TRANSLATING FOCUSED ULTRASOUND COMBINED NANOMEDICINES FOR TREATMENT OF BONE INFECTIONS AND CANINE CANCER PATIENTS

By

HARSHINI KAILASH ASHAR

Bachelor of Veterinary Sciences and Animal Husbandry
Nagpur Veterinary College
Nagpur, Maharashtra
2011

Master of Veterinary Science
Bombay Veterinary College
Mumbai, Maharashtra
2013

Submitted to the Faculty of the
Graduate College of the
Oklahoma State University
in partial fulfillment of
the requirements for
the Degree of
DOCTOR OF PHILOSOPHY
December, 2021

TRANSLATING FOCUSED ULTRASOUND COMBINED NANOMEDICINES FOR TREATMENT OF BONE INFECTIONS AND CANINE CANCER PATIENTS

Dissertation Approved:

Dr. Ashish Ranjan

Dissertation Adviser

Dr. Jerry Malayer

Dr. Jerry Ritchey

Dr. Daqing Piao

DEDICATED TO

MOM, DAD, JEET AND HERNAN

Name: HARSHINI KAILASH ASHAR

Date of Degree: DECEMBER, 2021

Title of Study: TRANSLATING FOCUSED ULTRASOUND COMBINED NANOMEDICINES FOR THE TREATMENT OF BONE INFECTIONS AND CANINE CANCER PATIENTS

Major Field: VETERINARY BIOMEDICAL SCIENCES

Abstract: High-intensity focused ultrasound (HIFU) is a non-invasive and non-ionizing sonic energy based therapeutic technology for inducing thermal and non-thermal effects in tissues. HIFU transducers are designed to focus high-energy pulses on a well-defined target region to minimize toxicities to healthy tissues. Depending on the parameters, HIFU can ablate tissue by heating them to $>55^0$C to induce denaturation and coagulative necrosis, improve radio- and chemo-sensitizations and local drug delivery from nanoparticles (NPs) at moderate hyperthermia (~ 41-43^0C), and mechanically fragment cells using acoustic cavitation (also known as histotripsy or HT). HIFU has already emerged as an attractive modality for treating human prostate cancer and neuromodulation. Based on this premise, the objective of this doctoral research was to investigate the feasibility of translating HIFU for treatment of veterinary cancers and bone-infections. Veterinary and human patients demonstrate anatomic and physiological similarities, and we hypothesize that HIFU will have a strong promise and translation basis for comparative oncology use. Veterinary research using HIFU can also inform on device innovations needed for human translation against various indications. In this project, we investigated several HIFU parameters to understand efficacy against a variety of veterinary cancers. We also determined immunopathological outcomes to provide the foundations for new treatment protocols. Unlike soft-tissue based tumors, the efficacy of HIFU in treating acoustically attenuating bone tissues that harbor metastasis or recalcitrant biofilm implant-associated osteomyelitis is still unclear. To address this question, a comprehensive assessment of HIFU against established implant-associated bone osteomyelitis was performed. Specifically, the ability of HIFU to induce bacterial killing and improve antibiotic treatments from NPs was determined. Our data from rodent and veterinary cancer studies provided important insights on the opportunities and challenges of HIFU technology, and we believe that the research studies can help jumpstart several clinical trials leading to greater use in patients.

TABLE OF CONTENTS

Chapter Page

LIST OF TABLES

Table Page

LIST OF FIGURES

Figure Page

Figure Page

Figure Page

CHAPTER I

INTRODUCTION AND LITERATURE REVIEW

1. MEDICAL ULTRASOUND

Ultrasound transducers transmit soundwaves with frequencies that are significantly higher than the range of human hearing (>20,000Hz). Medical ultrasound falls into two distinct categories: diagnostic and therapeutic. While diagnostic imaging is the most widely recognized for non-invasive image examination of internal body structures (e.g., obstetric ultrasonography), therapeutic ultrasound pre-dates diagnostic ultrasound by at least several decades [1]. The earliest investigation of focused ultrasound in experimental biology was reported by Lynn et al. in 1942 [2]. But despite its early start, the applications of therapeutic ultrasound did not see much use due to a lack of adequate image guidance to target and monitor treatments [3]. However, with recent advances in imaging, therapeutic ultrasound is making a resurgence in the medical community. Therapeutic ultrasound generates a biological effect as opposed to standard imaging and diagnostics by focusing acoustic energy in a defined region to produce thermal and nonthermal mechanisms including cavitation [4]. This approach is called high intensity focused ultrasound (HIFU) therapy. HIFU augments blood flow, stimulates tissue

regeneration, or destroys tissue by thermal and mechanical effects [5]. In the following sections, we describe HIFU elicited targeted physiological changes in tissue microenvironments, and ways this doctoral research leveraged those changes for treating soft and hard (calcified) tissues.

2. HIGH INTENSITY FOCUSED ULTRASOUND (HIFU)

HIFU is a non-invasive, therapeutic modality with acoustic intensities that are generally 1,000 to 10,000 time greater than traditional diagnostic devices (Table 1) [3, 6]. HIFU ultrasonic energy is deposited to a well-defined region of tissue (focal zone) resulting in thermal or mechanical ablation of tissue at the focal region. This ability to ablate millimeter sized targets without harming surrounding tissues has made HIFU a highly appealing alternative to other treatment modalities like radiation and surgery. Currently, there are 152 clinical indications or disorders utilizing HIFU in various stages of development, most of which are in early stages of investigation. Worldwide, 34 indications have obtained regulatory approval for HIFU use. In the United States, HIFU has been approved by the FDA for 7 indications [7] .

	HIFU [3]	Diagnostic [6]
Intensity (W/cm^2)	1000 to >25000	1.75
Power (W)	>10	0.05
Frequency (MHz)	0.8-20	1-20
Intended tissue temperature (^0C)	>56	37

Table 1. Typical parameters of HIFU versus diagnostic ultrasound [3, 6].

2.1. PROPAGATION AND FOCUSING OF ULTRASOUND WAVES

To achieve localized effects, HIFU transducers are designed to converge beams of ultrasound waves at a single focal point. A transducer is a device that converts energy from one form to another. In HIFU, electrical energy is converted to sound energy using piezoelectric crystals that oscillate upon application of an alternating voltage, resulting in the generation of ultrasound waves in the receiving medium. Focusing can be geometrically achieved by using a spherical/ concave curved transducer or by using a plane transducer with an acoustic lens to mimic a concave surface transducer [8]. Beam focusing can also be achieved via electronic steering in phased array transducers, composed of multiple piezoelectric elements (Figure 1) [8, 9]. The overall geometry of the transducer and frequency of the piezoelectric elements determine the characteristics of the transducer, including focal depth and width and length of the focal zone.

An ultrasound wave from a transducer outside the body must travel through multiple tissue layers, (including skin, subcutaneous fat, muscle), prior to reaching the target organ. At each tissue interface, part of the energy carried by the sound wave is reflected, whilst the remaining energy is transmitted into the tissue. The acoustic impedance, Z, which is the product of the speed of sound and density of tissue, determines the transmission coefficient. Apart from fat, air and bone, most human tissues have acoustic properties like those of water. Therefore, aqueous media are optimal for transmitting ultrasound energy from the transducer into the body. Furthermore, the loss in incident acoustic energy (due to absorption/heating or scattering) in a medium is characterized by its attenuation coefficient, which in turn is inversely related to the ultrasound frequency [10]. An increasing attenuation is correlated with decreased water content and increased

protein content [11]. For example, tissues such as tendons, with high protein content, have higher absorption of ultrasound waves and therefore greater heating effects compared to high water containing tissues like blood and fat [12]. Therefore, target tissue properties also need to be considered when deciding on the HIFU treatment parameters.

3. BIOLOGICAL EFFECTS OF HIFU:

Application of HIFU can result in one or more diverse bioeffects that may be broadly categorized as tissue destruction, localized drug delivery, immunomodulation, or other effects.

3.1. TISSUE DESTRUCTION

This is the most common application of HIFU [13]. HIFU induced tissue destruction can be achieved by either using thermal energy to induce tissue protein denaturation [14] or mechanical energy to induce cell membrane destruction via cell stress [15].

3.1.1. Thermal Ablation

During ablative treatment, high intensities of acoustic energy deposited in the focal region by HIFU leads to rapid heating. Temperatures quickly rise to more than 55^0C to 60^0C within seconds, that causes rapid cellular necrosis in the targeted area with minimal damage to the surrounding tissue, as shown in Figure 2 [3]. These exposures are usually high power, short duration exposures producing well demarcated coagulated lesions surrounded by apoptotic viable cells in the order of a few cellular layers [16] [17]. The classic individual thermal lesion can be the size of a rice grain [8], depending on the equipment and parameters used, allowing for an extremely localized treatment and sharp treatment borders. The threshold for thermal necrosis depends on the temperature reached

in the tissue, the rate of HIFU application and the thermal sensitivity of the target tissue [18]. Magnetic Resonance (MR)-guided imaging allows for the monitoring of temperature rise in real time, allowing quantification of the therapeutic dose [19]. Additionally, ultrasound imaging and tissue characterization techniques can be used for treatment monitoring for many clinical applications [20].

The thermal effects of ultrasound for therapeutic purposes [2] [21] has been extensively explored for non-invasive treatment of a variety of clinical conditions such as uterine fibroids [22, 23], tumors in the prostate [24], breast and liver [8], musculoskeletal pain [25] and neurologic disorders such as essential tremor, Parkinson's and neuropathic pain [26-28] among many other conditions.

3.1.2. Mechanical destruction

Using high power and very short pulse durations create a large pressure change in the tissues, low energy deposition and minimal thermal rise in tissues. However, the high-pressure exposure conditions lead to occurrence of acoustic cavitation [29]. This is the most prominent mechanical effect of HIFU. In general, acoustic cavitation can be thought of as the formation of a bubble cloud, as the traveling ultrasound waves interact with dissolved gases in the tissues, in response to an acoustic pressure field. This phenomenon can occur during ultrasound propagation in water [30] as well as biological tissues. The threshold of pressure amplitude that is required to initiate thermally significant cavitation, in vivo, is inversely proportional to the frequency of ultrasound treatment [31]. The nucleation of bubbles within tissue can also be injected in the form of microbubbles apart from being generated by the ultrasonic peak negative pressure itself [32, 33]. The

pressure threshold for cavitation to happen is dependent on the acoustic parameters such as frequency, pulse length, and peak pressure as well as environmental properties such as the tissue type and tissue temperature [34].

Types of acoustic cavitation include stable and inertial cavitation (Figure 3) [35]. Stable cavitation occurs when bubbles oscillate steadily and grow in size , as the pressure changes at the focal point, creating shear stress and microstreaming of the surrounding fluid [8]. It can induce moderate changes at the cellular level, such as enhancing cell membrane permeability to drugs and other molecules [36]. The main application of stable cavitation is to alter vascular permeability for increased drug/gene/nanoparticle extravasation, penetration, and thus improved delivery to whole tissues [37]. By altering cell permeability and action potential, via ion channel and receptor stimulation, it also facilitates drug delivery to cells [38].

Inertial cavitation occurs when above a certain pressure threshold causes a violent collapse of the microbubbles releasing a shockwave capable of destroying cell membranes and even liquefying or ‘ablating’ cells at the focal point [33, 39]. The use of inertial cavitation to create mechanical lesions with clearly demarcated margins of tissue fractionation is known as histotripsy [40]. Using injected microbubbles, which are easily visible with ultrasound imaging, to lower the threshold for inertial cavitation only at the target, acoustic cavitation can be monitored in real-time to guide accurate targeting with the goal of minimizing unwanted tissue damage [39, 41, 42]. High precision and tissue selectivity are thus the well-established hallmarks of histotripsy procedure [43-45]. Other physical phenomena like acoustic streaming and radiation forces also contribute to mechanical-based bioeffects [46]. Unlike most other ablation therapies, because

histotripsy is non-thermal in most cases, it is not affected by the heat-sink effect, and therefore remains safe and efficacious for use near the selective tissues such as vasculature [47]. Histotripsy treated tissues have shown rapid dissolution after treatment, compared to the other ablation modalities [48, 49]. For e.g., healthy rat livers treated with cavitation-cloud histotripsy showed rapid shrinkage of treated volumes, granulation and growth of healthy hepatocytes within 28 days post treatment, with minimal scarring [48]. Histotripsy has been investigated for a wide range of preclinical applications in large and small animal models for tumors including liver cancer [48, 50], prostate cancer [41], renal cancer [51, 52], pancreatic cancer [53, 54], musculoskeletal tumors [55], as well as brain applications [40, 56, 57]. Clinically, three Phase I trials have been conducted to investigate the safety of histotripsy in patients with liver cancer [58], calcified aortic stenosis [59], and benign prostatic hyperplasia [60].

3.2. TARGETED DRUG DELIVERY

HIFU assisted delivery of drugs has gained increasing attention in recent years as it permits spatially confined delivery of therapeutic compounds in target areas, such as tumors [61]. Different HIFU mechanisms can be used for enhanced cellular drug uptake, namely, sonoporation, vasodilation and increased vascular permeability, local hyperthermia and drug delivery vehicles [38] .

3.2.1. Sonoporation

Sonoporation is the process where the pore size in the cell membrane increases because of ultrasound induced mechanical impact via stable cavitation. Stable cavitation

physically disrupts the integrity of membrane assembly leading to membrane poration [36]. The reversible changes thus formed at the cellular level, allow passive entry of drug molecules, genes or nanoparticles into cells [36]. Additionally, stable cavitation produces microstreaming, which increases the flow of fluid in a cell's environment. This increase in flow may further assist the opening of pores, allowing a greater volume of drugs/compounds to be directed towards the cells, which enhances cellular uptake [62]. Ultrasound-induced sonoporation for improved delivery of DNA to mammalian cell was first demonstrated by Fechheimer et al. (1986) [63]. This method can also be used in vivo for delivery of genetic material compared to the alternatives and greatly increase the specificity of treatments [64]. Focused ultrasound-assisted gene therapy can be used to treat several indications ranging from glioblastoma, cardiovascular indications, Parkinson's disease, and even certain types of cancer [65-69].

3.2.2. Vasodilation and increased vascular permeability

Physiological barriers between the blood vessels and their surrounding tissue can limit delivery of drugs to the intended targets. Focused ultrasound can reversibly cause widening of blood vessels, vasodilation, and increase their permeability, thereby increasing blood flow and temporarily allowing drugs to pass through them and into the targeted region.

Focused ultrasound can create a pressure change at the applied location, triggering the endothelium of targeted blood vessels to release nitric oxide, the chemical signal that causes smooth muscle relaxation and the dilation of blood vessels [70]. Vasodilation can be induced in ischemic tissue to enhance the effects of radiotherapy by increasing the

delivery of oxygen and blood to the target. Vasodilation can also aid treatments by increasing the amount of the drug delivered in the targeted tissue/region. It is a reversible process, with no permanent damage to targeted tissue. Moreover, pulsed HIFU causes minimal thermal effects [71]. There are numerous clinical indications that could be more effectively treated with the enhanced drug delivery effects of vasodilation, and it can also be used as a neo-adjuvant therapy to enhance efficacy of other therapies like radiotherapy. The delivery of drugs across vessel walls is controlled by a network of endothelial cells joined by tight junctions. The mechanical effects of HIFU disrupt these tight junctions to increase permeability, which can be more efficiently induced by using microbubbles [72]. This same effect had been employed to non-invasively open the blood-brain barrier, which has unlocked a vast array of potential treatments for many neurological disorders Parkinson's disease, Alzheimer's disease, and glioblastoma [73-75].

3.2.3. Local hyperthermia

Hyperthermia involves heating of tissues to 40-450C for longer period as opposed to ablative heating which induces rapid heating of targeted tissue to temperatures >600C within seconds leading to coagulative necrosis. Elevating and maintaining tissue temperature to a mild~ 40-45°C for several minutes can increase blood flow and drug absorption in the targeted region [76]. Hyperthermia increases blood flow to the heated region, increasing tissue perfusion drastically [77] which also increases oxygen delivery to the area, thus enhancing the metabolic activity and sensitivity of the targeted cells to drugs [78]. This has been used clinically to enhance drug delivery and efficacy in regions with restricted blood flow, especially tumors. Since HIFU has the ability to penetrate into

the deeper tissues of the body, with precision, it has numerous and wide-ranging potential clinical applications [79]. Tissue temperatures can be monitored in real-time using MRIor interstitial temperature sensors such as thermocouples, which allows for accurate temperature control. This approach has been applied in patients since the 1970's [80]. Some of the earlier patient treatments with Focused Ultrasound for hyperthermia used invasive thermocouples to monitor the temperature of heated tumors [81]. However, use of invasive thermocouples could introduce errors when placed within the focus of an ultrasound field [82], so non-invasive methods such as magnetic resonance thermometry are preferred.

HIFU-induced hyperthermia has shown to significantly enhance the delivery of anticancer treatments to targeted tumor sites in vivo [83]. For hyperthermia applications, it is desirable to achieve a stable temperature for a specific duration of time (tens of minutes to several hours) with a maximum volume of the target treated. For example, in the case of drug delivery systems using systemically administered temperature-sensitive liposomes, blood circulation continuously brings the liposomes to the targeted location, and prolonged hyperthermic heating at 400C to 450C would allow localized drug release and accumulation at therapeutic levels (Figure 4) [84]. Stable hyperthermia at 410C has been shown to be the most effective for drug deployment via temperature-sensitive liposomal systems [85]. Kong et al., 2001, observed that there is a much higher probability for tumor blood vessels to collapse above temperatures of 440C, resulting in significant decrease in liposomes arriving via the microcirculation and hence, a decrease in drug release in those regions. Other studies have shown that the application of moderate HIFU hyperthermia (~420C to 460C) can significantly increase perfusion

within the infected tissues, enhance tissue delivery of antibiotic from temperature sensitive liposomes and consequently improve bacterial killing in mice [86], without damage to surrounding tissues.

3.3. HIFU BASED IMMUNOMODULATION

A healthy immune system can identify a broad range of pathogens and cancer cells. It is when the immune system is compromised that leads to the advancement of chronic conditions like cancer, chronic infections, and others. During chronic infections, the pathogens (e.g., Staphylococcus aureus) or cancer cells develop various ‘acts’ of immune evasion by intracellular colonization of host/immune cells [87], releasing immune-suppressive cytokines, or depleting the tumor associated antigens [88]. Extensive research has been done in the field of cancer immunology and its application, cancer immunotherapy since the concept of cancer immunosurveillance was first proposed in 1957 by Burnet and Thomas [89]. Anti-tumor immunity requires specific identification of cancer cells by the immune system of the patient, for cancer elimination. To produce a cancer specific response, the cancer cells need to indicate tumor associated antigens. However, majority of cancer types are immunologically unresponsive. HIFU is a noninvasive technique that can potentially turn immunologically ‘cold’ tumors to immune-responsive ‘hot’ tumors [90]. When a tumor is ablated, it releases cellular proteins and debris and neo-antigens which can trigger an immune response to the tumor, at the primary site as well as potentially at distant metastases [91, 92]. Depending on the

HIFU parameters used- thermal ablation, histotripsy (mechanical cavitation) or hyperthermia, there may be different immune responses.

3.3.1. Thermal ablation-induced immunomodulation

Thermal ablation of HIFU has been shown to upregulate the expression of intracellular molecular chaperones, i.e., HSP70, in vitro and ex vitro [93, 94], which can result in potent cellular immune responses. When a tumor is targeted with HIFU ablation, there is a marked increase in the antigen presenting cells (APC), such as dendritic cells [95]. The increased abundance of tumor antigens released are recognized by the APCs, which in turn activate lymphocytes for a specific immune response [96]. Increased tumor infiltrating lymphocytes (TILs) particularly cytotoxic CD8+ cells and NK cells along the ablated region can increase the clearance chance of surviving cancer cells [97]. Immunosuppression in a patient with malignant tumor is a major obstacle in cancer treatment. In a study investigating changes in the circulating level of immunosuppressive cytokines in patients with malignancy, before and after HIFU treatment, showed that serum immunosuppressive cytokine levels decreased after HIFU. Significant decrease in VEGF, TGF-beta1, and TGF-beta2 after HIFU treatment was observed in addition to direct tumor destruction [98]. Clinical evidence suggests that HIFU treatment may also enhance local antitumor immunity in prostate cancer patients [99] and upregulated expression of HSP70 in breast cancer tumor debris [100].

Additional studies have also defined B cell activation, the maintenance of plasma cells, and even the generation of tumor specific antibodies following local tumor ablation along with dendritic cell activation [101, 102]. In a prospective study investigating the adaptive

immune responses of radiofrequency ablation against tumor-associated antigens (TAA) in patients after treating secondary liver tumors, it was found that only 6 of 49 patients studied had increased antibodies, or TAA-reactive CD8+ T cells months after treatment. Although the number of TAA tested was limited, the study pointed to a weak effect of RF ablation on the adaptive immunity [101].

Although many promising pre-clinical and clinical studies have shown that ablation therapies can control tumor growth locally and have positive effects on systemic immune response, there have also been reports of the opposite. There are several pre-clinical reports of the RFA treatment of hepatocellular carcinoma tumors and colorectal metastases potentially stimulating growth of

existing and distant tumors [103, 104]. One main hypothesis to explain this phenomenon focuses on the sub ablative hyperthermia that affects peri-ablation zone tissues. Studies investigating this have linked these pro-oncogenic effects to upregulation of inflammatory pathways in this region, including the IL-6-HGF/c-Met-STAT3-VEGF axis and the HSP70 related pathways [103, 105, 106]. One study, Ahmed et al., demonstrated that a higher temperature/shorter duration treatment paradigm, alone or in combination with adjuvant HSP inhibitors, limited off-target systemic pro-oncogenic effects after hepatic RFA of rat livers [103]. Another cause associated with increased tumor growth after the minimally invasive ablation of tumors is the tumor cell seeding that can occur along the needle track [107]. This particular issue is avoided in HIFU ablation which uses a completely non-invasive extracorporeal transducer system for highly focused ultrasound treatment application. A study by Jenne et al., comparing HIFU ablation with other thermal ablation methods, noted that controlling the variability of lesion shape and

size was the major advantage of HIFU [108]. Other advantages of HIFU are its ability to ablate tumors in difficult locations such as close to the heart of diaphragm, where RFA would be technically impossible [109]. Furthermore, the HIFU- associated heat-sink effect was minimal due to extracorporeal energy delivery unlike RFA, where energy is delivered using an active treatment electrode, which can lead to incomplete tissue ablation [110].

3.3.2. Histotripsy-induced immunomodulation

Histotripsy induced cavitation breaks down tissues, ablating cells into subcellular fragments and acellular debris resulting in modulation of immune processes, cells, and molecules. Histotripsy's postulated roles in immunomodulation are summarized as- decrease in pro-tumor immune cells, cellular immunity, and systemic immunity [111, 112].

Studies by Pahk et al., demonstrated that the supernatant from breast cells treated with boiling histotripsy (BH) can polarize THP-1 human monocyte cells to M1 macrophages as well as repolarize M2 macrophages to M1 state [113]. Analysis found increased proinflammatory signaling molecules including TNF, which is a potent and well established M1 stimulating cytokine [114]. In vivo, this would help to decrease presence of pro-tumor immune cells and potentially alter the tumor microenvironment from 'cold' to 'hot'. Although not confirmed by literature, this hypothesis is consistent with results from some our preclinical studies. For example, we treated murine melanoma with Histotripsy, and showed a strong correlation between improved immune effects and an increase in mouse survival [115].

Histotripsy generates subcellular fragments through mechanical fractionation and induce sonic stress to enhance the expression of damage associated molecular patterns (DAMPs) which, in turn, enhance tumor inflammation, and anti-tumor immune effects [90, 116-118]. In addition, critical cytokines and chemokines have been found to be significantly altered, especially IFN-Y, in multiple histotripsy studies [90, 113, 119, 120]. An in vivo murine study of neuroblastoma treated with histotripsy showed an approximately 2-fold increase in IFN-Y [90]. While IFN-Y is the most consistently reported cytokine across therapies and tumor types, other important cytokines including IL-6, IL-2, TNF, IL-8, IL-13, and IL-10 have been reportedly upregulated post histotripsy treatment [90, 113, 119, 121]. In addition to cytokines, studies have reported changes in levels of growth factors including GM-CSF and VEGF post histotripsy [90], adding to the potential for histotripsy to shift a 'cold' tumor to a more proinflammatory and tumor-suppressive microenvironment.

In response to DAMPs and the anti-tumor mediators (cytokines and chemokines), the cells associated with innate immunity are most rapidly recruited. For histotripsy, this includes neutrophils, NK cells, dendritic cells, and macrophages [119, 122]. The consequent modulation of adaptive immune cells has been strongly correlated with clinical success [123, 124]. Reduction in the magnitude of T regulatory cells (Tregs) and increased ratio of CD8+ to Tregs in both the tumor-draining lymph nodes and spleens of treated mice was reported [125]. Furthermore, challenge tumors injected 6 days post histotripsy showed reduced tumor growth indicating treatment efficacy in generating systemic tumor-specific protection [118].

Notably, the effects of mechanical HIFU to minimize the growth rates of treated tumors were more effective than thermal ablation, despite primary tumor debulking being greater (43% and 85% tumor volume reduction respectively). This suggests that the mechanical fractionation using HIFU stimulated a stronger immune response and may be employed in combination with thermal ablations to increase efficacy of HIFU [118]. The increased release of DAMPs, altered inflammatory state, and enhanced cellular and systemic immune response can potentially improve the efficiency of immune checkpoint inhibitors (ICI) as demonstrated by Eranki et al., and Singh et al. [90, 115]. Combining boiling histotripsy with anti-CTLA-4 and anti-PDL1 can induce a potent systemic immunity and long-term immune memory to cure majority of mice with unilateral and bilateral neuroblastoma tumors [90]. In an ICI refractory melanoma model, combination of boiling histotripsy with anti-CD40 lead to improved immune sensitization of tumors via the CXCL9-cytotoxic T cell axis and consequently mice survival rates, compared to the monotherapies [115].

3.3.3. Hyperthermia-induced immunomodulation

HIFU mediated mild-moderate hyperthermia has been shown to increase vascular permeability, cellular permeability, and enhance the metabolic activity of the hyperthermic targets. This enables enhanced delivery/passage of drugs and immune cells, increased bioavailability of drug and sensitivity to chemotherapy. While mild hyperthermia does not cause immediate cell death typically, it has been shown to alter the tumor microenvironment by inducing a myriad of cellular effects [126]. HIFU hyperthermia can directly promote antigen cross-presentation and tumor specific T cell generation and expansion [127].

Originally based on the understanding of fever causing immunologic reactions, when cells are exposed to hyperthermia, they undergo a stress response. Viable tumor cells that evade the immune system experience an upregulation of HSP synthesis and surface expression. Consequent HSP-peptide complex formation activates NK cells which have direct antitumor activity. In addition, they also bind to dendritic cell receptors causing activation of cascade of T cell differentiation towards activated CD8+ cytotoxic T cells, which also have direct antitumor activity. In addition to a local response, locally applied hyperthermia is also capable of increasing systemic levels of antitumor immune cells [126, 128]. Wu et al. measured the levels of lymphocytes and natural killer cells in adults with solid tumors including osteosarcoma, hepatocellular carcinoma, and renal cell carcinoma. Patients treated with HIFU showed an increase in CD4+ lymphocytes in their peripheral blood, obtained at 7-10 days post treatment. CD4+ helper T cells play critical roles in initiating, regulating, and maintaining the antitumor immune response, esp. T cell mediated antitumor response [129].

Although the effects of HIFU hyperthermia against microbiological indications haven't been as thoroughly explored as cancer research, a sharp reduction in bacterial growth at temperatures above 400C was reported by Sturtevant et al., for S. aureus and S. epidermis planktonic strains. This was accompanied with upregulations of stress response genes- HSP60, which contributes to misfolded protein response, and murAB/Z, which is involved in cell wall synthesis and repair [130]. Another study reported structural damage to bacterial cells in a S. aureus biofilm and enhanced susceptibility to antibiotics, when exposed to mild HIFU hyperthermia of 420C- 460C [86].

Local hyperthermia has been reported to improve standard chemotherapy, especially with drug delivery systems, for a different disease [131-133], in addition to the radiosensitizing effects in cancer therapy [126]. With focus shifting to immunotherapy, hyperthermia continues to offer favorable combination approaches due to its ability to enhance both local and systemic antitumor immune responses. Singh et al., showed that a combination of HIFU hyperthermia and anti-CD-40 improved macrophage polarization dynamics and could enhance T cell functions to aid melanoma immunotherapy [134]. Another study assessed the combination of calreticulin nanoparticles with HIFU hyperthermia for immunogenic cell death associated immunomodulation in a melanoma model. Their *in vitro* and *in vivo* data suggested enhanced antigen presentation by macrophages and infiltration of activated CD8+ T cells in tumors. Addition of HIFU hyperthermia led to a modulation of the CRT-CD47-PDL1 axis, thus improving the overall therapeutic response against melanoma tumors [135].

4. DRUG DELIVERY SYSTEMS

Utilizing nanoparticles (NP) to aid in drug delivery has been a promising field of research. NP-based approaches have shown considerable promise for biomedical applications including diagnosis and therapy. Because of their large surface-area-to-volume ratio, as well as the flexibility in controlling the chemical and physical properties, nanotechnology is a powerful platform for enhancing the traditional chemotherapy [136]. Additionally, drug delivery systems protect the drug from rapid degradation or clearance, enhance drug concentrations in the target tissues. Consequently, lower doses of drug are required, and undesirable side effects of chemotherapy can be minimized [137]. This is

especially important when there is disparity between drug dose/ concentration and the resultant therapeutic/ toxic effects. Once the drug-loaded nanoparticles reach the diseased tissues, the therapeutic agents are delivered. This release of drugs can be controlled through changes in the physiological environment such as temperature, pH, osmolarity or an enzymatic activity [138].

Focused ultrasound can be used as a safe, non-invasive stimulus for controlled drug release from nanocarriers that are sensitive to elevated temperatures or pressures [139]. Therefore, although the encapsulated drug is circulating through the body, it is only released in the region where HIFU is applied. In this way, we can achieve triggered, 'on-demand' drug release in the diseased area, with zero to minimum side effects systemically (Figure 5). HIFU-induced hyperthermia [140, 141] and cavitation [36] have been shown to augment nanoparticle accumulation and increase local drug bioavailability.

A significant amount of recent scientific work has been devoted to optimizing the various types of drug delivery systems such as microbubbles [142], nanobubbles [143, 144], liposomes [145, 146], polymeric nanoparticles [147, 148], etc. as being ultrasound responsive. Fields of clinical applications include anticancer therapy, cardiovascular system, induction of an immune response, transdermal drug delivery, thrombolysis, disruption of the blood–brain barrier, and antibacterial applications [149, 150].

4.1. LIPOSOMES

Liposomes were first discovered by Dr. Alex D Bangham and R. W. Horne in 1963, at the Babraham Institute in Cambridge, when they were testing the institute's new electron

microscope by adding negative stain to dry phospholipids [151, 152]. Liposomes are spherical bilayer phospholipid-based membranes that can be fabricated anywhere between a few nanometers to micron sized. Liposomes are biocompatible and can be broken down and integrated into cell walls. They are capable of holding drugs in their hydrophilic core or within their hydrophobic phospholipid bilayer coat. Liposomes provide a larger drug payload per particle and protect the encapsulated drugs from metabolic processes [153]. Improved drug delivery is realized by interactions of liposomes with cells and enhancing drug solubility (via membrane fusion, endocytosis, lipid transfer, and stable adsorption of liposomes into cells), reducing toxicity to healthy cells, increasing the half-life of encapsulated drug, shielding from the phagocytic system, etc. [138]. The biophysical characteristics of these nanoparticles, like- vesicle size, lamellarity, surface charge, membrane fluidity, and surface, can be modified, by the lipid composition and/or preparation method, to confer various properties including active targeting to substrates, temperature sensitivity, and immunological responses. Numerous liposomal drug formulations are in clinical use for different pathologies such as anticancer drugs, neurological applications, antibiotics, antifungal drugs, anti-inflammatory, and antirheumatic drugs [154-156].

4.1.1. Temperature sensitive liposomes

The first formulation of liposomes to preferentially release their entrapped payload at transition temperatures was first described by Yatvin et al. in 1978 [157]. Temperature sensitive liposomes (TSLs) allow for external triggering of drug release both spatially and temporally. When the external temperature is raised above the melting phase transition temperature (Tm) of the lipids, forming the bilayer, the structure of the bilayer changes as

a transfer from a solid gel phase to a liquid-crystalline phase occurs. The permeability of hydrophilic drugs like doxorubicin HCl and ciprofloxacin HCl is highest at temperatures around the Tm when the bilayer membrane is in the liquid-crystalline phase [158]. This release generates high local drug concentrations and increased tissue penetration, when used in combination with external stimuli such as HIFU (as explained in the previous sections)[159]. DPPC is the major component of most TSL formulations since its T_m is above that of body temperature (i.e., 41.4^0C) [160, 161]. Unwanted drug leakage at body temperature can be reduced by mixing DPPC with small amounts of other phospholipids, such as DSPC (T_m= 54.9^0C) [162-164]. The overall T_m of the formulation is determined by the composition of miscible phospholipids [165]. Additionally, amphiphilic molecules (surfactants) are often used in liposomal formulations, but they potentially affect the vesicle stability to some extent [166]. Examples are- lipid-grafted PEG (e.g., 1,2-distearoyl-sn-glycero-3-phosphoethanolamine-N- [methoxy (polyethylene glycol)-2000], DSPE-PEG2000) is commonly used in liposomes to create a steric barrier for inhibition of uptake by the reticuloendothelial system and increased blood circulation time [167-169]; Lyso PC (e.g., 1-stearoyl-2-hydroxy-sn-glycero-3-phosphocholine) is incorporated to mediate drug release by formation of lysolipid-stabilized membrane pores in TSLs [170, 171]. Stable drug retention at body temperature in the presence of blood components and a long *in vivo* half-life, combined with a fast drug release rate around T_m are the pre-requisites for TSL formulations. In addition to phospholipid composition, the heat-triggered drug release depends to some degree on the drug molecule encapsulated, vesicle size, and the presence of serum components [164, 172-175]. Some of the first FDA-approved liposomal formulations included Doxil® (liposomal doxorubicin,

Janssen), and DaunoXome® (liposomal daunorubicin, Galen) for anti-cancer therapy, and Abelcet® (liposomal amphotericin B lipid complex, Sigma-tau) for fungal infections were non-thermosensitive in nature [176]. Since their approval in 1995, several other liposomal formulations were approved for clinical use, or are in clinical trials, for the treatment of various medical disorders including cancer, fungal infections, inflammatory conditions, neurological conditions, respiratory infections, infectious diseases, bacterial infections, and dermal conditions. Additionally, the route of administration for these formulations varies, depending on the active agent, indication, target tissue, and other factors, and include intravenous, intramuscular, intra-tumoral, ocular, oral, pulmonary, dermal, intranasal, intra-articular, and even vaginal [155, 156, 177, 178].

Incorporation of lysolipids in the membrane bilayer led to the development of low temperature-sensitive liposomes (LTSLs) by Needham et al. in 2000 [179]. This formulation is characterized by ultra-fast drug release upon heating and approximately 70% of lysolipid was found to dissociate within one hour post intravascular injection [180]. The LTSL formulation with encapsulated doxorubicin (ThermoDox), licensed to Celsion Corporation (Columbia, MD, USA), is designed to be used in combination with heat-based treatments, such as radiofrequency thermal ablation (RFA), microwave hyperthermia, or HIFU. It is currently under clinical investigation, in combination with MR-HIFU, for treatment of refractory/ recurrent solid tumors in humans as well as for sarcoma tumors in canine patients. Extensive research has been done and is underway to develop liposomal formulations for a variety of cancers [158] including studies done by our lab on colorectal tumor models which also demonstrate the feasibility of using HIFU-hyperthermia triggered drug release and accumulation in the mice models [132, 181].

Although not as well explored as cancer research, many studies have shown that liposome encapsulation improves the efficacy of antibacterial drugs against a broad range of pathogens both *in vitro* and *in vivo*. Localized delivery of antimicrobials to treat challenging infections like biofilms and intracellular infections is a promising approach[182, 183]. Research from our lab has demonstrated the use of LTSLs for localized antimicrobial delivery in combination with HIFU hyperthermia, *in vivo*. Additionally, at higher temperatures (42^0C), extended treatment caused *S. aureus* bacterial membrane deformation and structural changes in the biofilm matrix, and consequently reduced bacterial viability *in vitro* [131] and in a mouse chronic wound model [86]. Arikace™ (Transave, Inc.), a non-thermosensitive liposome-encapsulated amikacin, is clinically approved for the treatment of Mycobacterium avium complex lung disease. It was developed by the company as a site-specific treatment of serious lung infections. Arikace™ received orphan drug status from the FDA in the United States and the European Medicines Agency in Europe for the treatment of Pseudomonas aeruginosa infections in patients with Cystic Fibrosis (CF). It has also received orphan drug status by FDA for pseudomonas-associated non-CF bronchiectasis therapy as well as for lung infections due to nontuberculous mycobacteria. The product is currently in phase III clinical trials for these indications [155]. These indicate a strong promise to translate LTSL based systems with HIFU for wound treatments.

5. APPLICATIONS OF HIFU

HIFU is of interest to physicians and research scientists as it provides a non-invasive paradigm for treatment of a vast range of diseases for which the conventional therapies

pose major limitations. With advancement in technology such as phased array transducers, real- time feedback and temperature monitoring with ultrasound guidance or MR thermometry, new and exciting applications for HIFU have evolved. Currently HIFU is FDA approved for the treatment of uterine fibroids, breast tumors, bone metastases, prostate cancer, and neurological applications like essential tremor, Parkinson's disease, including others [8, 184, 185].

In oncology, promising research is being conducted for application of HIFU for immunomodulation as well as targeted drug delivery. More groups are reporting data on use of HIFU in conjunction with immunomodulation drugs and/or chemotherapeutic drugs to boost the anti-tumor responses in various tumor types. In addition to tumor ablation, application of HIFU has advanced to include targeted drug [186] and gene delivery [187] opening the blood-brain barrier [188] and thrombolysis [189]. Currently investigations are ongoing for treatment of polycystic ovarian syndrome and atherosclerosis [190, 191] with HIFU, among others. Additionally, HIFU clinical trials are ongoing for the treatment of soft tissue tumors and osteoid osteoma, with promising results [192, 193].

However, HIFU has its limitations including the lack of congruity between devices for effective treatment between its various applications. Thus, more research is required to expand the clinical applications of HIFU.

6. MOTIVATION FOR VETERINARY APPLICATION OF HIFU

Veterinary medicine is often running behind human medicine, despite the best of intentions. Domesticated dogs are exposed to the same environmental stimuli and are

afflicted with naturally occurring, inherited and genetic diseases as do humans [194]. Naturally occurring tumors in dogs share many molecular and clinical similarities to human cancers and that are difficult to replicate in other *in vivo* models [195]. Client-owned dogs with cancer are being increasingly recognized as a resource for pre-clinical/clinical assessment of the feasibility, pharmacology, and potential efficacy of novel anticancer therapies [196].

The employment of HIFU as a non-invasive cancer treatment tool in dogs is in its infancy. A recent retrospective clinical study by Ryu et al., suggested the use of HIFU as an alternative cancer treatment for dogs with solid tumors [197]. Another feasibility study demonstrated the potential of HIFU for treating soft tissue sarcomas in dogs [198]. Considering that these veterinary applications are also a possible model for treatment of similar tumors in humans, there exists and opportunity to explore the feasibility, safety, and efficacy of different HIFU parameters alone or in combination with chemo- or immunotherapy and nanomedicine.

The specific aims of this research project were to:

1. Determine if HIFU can non-invasively induce tumor regression in veterinary patients with and without chemotherapy
2. Evaluate and understand the local and systemic immune responses to HIFU ablation of tumors

7. MOTIVATION FOR MUSCULOSKELETAL APPLICATION OF HIFU AGAINST CALCIFIED TISSUES

As a noninvasive procedure, HIFU has shown promising results for management of numerous malignant and nonmalignant conditions, as discussed in this chapter. In the musculoskeletal field, HIFU is FDA approved for the treatment of bone metastasis and is currently being researched for application for osteoid osteoma, desmoid tumors, vascular malformations, and facet joint osteoarthritis [25]. Application of HIFU in management of musculoskeletal infections such as wound infections and osteomyelitis is yet unexplored and in early stage.

Our group has previously showed that HIFU can be applied for the treatment of acute and chronic wound infections by targeted antibiotic delivery using LTSLs and sensitizing the bacteria against the antibiotic by application of hyperthermia [131]. Furthermore, these non-healing wounds are often infested with bacterial biofilms, which have reduced perfusion, are resistant to antibiotics and have immune evasion mechanisms. Our group has previously reported HIFU in conjunction with antibiotics is improves non-invasive *S. aureus* biofilm killing in abscess wounds via enhanced antibiotic perfusion [86]. Building on prior success, we hypothesized that our combination therapy of HIFU with antibiotic laden LTSLs can be used to target biofilm-infested bone infections that currently require long duration antibiotic therapy and are limited by modest drug delivery within infected bones. In addition, biofilm implant associated bone infections, usually caused by MRSA, require multiple debridement and surgical interventions and the outcome greatly depends on extension of bone damage with limb amputation or septicemia being the most serious complications.

The specific aims of this research project were to:

1. Establish a rat model of biofilm implant associated osteomyelitis
2. Develop antibiotic loaded low-temperature sensitive liposomes
3. Assess the feasibility and optimize the application of combined HIFU + LTSL in the rat model of biofilm implant associated osteomyelitis

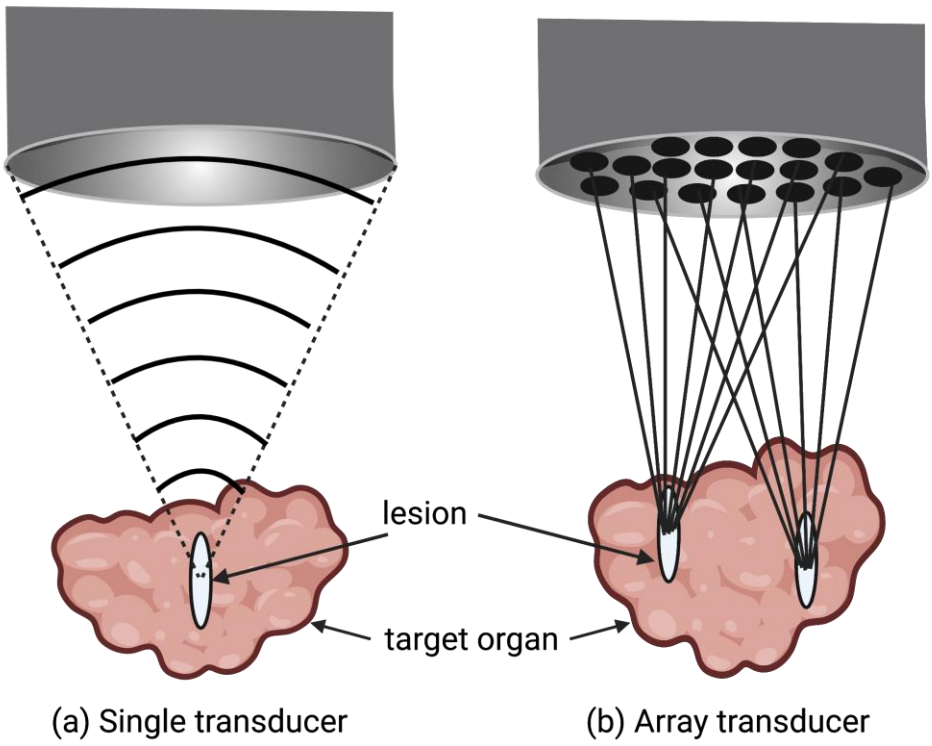

Figure 1. Focusing principles of high- intensity focused ultrasound (HIFU) in single (a) and array (b) transducers [9].

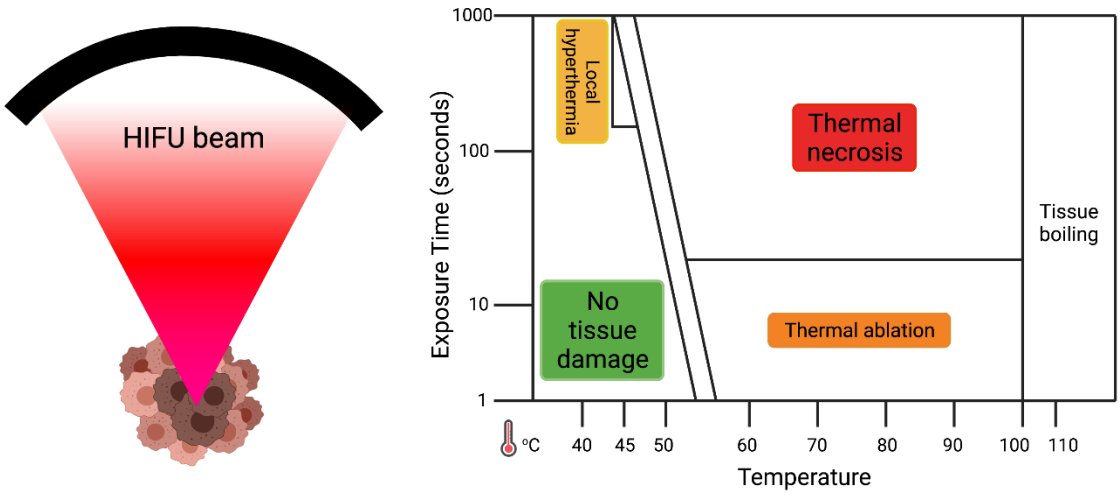

Figure 2. The threshold for thermal necrosis. As the temperature reached in the tissue increases, the exposure time needed for thermal necrosis decreases [79].

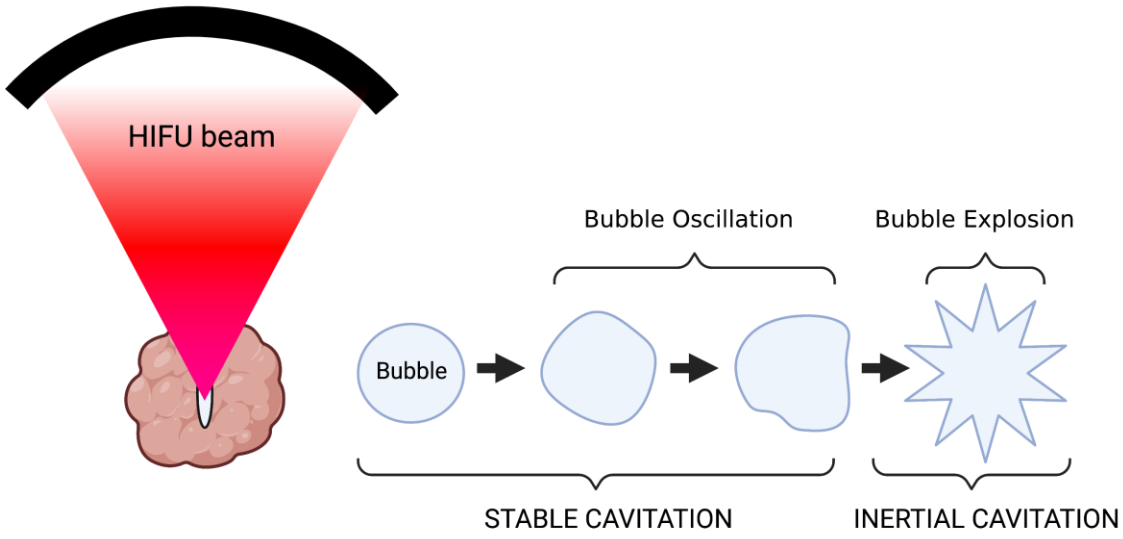

Figure 3. Cavitation effect of HIFU. Stable cavitation occurs when the ultrasound waves cause the tissue gas bubbles to oscillate steadily, creating shear stress and resultant cellular damage. Above a certain pressure threshold these bubbles violently explode resulting in shockwaves that causes tissue damage, this is known as inertial cavitation [35].

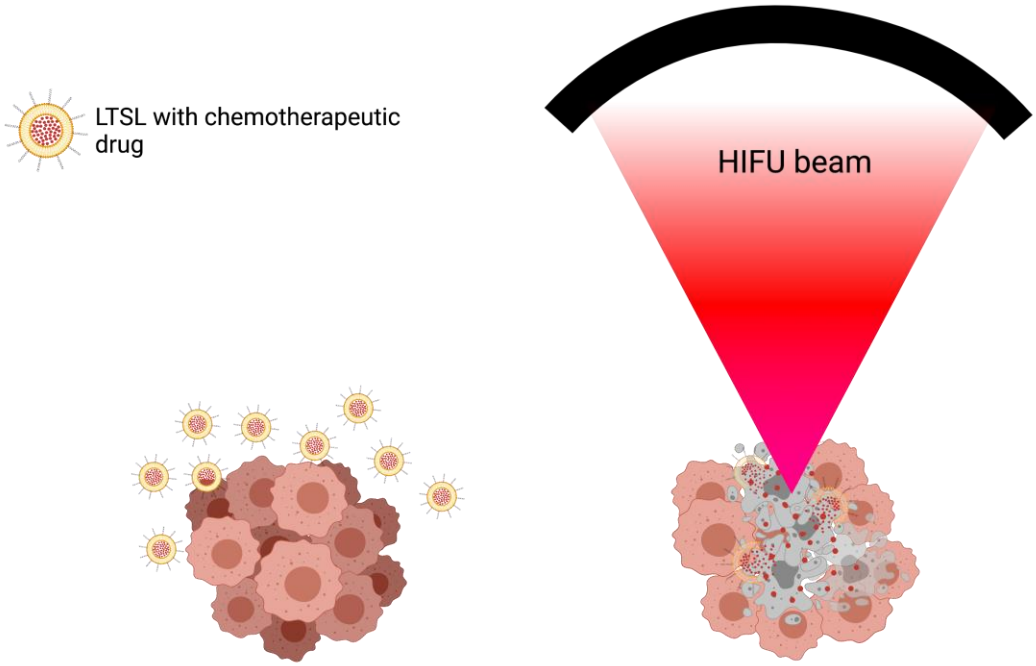

Figure 4. Schematic representation of targeted drug delivery using low-temperature sensitive liposomes (LTSLs). Application of HIFU causes localized temperature elevation (hyperthermia) which stimulates the release of drug from the LTSLs and sensitizes the cells to the chemotherapeutic drug.

References

1. Ter Haar, G., *The Resurgence of Therapeutic Ultrasound. A 21st Century Phenomenon.* Ultrasonics, 2008. **48**(4).
2. Lynn, J.G., et al., *A new method for the generation and use of focused ultrasound in experimental biology.* The Journal of general physiology, 1942. **26**(2): p. 179-193.
3. Ter Haar, G., *Therapeutic applications of ultrasound.* Progress in biophysics and molecular biology, 2007. **93**(1-3): p. 111-129.
4. Nyborg, W.L., *Biological effects of ultrasound: development of safety guidelines. Part II: general review.* Ultrasound in medicine & biology, 2001. **27**(3): p. 301-333.
5. Azhari, H., *Basics of biomedical ultrasound for engineers*. 2010: John Wiley & Sons.
6. Haar, G.t., *ACOUSTIC SURGERY.* Physics today, 2001. **54**(12): p. 29-34.
7. Elhelf, I.S., et al., *High intensity focused ultrasound: The fundamentals, clinical applications and research trends.* Diagnostic and interventional imaging, 2018. **99**(6): p. 349-359.
8. Malietzis, G., et al., *High-intensity focused ultrasound: advances in technology and experimental trials support enhanced utility of focused ultrasound surgery in oncology.* The British journal of radiology, 2013. **86**(1024): p. 20130044.
9. ter Haar, G. and C. Coussios, *High intensity focused ultrasound: physical principles and devices.* International journal of hyperthermia, 2007. **23**(2): p. 89-104.
10. O'Brien Jr, W.D., et al., *Acoustic propagation properties of normal, stunned, and infarcted myocardium: morphological and biochemical determinants.* Circulation, 1995. **91**(1): p. 154-160.
11. Watson, T., *Ultrasound in contemporary physiotherapy practice.* Ultrasonics, 2008. **48**(4): p. 321-329.
12. Al-Bataineh, O., J. Jenne, and P. Huber, *Clinical and future applications of high intensity focused ultrasound in cancer.* Cancer treatment reviews, 2012. **38**(5): p. 346-353.
13. Webb, H., M.G. Lubner, and J.L. Hinshaw. *Thermal ablation*. in *Seminars in roentgenology*. 2011. Elsevier.
14. Jang, H.J., et al., *Current and future clinical applications of high-intensity focused ultrasound (HIFU) for pancreatic cancer.* Gut and liver, 2010. **4**(Suppl 1): p. S57.
15. Ter Haar, G. and D. Robertson, *Tissue destruction with focused ultrasound in vivo.* European urology, 1993. **23**: p. 8-11.
16. Vykhodtseva, N., et al., *Apoptosis in ultrasound-produced threshold lesions in the rabbit brain.* Ultrasound in medicine & biology, 2001. **27**(1): p. 111-117.

17. Nikfarjam, M., V. Muralidharan, and C. Christophi, *Mechanisms of focal heat destruction of liver tumors.* Journal of Surgical Research, 2005. **127**(2): p. 208-223.
18. Jolesz, F.A., et al., *MR imaging–controlled focused ultrasound ablation: a noninvasive image-guided surgery.* Magnetic Resonance Imaging Clinics, 2005. **13**(3): p. 545-560.
19. Song, J.H., et al., *Real-time monitoring of HIFU treatment using pulse inversion.* Physics in Medicine & Biology, 2013. **58**(15): p. 5333.
20. Kennedy, J.E., *High-intensity focused ultrasound in the treatment of solid tumours.* Nature reviews cancer, 2005. **5**(4): p. 321-327.
21. Dobrotwir, A. and E. Pun, *Clinical 24 month experience of the first MRgFUS unit for treatment of uterine fibroids in Australia.* Journal of medical imaging and radiation oncology, 2012. **56**(4): p. 409-416.
22. Hesley, G.K., K.R. Gorny, and D.A. Woodrum, *MR-guided focused ultrasound for the treatment of uterine fibroids.* Cardiovascular and interventional radiology, 2013. **36**(1): p. 5-13.
23. Uchida, T., et al., *High-intensity focused ultrasound therapy for prostate cancer.* International Journal of Urology, 2012. **19**(3): p. 187-201.
24. Scipione, R., et al., *HIFU for Bone Metastases and other Musculoskeletal Applications.* Seminars in interventional radiology, 2018. **35**(4): p. 261-267.
25. Jeanmonod, D., et al., *Transcranial magnetic resonance imaging–guided focused ultrasound: noninvasive central lateral thalamotomy for chronic neuropathic pain.* Neurosurgical focus, 2012. **32**(1): p. E1.
26. Elias, W.J., et al., *A pilot study of focused ultrasound thalamotomy for essential tremor.* New England Journal of Medicine, 2013. **369**(7): p. 640-648.
27. Magara, A., et al., *First experience with MR-guided focused ultrasound in the treatment of Parkinson's disease.* Journal of therapeutic ultrasound, 2014. **2**(1): p. 1-8.
28. Leighton, T., *The Acoustic Bubble.| Academic.* Press, London, 1994: p. 234-243.
29. Atchley, A., et al., *Thresholds for cavitation produced in water by pulsed ultrasound.* Ultrasonics, 1988. **26**(5): p. 280-285.
30. Hynynen, K., *The threshold for thermally significant cavitation in dog's thigh muscle in vivo.* Ultrasound in medicine & biology, 1991. **17**(2): p. 157-169.
31. Deng, C.X., *Targeted drug delivery across the blood–brain barrier using ultrasound technique.* Therapeutic delivery, 2010. **1**(6): p. 819-848.
32. Chen, C.-J., et al., *Clinical experience with ultrasound-based real-time tracking lithotripsy in the single renal stone treatment.* Journal of endourology, 2009. **23**(11): p. 1811-1815.
33. Santos, M.A., *Towards Overcoming Limitations on MRI-Guided Focused Ultrasound Hyperthermia-Mediated Drug Delivery Using Thermosensitive Liposomes*. 2020, University of Toronto (Canada): Ann Arbor. p. 165.
34. Shehata, I.A., *Treatment with high intensity focused ultrasound: secrets revealed.* European journal of radiology, 2012. **81**(3): p. 534-541.

35. Liang, H., J. Tang, and M. Halliwell, *Sonoporation, drug delivery, and gene therapy.* Proceedings of the Institution of Mechanical Engineers, Part H: Journal of Engineering in Medicine, 2010. **224**(2): p. 343-361.
36. Yeh, C.-K., *Ultrasound microbubble contrast agents for diagnostic and therapeutic applications: current status and future design.* Chang Gung Med. J, 2012. **35**(2): p. 125-139.
37. Yang, C., et al., *Recent advances in ultrasound-triggered therapy.* Journal of drug targeting, 2019. **27**(1): p. 33-50.
38. Wrenn, S.P., et al., *Bursting bubbles and bilayers.* Theranostics, 2012. **2**(12): p. 1140.
39. Sukovich, J.R., et al., *In vivo histotripsy brain treatment.* Journal of neurosurgery, 2018. **131**(4): p. 1331-1338.
40. Hempel, C.R., et al., *Histotripsy fractionation of prostate tissue: local effects and systemic response in a canine model.* The Journal of urology, 2011. **185**(4): p. 1484-1489.
41. Kwan, J.J., S. Graham, and C.C. Coussios. *Inertial cavitation at the nanoscale*. in *Proceedings of Meetings on Acoustics ICA2013*. 2013. Acoustical Society of America.
42. Vlaisavljevich, E., et al., *Image-guided non-invasive ultrasound liver ablation using histotripsy: feasibility study in an in vivo porcine model.* Ultrasound in medicine & biology, 2013. **39**(8): p. 1398-1409.
43. Vlaisavljevich, E., et al., *Effects of ultrasound frequency and tissue stiffness on the histotripsy intrinsic threshold for cavitation.* Ultrasound in medicine & biology, 2015. **41**(6): p. 1651-1667.
44. Lin, K.-W., et al., *Histotripsy beyond the intrinsic cavitation threshold using very short ultrasound pulses: microtripsy.* IEEE transactions on ultrasonics, ferroelectrics, and frequency control, 2014. **61**(2): p. 251-265.
45. Dalecki, D., *Mechanical bioeffects of ultrasound.* Annu. Rev. Biomed. Eng., 2004. **6**: p. 229-248.
46. Pillai, K., et al., *Heat sink effect on tumor ablation characteristics as observed in monopolar radiofrequency, bipolar radiofrequency, and microwave, using ex vivo calf liver model.* Medicine, 2015. **94**(9).
47. Vlaisavljevich, E., et al., *Non-invasive ultrasound liver ablation using histotripsy: chronic study in an in vivo rodent model.* Ultrasound in medicine & biology, 2016. **42**(8): p. 1890-1902.
48. Smolock, A.R., et al., *Robotically assisted sonic therapy as a noninvasive nonthermal ablation modality: proof of concept in a porcine liver model.* Radiology, 2018. **287**(2): p. 485-493.
49. Vlaisavljevich, E., et al., *Non-invasive liver ablation using histotripsy: preclinical safety study in an in vivo porcine model.* Ultrasound in medicine & biology, 2017. **43**(6): p. 1237-1251.
50. Lake, A., et al., *Renal ablation by histotripsy—does it spare the collecting system?* The Journal of urology, 2008. **179**(3): p. 1150-1154.
51. Longo, K.C., et al., *Robotically assisted sonic therapy (RAST) for noninvasive hepatic ablation in a porcine model: Mitigation of body wall damage with a*

modified pulse sequence. Cardiovascular and interventional radiology, 2019. **42**(7): p. 1016-1023.
52. Hendricks, A.D., et al., *Determining the mechanism of the immune response to histotripsy ablation of pancreatic cancer*. 2020, Am Assoc Immnol.
53. Allen, I.C. and E. Vlaisavljevich, *Development of Novel Porcine Models of Orthotopic Pancreatic Cancer for FUS and Histotripsy Tumor Ablation Applications.* 2021.
54. Arnold, L., et al., *Histotripsy Ablation of Bone Tumors: Feasibility Study in Excised Canine Osteosarcoma Tumors.* Ultrasound in Medicine & Biology, 2021.
55. Sukovich, J.R., et al., *Targeted lesion generation through the skull without aberration correction using histotripsy.* IEEE transactions on ultrasonics, ferroelectrics, and frequency control, 2016. **63**(5): p. 671-682.
56. Ammi, A.Y., et al., *Characterization of ultrasound propagation through ex-vivo human temporal bone.* Ultrasound in medicine & biology, 2008. **34**(10): p. 1578-1589.
57. Vidal-Jove, J., *07 Dic Histotripsy-induced abscopal effect in liver tumors: Case Report.*
58. Messas, E., et al., *Feasibility and performance of noninvasive ultrasound therapy in patients with severe symptomatic aortic valve stenosis: a first-in-human study.* Circulation, 2021. **143**(9): p. 968-970.
59. Kaplan, S.A., *Re: Histotripsy Treatment of Benign Prostatic Enlargement Using the Vortx Rx System: Initial Human Safety and Efficacy Outcomes.* The Journal of urology, 2019. **202**(3): p. 434-434.
60. Zhu, L. and V.P. Torchilin, *Stimulus-responsive nanopreparations for tumor targeting.* Integrative Biology, 2013. **5**(1): p. 96-107.
61. Collis, J., et al., *Cavitation microstreaming and stress fields created by microbubbles.* Ultrasonics, 2010. **50**(2): p. 273-279.
62. Fechheimer, M., et al., *Measurement of cytoplasmic pH in Dictyostelium discoideum by using a new method for introducing macromolecules into living cells.* European journal of cell biology, 1986. **40**(2): p. 242-247.
63. Greenleaf, W.J., et al., *Artificial cavitation nuclei significantly enhance acoustically induced cell transfection.* Ultrasound in medicine & biology, 1998. **24**(4): p. 587-595.
64. Yang, Q., et al., *Gene therapy for drug-resistant glioblastoma via lipid-polymer hybrid nanoparticles combined with focused ultrasound.* International Journal of Nanomedicine, 2021. **16**: p. 185.
65. Han, H., et al., *Focused ultrasound-triggered chemo-gene therapy with multifunctional nanocomplex for enhancing therapeutic efficacy.* Journal of Controlled Release, 2020. **322**: p. 346-356.
66. Ziadloo, A., J. Xie, and V. Frenkel, *Pulsed focused ultrasound exposures enhance locally administered gene therapy in a murine solid tumor model.* The Journal of the Acoustical Society of America, 2013. **133**(3): p. 1827-1834.
67. Huber, P., et al., *Focused ultrasound (HIFU) induces localized enhancement of reporter gene expression in rabbit carotid artery.* Gene Therapy, 2003. **10**(18): p. 1600-1607.

68. Newman, C. and T. Bettinger, *Gene therapy progress and prospects: ultrasound for gene transfer.* Gene therapy, 2007. **14**(6): p. 465-475.
69. Maruo, A., et al., *Nitric oxide and prostacyclin in ultrasonic vasodilatation of the canine internal mammary artery.* The Annals of thoracic surgery, 2004. **77**(1): p. 126-132.
70. Yang, F.-Y., et al., *Functional changes in arteries induced by pulsed high-intensity focused ultrasound.* IEEE transactions on ultrasonics, ferroelectrics, and frequency control, 2009. **56**(12): p. 2643-2649.
71. Sheikov, N., et al., *Effect of focused ultrasound applied with an ultrasound contrast agent on the tight junctional integrity of the brain microvascular endothelium.* Ultrasound in medicine & biology, 2008. **34**(7): p. 1093-1104.
72. Tsai, S.-J., *Transcranial focused ultrasound as a possible treatment for major depression.* Medical hypotheses, 2015. **84**(4): p. 381-383.
73. Samiotaki, G., et al., *Enhanced delivery and bioactivity of the neurturin neurotrophic factor through focused ultrasound—mediated blood—brain barrier opening in vivo.* Journal of Cerebral Blood Flow & Metabolism, 2015. **35**(4): p. 611-622.
74. Fan, C.-H., et al., *Drug-loaded bubbles with matched focused ultrasound excitation for concurrent blood–brain barrier opening and brain-tumor drug delivery.* Acta biomaterialia, 2015. **15**: p. 89-101.
75. Thanou, M. and W. Gedroyc, *MRI-guided focused ultrasound as a new method of drug delivery.* Journal of drug delivery, 2013. **2013**.
76. PAWAR, P. and M. JOSHI, *Hyperthermia Therapy in Cancer Treatment.* 2013.
77. Ko, A. and M. Dollinger, *Everyone's guide to cancer therapy: How cancer is diagnosed, treated, and managed day to day*. 2008: Andrews McMeel Publishing.
78. Foundation, F.U. *An Overview of the Biological Effects of Focused Ultrasound*. 2015.
79. Marmor, J.B., et al., *Treatment of superficial human neoplasms by local hyperthermia induced by ultrasound.* Cancer, 1979. **43**(1): p. 188-197.
80. Shimm, D.S., et al., *Scanned focussed ultrasound hyperthermia: initial clinical results.* International Journal of Radiation Oncology* Biology* Physics, 1988. **15**(5): p. 1203-1208.
81. Hynynen, K., et al., *Errors in temperature measurement by thermocouple probes during ultrasound induced hyperthermia.* The British journal of radiology, 1983. **56**(672): p. 969-970.
82. Zhou, Y., *High-intensity focused ultrasound treatment for advanced pancreatic cancer.* Gastroenterology research and practice, 2014. **2014**.
83. Kong, G., R.D. Braun, and M.W. Dewhirst, *Characterization of the effect of hyperthermia on nanoparticle extravasation from tumor vasculature.* Cancer research, 2001. **61**(7): p. 3027-3032.
84. Ponce, A.M., et al., *Hyperthermia mediated liposomal drug delivery.* International Journal of Hyperthermia, 2006. **22**(3): p. 205-213.
85. Wardlow, R., et al., *High Intensity Focused Ultrasound (HIFU) Heating Improves Perfusion and Antimicrobial Efficacy in Mouse Staphylococcus Abscess.* Ultrasound in Medicine and Biology, 2018. **44**(4): p. 909-914.

86. Muthukrishnan, G., et al., *Mechanisms of Immune Evasion and Bone Tissue Colonization That Make Staphylococcus aureus the Primary Pathogen in Osteomyelitis.* Current Osteoporosis Reports, 2019. **17**(6): p. 395-404.
87. Lindau, D., et al., *The immunosuppressive tumour network: myeloid-derived suppressor cells, regulatory T cells and natural killer T cells.* Immunology, 2013. **138**(2): p. 105-15.
88. Burnet, M., *Cancer-a biological approach. 3. Viruses associated with neoplastic conditions.* BMJ-BRITISH MEDICAL JOURNAL, 1957. **1**(APR 13): p. 841-846.
89. Eranki, A., et al., *High-Intensity Focused Ultrasound (HIFU) Triggers Immune Sensitization of Refractory Murine Neuroblastoma to Checkpoint Inhibitor Therapy.* Clinical Cancer Research, 2020. **26**(5): p. 1152-1161.
90. Finley, D.S., et al., *Ultrasound-based combination therapy: potential in urologic cancer.* Expert review of anticancer therapy, 2011. **11**(1): p. 107-113.
91. Haen, S.P., et al., *More than just tumor destruction: immunomodulation by thermal ablation of cancer.* Clinical and Developmental Immunology, 2011. **2011**.
92. Kruse, D., et al., *Short-duration-focused ultrasound stimulation of Hsp70 expression in vivo.* Physics in Medicine & Biology, 2008. **53**(13): p. 3641.
93. Hundt, W., et al., *In vitro effect of focused ultrasound or thermal stress on HSP70 expression and cell viability in three tumor cell lines.* Academic radiology, 2007. **14**(7): p. 859-870.
94. Dromi, S.A., et al., *Radiofrequency ablation induces antigen-presenting cell infiltration and amplification of weak tumor-induced immunity.* Radiology, 2009. **251**(1): p. 58-66.
95. den Brok, M.H., et al., *In situ tumor ablation creates an antigen source for the generation of antitumor immunity.* Cancer research, 2004. **64**(11): p. 4024-4029.
96. Lu, P., et al., *Increased infiltration of activated tumor-infiltrating lymphocytes after high intensity focused ultrasound ablation of human breast cancer.* Surgery, 2009. **145**(3): p. 286-293.
97. Zhou, Q., et al., *Changes in Circulating Immunosuppressive Cytokine Levels of Cancer Patients After High Intensity Focused Ultrasound Treatment.* Ultrasound in Medicine & Biology, 2008. **34**(1): p. 81-87.
98. Kramer, G., et al., *Response to sublethal heat treatment of prostatic tumor cells and of prostatic tumor infiltrating T-cells.* The Prostate, 2004. **58**(2): p. 109-120.
99. Wu, F., et al., *Expression of tumor antigens and heat-shock protein 70 in breast cancer cells after high-intensity focused ultrasound ablation.* Annals of surgical oncology, 2007. **14**(3): p. 1237-1242.
100. Widenmeyer, M., et al., *Analysis of tumor antigen-specific T cells and antibodies in cancer patients treated with radiofrequency ablation.* International Journal of Cancer, 2011. **128**(11): p. 2653-2662.
101. Wissniowski, T.T., et al., *Activation of tumor-specific T lymphocytes by radio-frequency ablation of the VX2 hepatoma in rabbits.* Cancer research, 2003. **63**(19): p. 6496-6500.
102. Ahmed, M., et al., *Radiofrequency ablation (RFA)-induced systemic tumor growth can be reduced by suppression of resultant heat shock proteins.* International Journal of Hyperthermia, 2018. **34**(7): p. 934-942.

103. Ahmed, M., et al., *Radiofrequency (RF) ablation of normal liver increases tumor growth of remote subcutaneous tumors in an animal tumor model.* Journal of Vascular and Interventional Radiology, 2013. **24**(4): p. S44.
104. Velez, E., et al., *Hepatic thermal ablation: effect of device and heating parameters on local tissue reactions and distant tumor growth.* Radiology, 2016. **281**(3): p. 782-792.
105. Ahmed, M., et al., *Hepatic radiofrequency ablation–induced stimulation of distant tumor growth is suppressed by c-Met inhibition.* Radiology, 2016. **279**(1): p. 103-117.
106. Distelmaier, M., et al., *Midterm safety and efficacy of irreversible electroporation of malignant liver tumors located close to major portal or hepatic veins.* Radiology, 2017. **285**(3): p. 1023-1031.
107. Jenne, J.W., et al. *HIFU Therapy Compared with Other Thermal Ablation Methods in a Perfused Organ Model*. in *AIP Conference Proceedings*. 2007. American Institute of Physics.
108. Cheung, T.T., et al., *High-intensity focused ultrasound as a treatment for colorectal liver metastasis in difficult position.* International journal of colorectal disease, 2012. **27**(7): p. 987-988.
109. Cheung, T.T., K.W. Ma, and W.H. She, *A review on radiofrequency, microwave and high-intensity focused ultrasound ablations for hepatocellular carcinoma with cirrhosis.* Hepatobiliary Surgery and Nutrition, 2021. **10**(2): p. 193.
110. Vlaisavljevich, E., et al., *Visualizing the histotripsy process: Bubble cloud–cancer cell interactions in a tissue-mimicking environment.* Ultrasound in medicine & biology, 2016. **42**(10): p. 2466-2477.
111. Hendricks-Wenger, A., et al., *Immunological Effects of Histotripsy for Cancer Therapy.* Frontiers in Oncology, 2021. **11**: p. 1999.
112. Pahk, K.J., et al., *Boiling Histotripsy-induced Partial Mechanical Ablation Modulates Tumour Microenvironment by Promoting Immunogenic Cell Death of Cancers.* Scientific reports, 2019. **9**(1): p. 1-12.
113. Kratochvill, F., et al., *TNF counterbalances the emergence of M2 tumor macrophages.* Cell reports, 2015. **12**(11): p. 1902-1914.
114. Singh, M.P., et al., *Boiling histotripsy and in-situ CD40 stimulation improve the checkpoint blockade therapy of poorly immunogenic tumors.* Theranostics, 2021. **11**(2): p. 540.
115. Khokhlova, T.D., et al., *Controlled tissue emulsification produced by high intensity focused ultrasound shock waves and millisecond boiling.* The Journal of the Acoustical Society of America, 2011. **130**(5): p. 3498-3510.
116. Eranki, A., et al., *Mechanical fractionation of tissues using microsecond-long HIFU pulses on a clinical MR-HIFU system.* International Journal of Hyperthermia, 2018. **34**(8): p. 1213-1224.
117. Hu, Z., et al., *Investigation of HIFU-induced anti-tumor immunity in a murine tumor model.* Journal of translational medicine, 2007. **5**(1): p. 1-11.
118. Qu, S., et al., *Non-thermal histotripsy tumor ablation promotes abscopal immune responses that enhance cancer immunotherapy.* Journal for immunotherapy of cancer, 2020. **8**(1).

119. Schade, G.R., et al., *Boiling histotripsy ablation of renal cell carcinoma in the eker rat promotes a systemic inflammatory response.* Ultrasound in medicine & biology, 2019. **45**(1): p. 137-147.
120. Schade, G.R., *Evaluation of the Systemic Response to Boiling Histotripsy Treatment for Renal Carcinoma.*
121. Hu, Z., et al., *Release of endogenous danger signals from HIFU-treated tumor cells and their stimulatory effects on APCs.* Biochemical and biophysical research communications, 2005. **335**(1): p. 124-131.
122. Kepp, O., et al., *Oncolysis without viruses—inducing systemic anticancer immune responses with local therapies.* Nature Reviews Clinical Oncology, 2020. **17**(1): p. 49-64.
123. Keisari, Y., *Tumor abolition and antitumor immunostimulation by physico-chemical tumor ablation.* Front Biosci (Landmark Ed), 2017. **22**: p. 310-347.
124. Huang, X., et al., *M-HIFU inhibits tumor growth, suppresses STAT3 activity and enhances tumor specific immunity in a transplant tumor model of prostate cancer.* PloS one, 2012. **7**(7): p. e41632.
125. Tydings, C., et al., *Emerging hyperthermia applications for pediatric oncology.* Advanced Drug Delivery Reviews, 2020.
126. Baronzio, G.F., et al., *Effects of local and whole body hyperthermia on immunity.* Hyperthermia in Cancer Treatment: A Primer, 2006: p. 247-275.
127. Baronzio, G., A. Gramaglia, and G. Fiorentini, *Hyperthermia and immunity. A brief overview. in vivo*, 2006. **20**(6A): p. 689-695.
128. Wu, F., et al., *Activated anti-tumor immunity in cancer patients after high intensity focused ultrasound ablation.* 2004. **30**(9): p. 1217-1222.
129. Sturtevant, R.A., et al., *Thermal Augmentation of Vancomycin Against Staphylococcal Biofilms.* Shock, 2015. **44**(2): p. 121-7.
130. Wardlow, R., et al., *Targeted antibiotic delivery using low temperature-sensitive liposomes and magnetic resonance-guided high-intensity focused ultrasound hyperthermia.* International Journal of Hyperthermia, 2016. **32**(3): p. 254-264.
131. VanOsdol, J., et al., *Sequential HIFU heating and nanobubble encapsulation provide efficient drug penetration from stealth and temperature sensitive liposomes in colon cancer.* Journal of controlled release : official journal of the Controlled Release Society, 2017. **247**: p. 55-63.
132. Partanen, A., et al., *Mild hyperthermia with magnetic resonance-guided high-intensity focused ultrasound for applications in drug delivery.* International journal of hyperthermia, 2012. **28**(4): p. 320-336.
133. Singh, M.P., et al., *In-situ vaccination using focused ultrasound heating and anti-CD-40 agonistic antibody enhances T-cell mediated local and abscopal effects in murine melanoma.* International Journal of Hyperthermia, 2019. **36**(sup1): p. 64-73.
134. Sethuraman, S.N., et al., *Novel calreticulin-nanoparticle in combination with focused ultrasound induces immunogenic cell death in melanoma to enhance antitumor immunity.* Theranostics, 2020. **10**(8): p. 3397.
135. Kim, M.H., *Nanoparticle-Based Therapies for Wound Biofilm Infection: Opportunities and Challenges.* IEEE Trans Nanobioscience, 2016. **15**(3): p. 294-304.

136. Nevozhay, D., et al., *Current status of research on conjugates and related drug delivery systems in the treatment of cancer and other diseases.* Postepy higieny i medycyny doswiadczalnej (Online), 2007. **61**: p. 350-360.
137. Wilczewska, A.Z., et al., *Nanoparticles as drug delivery systems.* Pharmacological reports, 2012. **64**(5): p. 1020-1037.
138. Couture, O., et al., *Review of ultrasound mediated drug delivery for cancer treatment: updates from pre-clinical studies.* Transl Cancer Res, 2014. **3**(5): p. 494-511.
139. May, J.P. and S.-D. Li, *Hyperthermia-induced drug targeting.* Expert opinion on drug delivery, 2013. **10**(4): p. 511-527.
140. Frazier, N., et al., *High intensity focused ultrasound hyperthermia for enhanced macromolecular delivery.* Journal of Controlled Release, 2016. **241**: p. 186-193.
141. Han, H., et al., *Effect of high intensity focused ultrasound (HIFU) in conjunction with a nanomedicines-microbubble complex for enhanced drug delivery.* Journal of Controlled Release, 2017. **266**: p. 75-86.
142. Batchelor, D.V., et al., *Nested nanobubbles for ultrasound-triggered drug release.* ACS applied materials & interfaces, 2020. **12**(26): p. 29085-29093.
143. Yao, Y., et al., *Comparison of the synergistic effect of lipid nanobubbles and SonoVue microbubbles for high intensity focused ultrasound thermal ablation of tumors.* PeerJ, 2016. **4**: p. e1716.
144. Zangabad, P.S., et al., *Stimulus-responsive liposomes as smart nanoplatforms for drug delivery applications.* Nanotechnology reviews, 2018. **7**(1): p. 95-122.
145. Haemmerich, D. and A. Motamarry, *Thermosensitive liposomes for image-guided drug delivery.* Advances in cancer research, 2018. **139**: p. 121-146.
146. Yildirim, A., N.T. Blum, and A.P. Goodwin, *Colloids, nanoparticles, and materials for imaging, delivery, ablation, and theranostics by focused ultrasound (FUS).* Theranostics, 2019. **9**(9): p. 2572.
147. Zeng, Z., J.-B. Liu, and C.-Z. Peng, *Phase-changeable Nanoparticle-mediated Energy Conversion Promotes Highly Efficient High-Intensity Focused Ultrasound Ablation.* Current Medicinal Chemistry, 2021.
148. Zhao, Y.-Z., et al., *Potential and problems in ultrasound-responsive drug delivery systems.* International journal of nanomedicine, 2013. **8**: p. 1621.
149. Kasimanickam, R.K., et al., *Prevention and treatment of biofilms by hybrid- and nanotechnologies.* Int J Nanomedicine, 2013. **8**: p. 2809-19.
150. Kumar, A., et al., *Development and characterization of liposomal drug delivery system for nimesulide.* Int J Pharm Pharm Sci, 2010. **2**(4): p. 87-89.
151. Bangham, A., *Liposomes: the Babraham connection.* Chemistry and physics of lipids, 1993. **64**(1-3): p. 275-285.
152. Daraee, H., et al., *Application of liposomes in medicine and drug delivery.* Artificial cells, nanomedicine, and biotechnology, 2016. **44**(1): p. 381-391.
153. Mishra, D.K., R. Shandilya, and P.K. Mishra, *Lipid based nanocarriers: a translational perspective.* Nanomedicine: Nanotechnology, Biology and Medicine, 2018. **14**(7): p. 2023-2050.
154. Bulbake, U., et al., *Liposomal formulations in clinical use: an updated review.* Pharmaceutics, 2017. **9**(2): p. 12.

155. Antimisiaris, S., et al., *Overcoming barriers by local drug delivery with liposomes.* Advanced Drug Delivery Reviews, 2021.
156. Yatvin, M.B., et al., *Design of liposomes for enhanced local release of drugs by hyperthermia.* Science, 1978. **202**(4374): p. 1290-1293.
157. Kneidl, B., et al., *Thermosensitive liposomal drug delivery systems: state of the art review.* International journal of nanomedicine, 2014. **9**: p. 4387.
158. Grüll, H. and S. Langereis, *Hyperthermia-triggered drug delivery from temperature-sensitive liposomes using MRI-guided high intensity focused ultrasound.* Journal of Controlled Release, 2012. **161**(2): p. 317-327.
159. Demel, R.A. and B. De Kruyff, *The function of sterols in membranes.* Biochimica et Biophysica Acta (BBA)-Reviews on Biomembranes, 1976. **457**(2): p. 109-132.
160. Mabrey, S. and J.M. Sturtevant, *Investigation of phase transitions of lipids and lipid mixtures by sensitivity differential scanning calorimetry.* Proceedings of the National Academy of Sciences, 1976. **73**(11): p. 3862-3866.
161. Bassett, J.B., R.U. Anderson, and J.R. Tacker, *Use of temperature-sensitive liposomes in the selective delivery of methotrexate and cis-platinum analogues to murine bladder tumor.* The Journal of urology, 1986. **135**(3): p. 612-615.
162. Maruyama, K., et al., *Enhanced delivery of doxorubicin to tumor by long-circulating thermosensitive liposomes and local hyperthermia.* Biochimica et Biophysica Acta (BBA)-Biomembranes, 1993. **1149**(2): p. 209-216.
163. Gaber, M.H., et al., *Thermosensitive sterically stabilized liposomes: formulation and in vitro studies on mechanism of doxorubicin release by bovine serum and human plasma.* Pharmaceutical research, 1995. **12**(10): p. 1407-1416.
164. Hossann, M., et al., *In vitro stability and content release properties of phosphatidylglyceroglycerol containing thermosensitive liposomes.* Biochimica et Biophysica Acta (BBA)-Biomembranes, 2007. **1768**(10): p. 2491-2499.
165. Ickenstein, L.M., et al., *Disc formation in cholesterol-free liposomes during phase transition.* Biochimica et Biophysica Acta (BBA)-Biomembranes, 2003. **1614**(2): p. 135-138.
166. Papahadjopoulos, D. and A. Gabizon, *Liposomes designed to avoid the reticuloendothelial system.* Progress in clinical and biological research, 1990. **343**: p. 85-93.
167. Allen, T., et al., *Liposomes containing synthetic lipid derivatives of poly (ethylene glycol) show prolonged circulation half-lives in vivo.* Biochimica et Biophysica Acta (BBA)-Biomembranes, 1991. **1066**(1): p. 29-36.
168. Needham, D., T. McIntosh, and D. Lasic, *Repulsive interactions and mechanical stability of polymer-grafted lipid membranes.* Biochimica et Biophysica Acta (BBA)-Biomembranes, 1992. **1108**(1): p. 40-48.
169. Mills, J.K. and D. Needham, *Lysolipid incorporation in dipalmitoylphosphatidylcholine bilayer membranes enhances the ion permeability and drug release rates at the membrane phase transition.* Biochimica et Biophysica Acta (BBA)-Biomembranes, 2005. **1716**(2): p. 77-96.
170. Landon, C.D., et al., *Nanoscale drug delivery and hyperthermia: the materials design and preclinical and clinical testing of low temperature-sensitive liposomes used in combination with mild hyperthermia in the treatment of local cancer.* The open nanomedicine journal, 2011. **3**: p. 38.

171. Limmer, S., et al., *Gemcitabine treatment of rat soft tissue sarcoma with phosphatidyldiglycerol-based thermosensitive liposomes.* Pharmaceutical research, 2014. **31**(9): p. 2276-2286.
172. Ranjan, A., et al., *Antibacterial efficacy of core-shell nanostructures encapsulating gentamicin against an in vivo intracellular Salmonella model.* International journal of nanomedicine, 2009. **4**: p. 289-297.
173. Hossann, M., et al., *Size of thermosensitive liposomes influences content release.* Journal of controlled release, 2010. **147**(3): p. 436-443.
174. Hossann, M., et al., *Proteins and cholesterol lipid vesicles are mediators of drug release from thermosensitive liposomes.* Journal of controlled release, 2012. **162**(2): p. 400-406.
175. Patra, J.K., et al., *Nano based drug delivery systems: recent developments and future prospects.* Journal of nanobiotechnology, 2018. **16**(1): p. 1-33.
176. Kim, E.-M. and H.-J. Jeong, *Liposomes: Biomedical Applications.* Chonnam medical journal, 2021. **57**(1): p. 27.
177. Crommelin, D.J., P. van Hoogevest, and G. Storm, *The role of liposomes in clinical nanomedicine development. What now? Now what?* Journal of Controlled Release, 2020. **318**: p. 256-263.
178. Needham, D. and M.W. Dewhirst, *The development and testing of a new temperature-sensitive drug delivery system for the treatment of solid tumors.* Advanced drug delivery reviews, 2001. **53**(3): p. 285-305.
179. Banno, B., et al., *The functional roles of poly (ethylene glycol)-lipid and lysolipid in the drug retention and release from lysolipid-containing thermosensitive liposomes in vitro and in vivo.* Journal of pharmaceutical sciences, 2010. **99**(5): p. 2295-2308.
180. Ektate, K.P., *Development of Targeted Liposomal Formulation Approaches for Enhanced Colorectal Cancer Therapy*. 2019, Oklahoma State University: Ann Arbor. p. 137.
181. Rukavina, Z. and Ž. Vanić, *Current trends in development of liposomes for targeting bacterial biofilms.* Pharmaceutics, 2016. **8**(2): p. 18.
182. Gao, W., et al., *Nanoparticle-based local antimicrobial drug delivery.* Adv Drug Deliv Rev, 2018. **127**: p. 46-57.
183. Izadifar, Z., et al., *An introduction to high intensity focused ultrasound: systematic review on principles, devices, and clinical applications.* Journal of clinical medicine, 2020. **9**(2): p. 460.
184. She, W., et al., *Clinical applications of high-intensity focused ultrasound.* Hong Kong Medical Journal, 2016.
185. McClure, A., *Using high-intensity focused ultrasound as a means to provide targeted drug delivery: a literature review.* Journal of Diagnostic Medical Sonography, 2016. **32**(6): p. 343-350.
186. Rahim, A.A., et al., *Spatial and acoustic pressure dependence of microbubble-mediated gene delivery targeted using focused ultrasound.* The Journal of Gene Medicine: A cross-disciplinary journal for research on the science of gene transfer and its clinical applications, 2006. **8**(11): p. 1347-1357.
187. Hynynen, K., et al., *Noninvasive MR imaging–guided focal opening of the blood-brain barrier in rabbits.* Radiology, 2001. **220**(3): p. 640-646.

188. Pajek, D., et al., *High-intensity focused ultrasound sonothrombolysis: the use of perfluorocarbon droplets to achieve clot lysis at reduced acoustic power.* Ultrasound in medicine & biology, 2014. **40**(9): p. 2151-2161.
189. Shehata, I.A., et al., *High-intensity focused ultrasound for potential treatment of polycystic ovary syndrome: toward a noninvasive surgery.* Fertility and sterility, 2014. **101**(2): p. 545-551. e2.
190. Shehata, I.A., et al., *Feasibility of targeting atherosclerotic plaques by high-intensity–focused ultrasound: An in vivo study.* Journal of Vascular and Interventional Radiology, 2013. **24**(12): p. 1880-1887. e2.
191. Ghanouni, P., et al., *Magnetic resonance-guided focused ultrasound treatment of extra-abdominal desmoid tumors: a retrospective multicenter study.* European radiology, 2017. **27**(2): p. 732-740.
192. Sharma, K.V., et al., *Comparison of noninvasive high-intensity focused ultrasound with radiofrequency ablation of osteoid osteoma.* The Journal of pediatrics, 2017. **190**: p. 222-228. e1.
193. Fan, T.M. and K.A. Selting, *Exploring the Potential Utility of Pet Dogs With Cancer for Studying Radiation-Induced Immunogenic Cell Death Strategies.* Front Oncol, 2018. **8**: p. 680.
194. Khanna, C., et al., *Guiding the optimal translation of new cancer treatments from canine to human cancer patients.* Clinical cancer research, 2009. **15**(18): p. 5671-5677.
195. Thamm, D.H., *Canine cancer: strategies in experimental therapeutics.* Frontiers in oncology, 2019. **9**: p. 1257.
196. Ryu, M.O., et al., *Treatment of solid tumors in dogs using veterinary high-intensity focused ultrasound: A retrospective clinical study.* The Veterinary Journal, 2018. **234**: p. 126-129.
197. Seward, M.C., et al., *Feasibility of targeting canine soft tissue sarcoma with MR-guided high-intensity focused ultrasound.* International Journal of Hyperthermia, 2018. **35**(1): p. 205-215.

CHAPTER II

FOCUSED ULTRASOUND ABLATIONS OF A LARGE CANINE ORAL TUMOR ACHIEVES EFFICIENT TUMOR REMISSION: A CASE REPORT

This chapter is based on:

Ashish Ranjan*, Deepan Kishore*, **Harshini Ashar***, Tina Neel, Akansha Singh & Sunil More (2021) Focused ultrasound ablation of a large canine oral tumor achieves efficient tumor remission: a case report, *International Journal of Hyperthermia*, 38:1, 552-560

* These authors contributed equally to this work.

Abstract

Purpose: Oral cancers are one of the commonly diagnosed tumors worldwide in human and veterinary patients. Most oral cancers are surgically resected; however, obtaining an adequate margin of safety in patients without compromising their quality of life is often challenging. Herein, we investigated the ability of non-invasive focused ultrasound (FUS) to thermally ablate a biopsy confirmed canine oral cancer.

Materials and Methods: A male canine patient with a large neurilemmoma (schwannoma) mass on the left maxilla, with evidence of thinning and loss of alveolar bone and pressure

necrosis, was treated with FUS ablation instead of the traditional maxillectomy ablations were performed in three sessions over three weeks. Tumor remission was determined with computed tomography and histopathological examination of the treated site. Additionally, the anti-tumor immune effects of FUS were assessed by flow cytometry analysis of blood and tumor samples.

Results: Complete tumor remission was noted at the treated site. Treatment related adverse events were primarily thermal burns of the buccal mucosa, which were managed with periodic hyperbaric oxygen therapy and surgical coverage of the underlying exposed bones with gingival flaps. Enhanced proliferation of adaptive immunity cells (e.g., T-cells) was observed in tumor and blood samples.

Conclusion: Our limited investigation in a canine oral cancer patient suggests that FUS may avoid the need for large-scale resection of bony tissues, thus potentially improving quality of life.

1. Introduction

Cancers of the oral cavity have a substantial incidence worldwide, and 3% of cancers diagnosed in the United States are oral cancers [1]. Oral cancers can occur in various regions of the mouth, including the buccal mucosa, tongue, lips, palate, gums, and floor [2]. Depending on the severity and extent of progression, they are treated with a combination of surgery, chemotherapy, and radiotherapy [3,4]. However, oral cancers recur in 18–76% of patients after standard treatment [5]. For example, primary squamous cell carcinomas have high local recurrence rates in patients [6], and the pattern of local

invasion and lymph node metastasis significantly affects survival rates. In fact, 50% of patients receiving local resection with involved and close margins die within 5 years [7]. In canine and feline species, benign and malignant oral tumors are also common [8] and have an incidence rate similar to that in humans. For example, 6–7% of all cancers are of oral origin in dogs [9]. These oral cancers in veterinary patients mainly include melanomas, squamous cell carcinomas, and fibrosarcomas [10]. Herein, we evaluated the ability of focused ultrasound (FUS) ablation to treat a relatively uncommon oral schwannoma in a canine patient. Schwannomas are peripheral nerve sheath tumors originating from Schwann cells in dogs and cats. Although they are typically benign, malignant cases have been reported [11,12]. Malignant schwannoma cells demonstrate immunoreactivity to glial fibrillary acidic protein (GFAP) [13], laminin, and S100 [14,15], and are devoid of melanoma associated antigens [12]. In humans, as in small animals, schwannomas of neurofibromatosis type I origin in the tongue, palate, floor of the mouth, buccal mucosa, lips, and jaws have been reported [16]. Therefore, we believe that our case report is important because it provides insights into the feasibility of leveraging FUS for the therapeutic management of aggressive oral cancers. FUS is an emerging noninvasive and non-ionizing clinical modality that uses sonic energy under image guidance to treat target tissue with high spatial precision at various locations in the body. We and others have shown that FUS improves the delivery of both genes and drugs and enhances the therapeutic clearance of murine tumors [17–20]. A key benefit of FUS is its unique ability to generate both thermal and mechanical effects in tissues without the use of any photoreactive or magnetic agents. FUS parameters are tunable and can elicit ablative, boiling, mild heating, and low intensity mechanical stress in tumors [18,21,22].

In particular, ablative FUS generates temperatures >60^0C at the focus, thus inducing protein denaturation, coagulative necrosis, tumor cell killing, and antitumor immunity [23]. FUS exposure is generally performed under noninvasive magnetic resonance or ultrasound imaging and is thus generally considered minimally toxic. Although large randomized clinical trials emphasizing the assessment of normal tissue toxicity of FUS are rare, some breast and liver cancer trials have reported mild to moderate skin burns in some patients [24,25]. This outcome is probably due to damage to tumor adjacent healthy tissues in the absence of reliable real-time thermometry [26]. Therefore, methods to decrease the adverse effects are needed to overcome this limitation of FUS. One approach can be through the application of hyperbaric oxygen therapy (HBOT) following FUS in patients. HBOT allows patients to inspire 100% oxygen for a defined period to increase the oxygen supply, angiogenesis, and fibroblast proliferation in wounds, thereby decreasing tissue edema and infections [27–29]. HBOT has been found to enhance the healing of thermal burns and diabetic foot ulcers [29–31], radiation induced ulcerations of skin [32], and osteoradionecrosis of the jaw [33]. It can also reduce xerostomia in patients with oral or oropharyngeal carcinoma by improving the saliva quality post radiotherapy [34]. Based on this scientific premise, we reasoned that combining HBOT and FUS will similarly reduce the thermal burns and bone necrosis in oral regions and provide a future motivation for the investigation of this combined approach in large scale trials for ulceration reduction.

2. Methods

2.1 Canine patient: case history

Before the treatment, we obtained owner consent to the terms of the study, including a follow-up postmortem analysis and release from institutional/personal (researcher) liability. All animal related procedures were approved by the Oklahoma State University Animal Care and Use Committee. The canine patient was a 3 year and 8-month-old pit bull mix with an identifiable tumor of 4.3 3.8 3.8 cm (width length height) on the left maxilla. The initial examination of the patient revealed hematological and biochemical parameters in normal ranges. A pretreatment biopsy revealed an un-encapsulated multinodular mass with low cellularity, composed of oval to spindle-shaped neoplastic cells arranged in whorls or bundles supported by a loose fibrovascular stroma (Figure 1). The neoplastic cells had variably distinct cell borders with moderate amounts of eosinophilic fibrillar cytoplasm and single nuclei with finely stippled chromatin and indistinct nucleoli. Anisocytosis and anisokaryosis were mild. The neoplastic cells showed diffuse, moderate to strong cytoplasmic immunoreactivity toward GFAP, laminin, and S100 proteins—findings indicative of an aggressive neurilemmoma (schwannoma) tumor.

2.2 FUS setup and treatments

We performed the FUS treatment under ultrasound guidance with an Alpinion dry-type platform with a 1 MHz transducer capable of treating small animals (Figure 2(A)) [17,35–38]. In the dry-type system, the transducer sits inside an acoustically transparent membrane filled with degassed water for easy placement over tumor areas (Figure 2(B)).

The system allowed for mechanical translation of the transducer, with rotation 180^0 around the Z axis and $0–90^0$ around the X axis. The transducer moved in 3D space with 3 degrees of freedom to adjust to the shape and size of the treated region and allow the sonication to conform to the tumor, avoiding underlying bones as needed. Figure 2(C) shows the ultrasound image of the oral tumor. Sonication was targeted to the center of the oral tumor in the in the anesthetized patient, by using VIFU planning software under ultrasound guidance to define the target boundary and slice distance in the x, y, and z directions for automatic rastering of the transducer. The FUS parameters used were in the ablation range: 50% duty cycle, 90W acoustic power, and ~30 s to 1 min per focal point. Three FUS ablative treatments, each covering ~50% of the tumor core region, were performed over 1 month. Briefly, computed tomography (CT) scans were used to co-register with real-time ultrasound imaging at the time of FUS to improve ultrasound imaging, and the planning and monitoring of ongoing treatment. Vital signs were monitored with a fiber optic cuff placed around a shaved front paw, and degassed gel was used to provide acoustic coupling. For ultrasound exposure, the tumor was aligned at a fixed focal depth to cover a voxel size of 1 X 1 X 10 mm. VIFU-2000 software was used to define the target boundary and slice distance in the x, y, and z directions for automatic rastering of the transducer during treatment.

2.3 Histopathological and radiological examination

Biopsies were collected before treatment and then after each treatment. Briefly, the tumor region was scrubbed with 2% chlorhexidine solution, and a 6mm Baker's punch was used to obtain a sample (4–6mm in size) from the treated region. The defects in the biopsied regions were closed with one or two simple interrupted sutures. For histopathology,

formalin-fixed tissue sections were trimmed and processed, and hematoxylin and eosin (H&E) stained slides were analyzed by a veterinary pathologist at the Oklahoma Animal Disease Diagnostic Laboratory. Immunohistochemistry evaluations of GFAP (Dako, Denmark), S100 (Dako, Denmark), laminin (Cambridge, MA), and Cluster of differentiation 3 (CD3) (Leica, Buffalo Grove, IL) were performed with commercially available laboratory methods. Additionally, CT was performed before treatment, on days 30 and 90 after FUS treatments by a board-certified veterinary radiologist (Vimago, GT 30 Epica International).

2.4 HBOT treatment and post-treatment surgical management

HBOT exposure was performed with a 2800 Sechrist Monoplace Hyperbaric Chamber (Sechrist, USA) pressurized to 1.5 ATA. A total of 16 HBOT sessions were performed after the first FUS treatment between day 8 and day 28 (three times/week, two sessions/day). Each session lasted 45 min. Briefly, the patient was placed in the monoplace hyperbaric oxygen chamber and exposed daily (Figure 5). After the completion of FUS ablation and healing of thermal burns, the exposed bone tissues were gently debrided once on day 30, and a synthetic dental bone graft (Synergy) and clindamycin (clindoral 2% gel, VEDCO) were placed to encourage bone healing. Vertical diverging incisions were made in the gingiva around the alveolar bone, and a periosteal elevator was used to elevate the HBOT healed gingiva and cover the bony regions. The gingival flap was closed with a 3-0 suture with no tension in a simple interrupted pattern. The patient was administered carprofen (2.2 mg/kg BID for 7 days) for pain control, and follow-up evaluations were performed to assess patient eating and drinking, as well as flap healing.

2.5 Flow cytometry analysis of tumors and blood

Blood samples were collected in BD Vacutainer EDTA tubes, and biopsy samples were collected into RPMI supplemented with 2% FBS. Samples were transported and stored on ice or at 4^0C until further analysis. Single-cell suspensions were obtained through mechanical disruption of the tumor biopsy tissues followed by enzymatic digestion with 200 U/ml collagenase IV (Life Technologies, NY, USA). The lysates were filtered through a 70 mm cell strainer (Corning Inc, Corning, NY). Blood samples collected in EDTA tubes were incubated with 1X RBC lysis buffer (multispecies, Invitrogen) for 10–15 min before antibody staining. The following fluorochrome- conjugated anti-dog antibodies were used to stain cells for 30 min in the dark on ice: anti-CD3+, anti-CD4+, anti-CD-8+ (dog T lymphocyte cocktail, cat. 558699, BD Pharmingen), and APC labeled anti-CD45. (YKIX716.13, cat. MCA1042, Bio-Rad). For detecting interferon IFN-Y and Foxp3 positive T regulatory (Treg) cells, the cells were washed after surface marker staining, fixed, permeabilized with a transcription factor buffer set (BD Biosciences, San Jose, CA), and incubated with Alexa Fluor 700 labeled anti- IFN-Y (CC302, Novus biologicals) and e-fluor 450 labeled anti- Foxp3 (FJK-16s, cat. 5016374, Fisher) for 50 min in the dark on ice. Stained cells were sorted with a FACS Aria II (BD Biosciences) instrument within 24–48 h. Compensation was performed with single-stained Ultra Comp eBeads (Invitrogen). Datasets were analyzed in FlowJo software v.10.2 (Treestar Inc, Ashland, ORUSA).

3. Results

3.1 FUS induced efficient remission of the treated tumor, and HBOT enhanced wound healing

The efficacy of FUS at the indicated time points was evaluated with longest tumor diameter (mm) measurements and recording of new lesions according to Veterinary Cooperative Oncology Group (VCOG) response evaluation criteria in solid tumors (RECIST) v1.1 guidelines [39]. Complete response involved disappearance of all target lesions, partial response involved a>30% decrease in the sum of tumor diameters, and stable disease involved a<30% decrease in tumors or >20% increase in the sum of the diameters of target lesions after FUS treatments. Significant tumor regression after the first FUS exposure, as compared with the pretreatment value, was observed on day 8 by visual examination, and complete remission of the treated tumor was achieved after the 3rd FUS treatment (Figure 3(B, C)). The treated regions showed a calcified mass in the tumor, which probably caused thermal burns in the adjoining buccal mucosa, owing to high acoustic absorption (Figure 4(A)). The calcified mass was debrided on day 10 before the 2nd FUS exposure on day 14. After the completion of FUS treatments, the patient was followed for an additional 3 months. No new lesions were observed during the entire monitoring period (Figures 3 and 4). These findings were also verified by CT examination, which showed an absence of soft tissue mass in the treated regions from day 30 onward (Figure 4(B)). To aid in the healing of thermal burns, we administered HBOT from day 8 onward (Figure 5(A)). Compared with the pretreatment burn levels (42 X 22 mm) of the buccal mucosa (Figure 5(B)), the extent of ulceration decreased progressively by day 20 (24 X 10.4 mm; Figure 5(C)) and resolved completely by day 25. After the

thermal burns were replaced with healthy granulation tissues in the treated region, HBOT was stopped on day 28, and the exposed bones underlying the tumor were gently debrided on day 30 (Figure 5(D)); this region was then covered with a gingival flap (Figure 5(E)). At 2–3 days post-surgery, normal eating, drinking, and other behavioral responses were reported in the treated patient.

3.2 Histopathology showed an absence of viable tumor cells in the treated regions

H&E staining of post-treatment biopsy samples on day 10 and day 16 showed minimal areas of necrosis, and tumor cells were surrounded by inflammatory cells. On day 26, coagulative necrosis was observed within the mass, as characterized by hypereosinophilic neoplastic cells lacking nuclear details (Figure 6(A–C)). Additionally, moderate numbers of inflammatory cells including CD3+ T-cells surrounding tumor cells were observed (Figures 6(E–H) and 7(A)). In general, the tumor periphery showed large numbers of degenerate to non-degenerate neutrophils, low numbers of lymphocytes, and macrophages admixed with a sero-cellular crust. Evaluation of the treated region on day 102 showed an absence of tumor cells, and the submucosa mostly consisted of collagen bundles, a few lymphocytes, and melano-macrophages (Figure 6(D, H)).

3.3 FUS ablation enhanced antitumor immunity

Local and systemic evaluation of the immune responses of harvested tumor biopsy and blood samples after FUS ablation revealed an overall increase in CD3+ T cells from days 10 to 23, relative to the pretreatment levels (Figure 7(A,B)). Additional phenotypic characterization suggested an enhancement in CD3. CD8. and CD3. CD4. cells T cells with high IFN-Y expression, thus suggesting an activated cytotoxic phenotype.

Interestingly, a concurrent decrease in the population of Foxp3+ CD4+ Tregs, relative to the pretreatment paired control levels, was observed, particularly in the blood samples, and it became undetectable by day 102 (Figure 7(C)).

4. Discussion

Oral cancers are primarily treated surgically [3]. However, in advanced cases, resection of tumors is combined with external beam radiotherapy and chemotherapy [40]. The objective of this study was to investigate whether noninvasive FUS ablation might induce remission of a spontaneous oral tumor.

To investigate this possibility, we recruited a canine patient with schwannoma. Schwannoma or neurilemmoma is a rare tumor that can be found in areas such as the lips, jaws, tongue, and mucosa [41,42]. It is treated with transoral excision; however, excision may be challenging to perform in larger tumors requiring sufficient margins [43]. Like human schwannoma, canine schwannoma is a typically benign and solitary lesion; however, malignant cases have also been reported [15]. After enrollment, we performed FUS ablation of the tumor in three sessions over 3 weeks. The premise of this design stemmed from a study in a uterine myoma patient where FUS induced TLS and acute kidney injury [44]. Thus, we reasoned that a single ablative session might similarly induce tumor lysis syndrome (TLS), which occurs when tumor cells rapidly release their contents into the systemic circulation, thereby resulting in hyperuricemia, hyperkalemia, hyperphosphatemia, and hypocalcemia. These metabolic disturbances can cause cardiac toxicity and neurophysiological abnormalities [45,46]. Our longitudinal assessment

indicated that the patient tolerated the treatment and showed a normal appetite and mild pain at the treated region. Additionally, renal function examination did not indicate any signs of acute toxicity. Studies are currently underway in our laboratory to verify whether TLS is indeed a sequalae of FUS in a larger cohort of patients.

We performed the ablative treatments under ultrasound guidance (Figure 2). Unlike MR-guided FUS, which provides absolute temperature mapping by proton resonance frequency shifts, ultrasound is limited in providing real-time thermometry of the targeted region [47]. To overcome this barrier, we relied on temperature monitoring with fiber optic temperature sensors [17]. At the selected FUS parameters, we found that the temperatures were in ablative ranges. Progressive tumor remission was observed with each treatment, and the tumor became undetectable after approximately 4 weeks of treatment (Figure 3). Mechanistically, the FUS treatment induced coagulative necrosis and increased the populations of inflammatory cells in the treated tumor. Prior research has shown that FUS ablation enhances access to the intracellular tumor-associated antigens and the presentation to immune system components, thus improving the immunotherapeutic response [17,23,48,49]. Our findings were in line with those observations. For example, flow cytometry analysis of tumor and blood samples collected during the course of treatment suggested an increase in the populations CD4. and CD8. cells with IFN-Y production in tumor and blood samples, as compared with the pretreatment levels (Figure 7) [18,50,51]. We hypothesized that partial ablation of the tumor core generated a heat gradient and moderate hyperthermia in the tumor periphery, thereby releasing heat-shock proteins and tumor antigens and improving antigen presentation. The enhanced T-cell function was also associated with a decrease in the

local and systemic populations of Tregs, thereby indicating an activated antitumor immune system [52]. Longitudinal assessment of prophylaxis against local recurrence in more aggressive tumor types (e.g., squamous cell carcinoma) should be investigated in future studies to understand these mechanisms in greater detail.

Although our treatments were highly conformal, evaluation of the tumor after the first FUS treatment revealed the presence of a calcified mass in the tumor core (Figure 4). Calcified tissues (e.g., bone) have high acoustic absorption, exceeding the threshold of necrosis by >4-fold. Additionally, the reflected waves from such regions back to the transducer can induce fluctuations of $\pm 15^0$C, thus potentially damaging nearby healthy tissues [53]. On this basis, we believe that the unanticipated normal tissue toxicity in the buccal mucosa was probably induced by this process. To enhance healing of thermal wounds, close to the tumor, we used HBOT because it is known to decrease tissue hypoxia and infection and enhance neovascularization [54]. Visual examination of the oral regions suggested improved healing rates in the presence of HBOT (Figure 5). The ability to approve or disapprove HBOT in burn settings remains questionable, because of the high variability in individual outcomes [55]. However, enhanced microcirculation was found to aid the regeneration and healing of oral mucosal surgical flaps in HBOT group (2.5 bar O2/90 min) relative to the control group on days 7, 9, and 11 in a rabbit model via enhanced neo-angiogenesis in sub-ischemic region [56]. HBOT (28 sessions, 240 kPa for 90 min; n=14 patients) also improved oxygenation and vascularization of irradiated facial skin and gingival mucosa at 3- and 6-months post treatment compared to HBOT minus irradiated patients (n=8 patients), and transmucosal oxygen tension from 50 to ~80% in human oral mucosa of 10 patients [57]. These suggest that adding HBOT may

plausibly enhance vascularization in mucosal regions to hypothetically improve the healing of thermal burns. Because the recovery rates were not compared with controls without HBOT, a large veterinary clinical trial will be needed in the future to verify our findings. It may be noted that HBOT alone does not directly induce tumor cell death [58]. However, in mouse models, HBOT has been shown to decrease inflammation by downregulating Toll-like receptor expression, cytokine production, and NF-jB activation [59,60]. A mouse glioma study has also shown that HBOT decreases the populations of CD3+, CD3+/CD8+, CD3+/CD4+, and Treg cells via modulating reactive oxygen species signaling in thymus and tumor cells [61]. Our immunological analysis showed a trend toward enhanced CD8. and CD4. populations after FUS and HBOT exposure in the tumor and blood. In contrast, the proliferation of Tregs was markedly diminished in the blood 2–3 weeks post treatment. On the basis of our findings, we propose that local FUS increased the killing of tumor cells, and its combination with HBOT modulated the tumor microenvironment and hypoxia mediated stress pathways [62], thereby collectively enhancing the activated T-cell populations in the tumor and blood.

This case report has some limitations. The tumor was easily accessible for FUS therapy in the schwannoma patient. However, the ability of FUS to acoustically couple with tumors located in the soft palate region is likely to pose a challenge. Also, additional investigation is needed to determine whether HBOT exposure modifies tumor physiology. In summary, our data suggest that FUS ablation can induce regression of a large schwannoma. Local FUS also generated an inflamed tumor microenvironment that may possibly aid in antitumor immunity. Additional studies in malignant models are needed to shed more light on the therapeutic mechanisms.

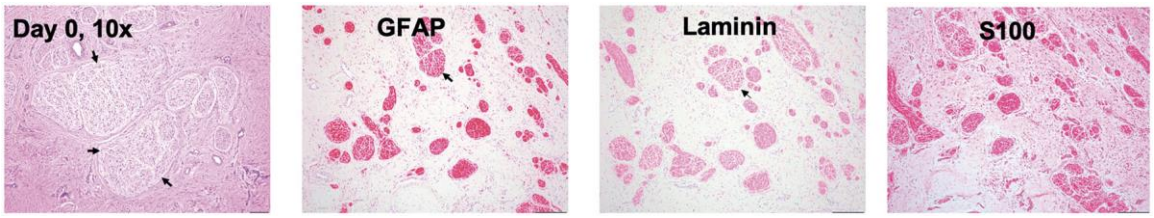

Figure 1. Schwannoma cells forming multinodular masses (arrow) supported by a loose fibrovascular stroma (H&E stain, 100X magnification). The neoplastic cells showed strong cytoplasmic immunoreactivity for GFAP, laminin, and S100 (immunostaining, 100X magnification).

Figure 2. FUS device and treatment setup. (A, B) Dry type FUS transducer for tumor treatment in an intubated dog lying on the right side. (C) FUS planning and targeting.

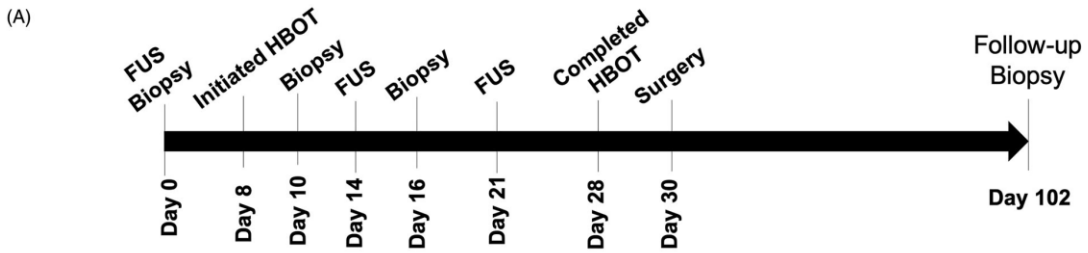

(B)

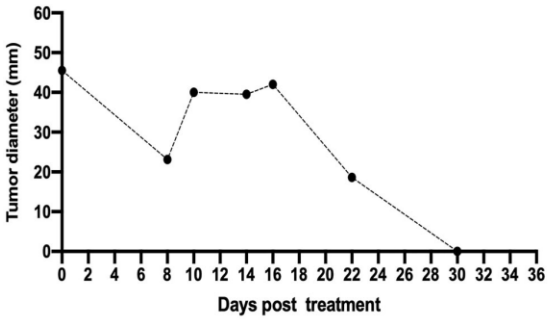

(C)

Time-points	Tumor	New lesions	Overall response
1-week follow-up after 1st treatment	PR	No	PR
2-weeks follow-up after 1st treatment	SD	No	SD
1-week follow-up after 2nd treatment	PR	No	PR
1-week follow-up after 3rd treatment	CR	No	CR
3 months follow-up after 3rd treatment	CR	No	CR

Figure 3. Treatment timeline and response rates. (A) Three partial FUS treatments (~50% of tumor volume/session) were performed over 3 weeks. Tumor biopsies were collected before and after FUS treatment. HBOT was administered between day 10 to day 28. (B) Caliper measurements of the longest diameter of treated tumor after various FUS sessions. Complete local tumor remission was observed by the end of the 4th week; (C) Therapeutic efficacy evaluated with the response evaluation criteria in solid tumors (RECIST v1.1) suggested complete response at the treated site without emergence of new lesions at 3 months post-treatment (CR: complete response; PR: partial response; SD: stable disease).

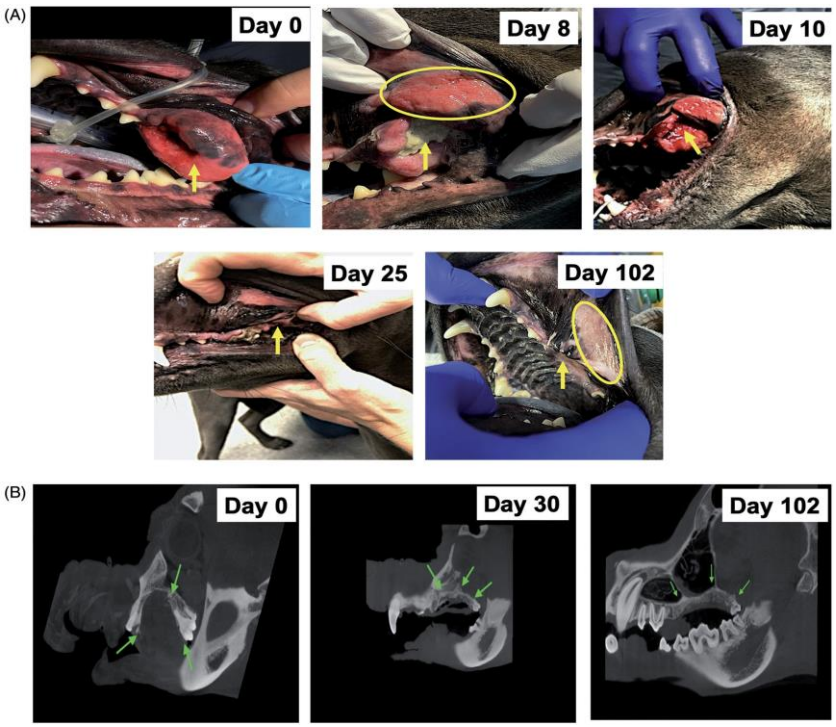

Figure 4. Representative images of the treated tumor regions over 102 days. (A) Complete remission of the treated tumor (arrow) was observed as time progressed. Briefly, necrosis and a calcified mass in the treated tumor were observed 1 week after the first FUS treatment and were associated with thermal burns (ellipse) of the regional buccal mucosa, probably because of high acoustic absorption and heating of the calcified mass during FUS treatment. The calcified mass was debrided on day 10. Additional FUS treatments were administered on days 14 and 21 to induce complete tumor remission. Longitudinal monitoring of the treated regions from days 25 to 102 showed an absence of the tumor in the treated region. (B) CT revealed a central gas filled defect in the left caudal maxilla (green arrow) in the area of FUS focus on days 30 and 102 post-treatment. New bone formation appeared to fill the depth of the osseous defect in the left caudal maxillary crest by day 30. A mild amount of amorphous new bone on the floor of the left orbital dorsal region of the removed soft tissue mass was also observed.

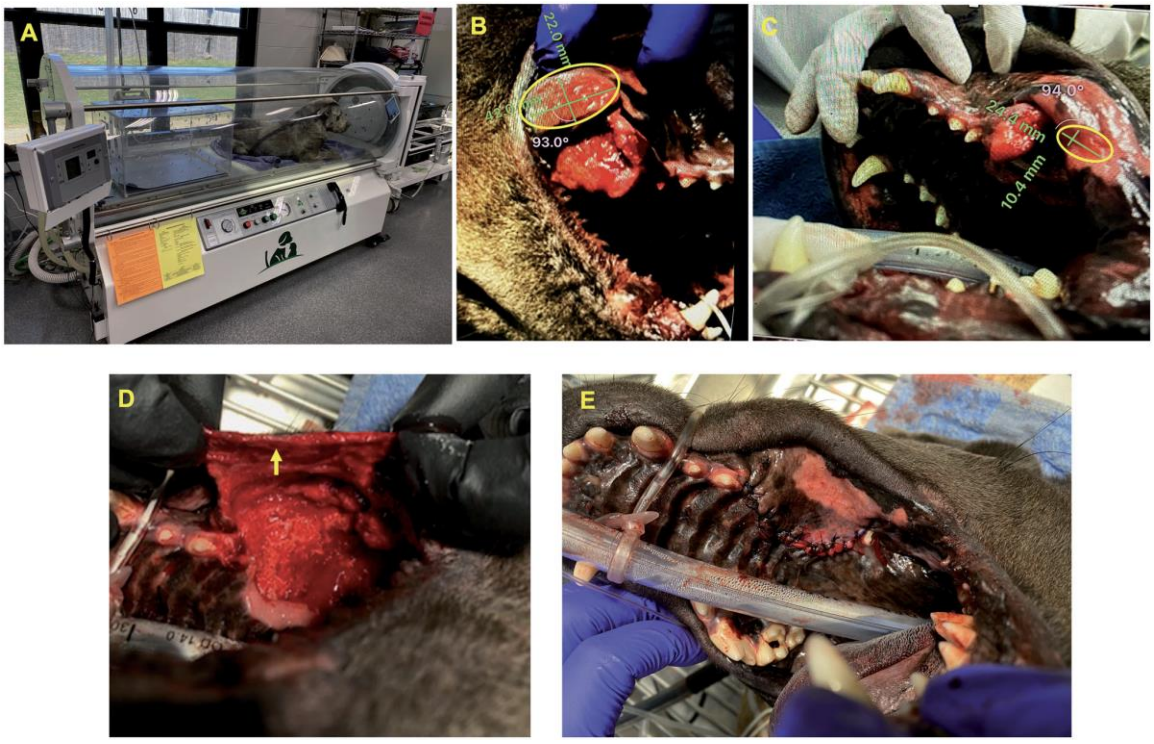

Figure 5. HBOT chamber for management of thermal burns. (A) HBOT device and setup. (B) A thermal burn (42 X 22 mm) was observed in the buccal mucosa (ellipse) region close to the treated tumor on day 8. (C) HBOT administration decreased the zone of thermal burns (24 X 10.4 mm; ellipse), as compared with the pretreatment levels. (D, E) The exposed bones underlying the tumors were closed with a gingival flap (arrow) after complete tumor remission and healing of thermal burns on day 30.

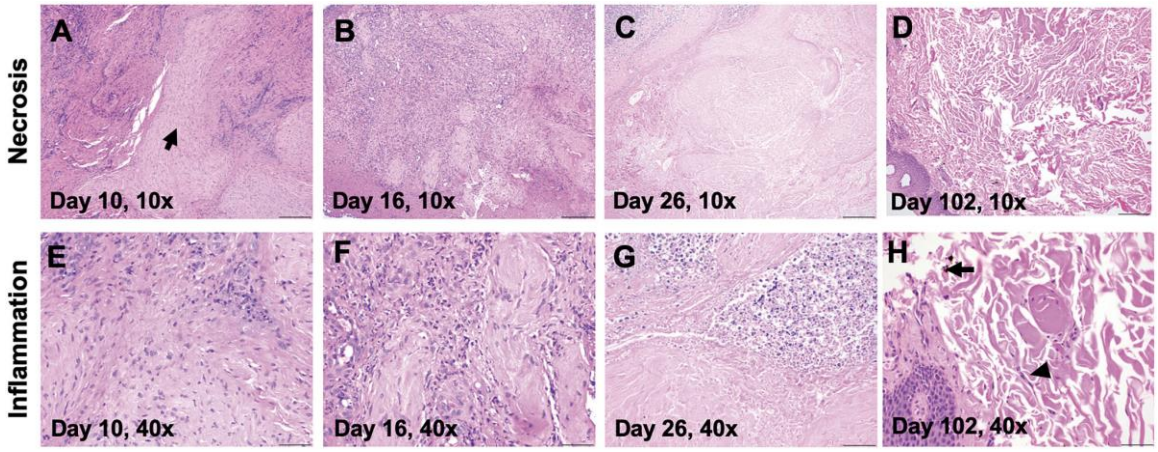

Figure 6. Longitudinal histopathological analysis. (A–C) Marked areas of coagulative necrosis within the mass, characterized by hyper-eosinophilic neoplastic cells lacking nuclear details. (D, H) Evaluation of treated regions on day 102 showed an absence of tumor cells with submucosa composed of collagen, fibroblasts (arrowhead), and melanomacrophages (arrow). (E–H) The tumor showed infiltrated neutrophils, lymphocytes, and macrophages admixed with tumor cells between day 10 and day 26, and they became rare by day 102.

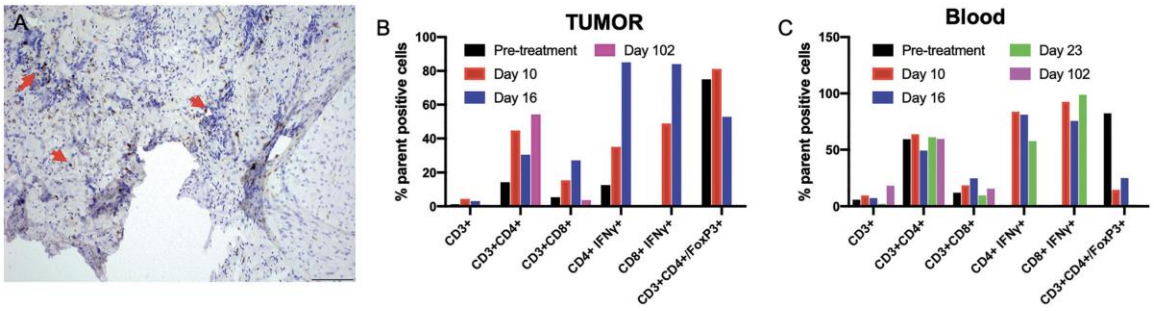

Figure 7. Local and systemic evaluation of immune response to FUS treatments. (A) A day 10 tumor biopsy sample showed low to moderate numbers of CD3. lymphocytes surrounding the tumor cells (arrow, 200X magnification). (B, C) Trends in the treatment effects on T cells in the tumor and blood over time, relative to the pretreatment controls. FUS ablation increased the frequency of CD3+, and IFN-Y expressing CD3+ CD4+ T cells and CD3+ CD8+ T cells at 1–3 weeks post-treatment in the tumor, as compared with the pretreatment levels. The population of T-cells became undetectable on day 102 in the tumor region. Similarly, an elevated population of IFN-Y expressing CD3+ CD4+ T cells and CD3+ CD8+ T cells was observed in the blood 2–3 weeks post-treatment, and these cells became undetectable by day 102. A consistent decrease in the populations of the immunosuppressive Treg cells in the blood was observed post-treatment, and these cells became undetectable in both the blood and tumor by day 102.

References

1. Ellington TD, Henley SJ, Senkomago V, et al. Trends in incidence of cancers of the oral cavity and pharynx – United States 2007–2016. MMWR Morb Mortal Wkly Rep. 2020; 69:433–438.
2. Joo YH, Cho JK, Koo BS, et al. Guidelines for the surgical management of oral cancer: Korean society of thyroid-head and neck surgery. Clin Exp Otorhinolaryngol. 2019; 12:107–144.
3. Omura K. Current status of oral cancer treatment strategies: surgical treatments for oral squamous cell carcinoma. Int J Clin Oncol. 2014; 19:423–430.
4. Shanti RM, O'Malley BW Jr. Surgical management of oral cancer. Dent Clin North Am. 2018; 62:77–86.
5. da Silva SD, Hier M, Mlynarek A, et al. Recurrent oral cancer: current and emerging therapeutic approaches. Front Pharmacol. 2012; 3:149.
6. Wang B, Zhang S, Yue K, et al. The recurrence and survival of oral squamous cell carcinoma: a report of 275 cases. Chin J Cancer. 2013; 32:614–618.
7. Woolgar JA, Scott J, Vaughan ED, et al. Survival, metastasis and recurrence of oral cancer in relation to pathological features. Ann R Coll Surg Engl. 1995; 77:325–331.
8. Mikiewicz M, Pa zdzior-Czapula K, Gesek M, et al. Canine and feline oral cavity tumours and tumour-like lesions: a retrospective study of 486 cases (2015–2017). J Comp Pathol. 2019; 172:80–87.
9. Cray M, Selmic LE, Ruple A. Demographics of dogs and cats with oral tumors presenting to teaching hospitals: 1996–2017. J Vet Sci. 2020;21: e70.
10. Dorn CR, Taylor DO, Schneider R, et al. Survey of animal neoplasms in Alameda and Contra Costa Counties, California. II. Cancer morbidity in dogs and cats from Alameda County. J Natl Cancer Inst. 1968; 40:307–318.
11. Silva EO, Goiozo PFI, Pereira LG, et al. Concomitant malignant pulmonary peripheral nerve sheath tumour and benign cutaneous peripheral nerve sheath tumour in a dog. J Comp Pathol. 2017; 157:46–50.
12. Boonsriroj H, Kimitsuki K, Akagi T, et al. Malignant epithelioid schwannoma of the oral cavity in a cat. J Vet Med Sci. 2014;76: 927–930.
13. Giangaspero F, Fratamico FC, Ceccarelli C, et al. Malignant peripheral nerve sheath tumors and spindle cell sarcomas: an immunohistochemical analysis of multiple markers. Appl Pathol. 1989;7: 134–144.
14. Gaitero L, A~nor S, Fondevila D, et al. Canine cutaneous spindle cell tumours with features of peripheral nerve sheath tumours: a histopathological and immunohistochemical study. J Comp Pathol. 2008; 139:16–23.
15. Ottinger T, Lindberg R, Ekman S. Malignant acoustic schwannoma in a dog. J Vet Diagn Invest. 2009; 21:129–13

16. Lambade PN, Palve D, Lambade D. Schwannoma of the cheek: clinical case and literature review. J Maxillofac Oral Surg. 2015;14: 327–331.
17. VanOsdol J, Ektate K, Ramasamy S, et al. Sequential HIFU heating and nanobubble encapsulation provide efficient drug penetration from stealth and temperature sensitive liposomes in colon cancer. J Control Release. 2017; 247:55–63.
18. Sethuraman SN, Singh MP, Patil G, et al. Novel calreticulin-nanoparticle in combination with focused ultrasound induces immunogenic cell death in melanoma to enhance antitumor immunity. Theranostics. 2020; 10:3397–3412.
19. Stavarache MA, Petersen N, Jurgens EM, et al. Safe and stable noninvasive focal gene delivery to the mammalian brain following focused ultrasound. J Neurosurg. 2018; 130:989–998.
20. Timbie KF, Mead BP, Price RJ. Drug and gene delivery across the blood–brain barrier with focused ultrasound. J Control Release. 2015; 219:61–75.
21. Bandyopadhyay S, Quinn TJ, Scandiuzzi L, et al. Low-intensity focused ultrasound induces reversal of tumor-induced T cell tolerance and prevents immune escape. J Immunol. 2016;196: 1964–1976.
22. Wu F, Zhou L, Chen WR. Host antitumour immune responses to HIFU ablation. Int J Hyperthermia. 2007; 23:165–171.
23. Mauri G, Nicosia L, Xu Z, et al. Focused ultrasound: tumour ablation and its potential to enhance immunological therapy to cancer. Br J Radiol. 2018; 91:20170641.
24. Li S, Wu PH. Magnetic resonance image-guided versus ultrasound- guided high-intensity focused ultrasound in the treatment of breast cancer. Chin J Cancer. 2013; 32:441–452.
25. Leslie T, Ritchie R, Illing R, et al. High-intensity focused ultrasound treatment of liver tumours: post-treatment MRI correlates well with intra-operative estimates of treatment volume. BJR. 2012;85: 1363–1370.
26. Schmitz AC, Gianfelice D, Daniel BL, et al. Image-guided focused ultrasound ablation of breast cancer: current status, challenges, and future directions. Eur Radiol. 2008; 18:1431–1441.
27. Kirby JP, Snyder J, Schuerer DJE, et al. Essentials of hyperbaric oxygen therapy: 2019 review. Mol Med. 2019; 116:176–179.
28. Bhutani S, Vishwanath G. Hyperbaric oxygen and wound healing. Indian J Plast Surg. 2012; 45:316–324.
29. Oley MH, Oley MC, Aling DMR, et al. Effects of hyperbaric oxygen therapy on the healing of thermal burns and its relationship with ICAM-1: a case–control study. Ann Med Surg. 2021; 61:104–109.
30. Kranke P, Bennett M, Roeckl-Wiedmann I, et al. Hyperbaric oxygen therapy for chronic wounds. Cochrane Database Syst Rev. 2004:CD004123.
31. Cianci P, Slade JB, Jr., Sato RM, et al. Adjunctive hyperbaric oxygen therapy in the treatment of thermal burns. Undersea Hyperb Med. 2013; 40:89–108.
32. Enomoto M, Yagishita K, Okuma K, et al. Hyperbaric oxygen therapy for a refractory skin ulcer after radical mastectomy and radiation therapy: a case report. J Med Case Rep. 2017; 11:5–5.

33. Sultan A, Hanna GJ, Margalit DN, et al. The use of hyperbaric oxygen for the prevention and management of osteoradionecrosis of the jaw: a Dana-Farber/Brigham and Women's Cancer Center Multidisciplinary Guideline. Oncologist. 2017;22(3):343–350 [published correction appears in Oncologist. 2017 Nov;22(11):1413].
34. Gerlach NL, Barkhuysen R, Kaanders JHAM, et al. The effect of hyperbaric oxygen therapy on quality of life in oral and oropharyngeal cancer patients treated with radiotherapy. Int J Oral Maxillofac Surg. 2008; 37:255–259.
35. Wardlow R, Sahoo K, Dugat D, et al. High intensity focused ultrasound (HIFU) heating improves perfusion and antimicrobial efficacy in mouse Staphylococcus abscess. Ultrasound Med Biol. 2018; 44:909–914.
36. Wardlow R, Bing C, VanOsdol J, et al. Targeted antibiotic delivery using low temperature-sensitive liposomes and magnetic resonance-guided high-intensity focused ultrasound hyperthermia. Int J Hypertherm. 2016; 32:254–264.
37. Ranjan A, Jacobs GC, Woods DL, et al. Image-guided drug delivery with magnetic resonance guided high intensity focused ultrasound and temperature sensitive liposomes in a rabbit Vx2 tumor model. J Controlled Release. 2012; 158:487–494.
38. Maples D, et al. Synthesis and characterisation of ultrasound imageable heat-sensitive liposomes for HIFU therapy. Int J Hypertherm. 2015; 31:674–685.
39. Nguyen SM, Thamm DH, Vail DM, et al. Response evaluation criteria for solid tumours in dogs (v1.0): a Veterinary Cooperative Oncology Group (VCOG) consensus document. Vet Comp Oncol. 2015; 13:176–183.
40. Kim D, Li R. Contemporary treatment of locally advanced oral cancer. Curr Treat Options Oncol. 2019; 20:32.
41. Martins MD, Anunciato de Jesus L, Fernandes KPS, et al. Intra-oral schwannoma: case report and literature review. Indian J Dent Res. 2009; 20:121–125.
42. Santos PP, Freitas VS, Pinto LP, et al. Clinicopathologic analysis of 7 cases of oral schwannoma and review of the literature. Ann Diagn Pathol. 2010; 14:235–239.
43. Cohen M, Wang MB. Schwannoma of the tongue: two case reports and review of the literature. Eur Arch Otorhinolaryngol. 2009; 266:1823–1829.
44. Park J, Lee JS, Cho JH, et al. Effects of high-intensity-focused ultrasound treatment on benign uterine tumor. J Korean Med Sci. 2016; 31:1279–1283.
45. Howard SC, Jones DP, Pui CH. The tumor lysis syndrome. N Engl J Med. 2011; 364:1844–1854.
46. Strauss PZ, Hamlin SK, Dang J. Tumor lysis syndrome: a unique solute disturbance. Nurs Clin North Am. 2017; 52:309–320.
47. Fernando R, Downs J, Maples D, et al. MRI-guided monitoring of thermal dose and targeted drug delivery for cancer therapy. Pharm Res. 2013; 30:2709–2717.
48. D'Souza AL, Chevillet JR, Ghanouni P, et al. Tumor characterization by ultrasound-release of multiple protein and microRNA biomarkers, preclinical and clinical evidence. PLoS One. 2018;13: e0194268.
49. Xu ZL, Zhu XQ, Lu P, et al. Activation of tumor-infiltrating antigen presenting cells by high intensity focused ultrasound ablation of human breast cancer. Ultrasound Med Biol. 2009; 35:50–57.

50. Castro F, Cardoso AP, Gonc¸alves RM, et al. Interferon-gamma at the crossroads of tumor immune surveillance or Evasion. Front Immunol. 2018; 9:847.
51. Ektate K, Munteanu MC, Ashar H, et al. Chemo-immunotherapy of colon cancer with focused ultrasound and Salmonella-laden temperature sensitive liposomes (thermobots). Sci Rep. 2018; 8:13062.
52. Facciabene A, Motz GT, Coukos G. T-regulatory cells: key players in tumor immune escape and angiogenesis. Cancer Res. 2012;72: 2162–2171.
53. Nell DM, Myers MR. Thermal effects generated by high-intensity focused ultrasound beams at normal incidence to a bone surface. J Acoust Soc Am. 2010; 127:549–559.
54. Weitgasser L, Ihra G, Sch€afer B, et al. Update on hyperbaric oxygen therapy in burn treatment. Wien Klin Wochenschr. 2021; 133(3-4):137–143.
55. Weitgasser L, Ihra G, Sch€afer B, et al. Update on hyperbaric oxygen therapy in burn treatment. Wien Klin Wochenschr. 2021;133: 137–143.
56. Helmers R, Milstein DM, van Hulst RA, et al. Hyperbaric oxygen therapy accelerates vascularization in keratinized oral mucosal surgical flaps. Head Neck. 2014; 36:1241–1247.
57. Thorn JJ, Kallehave F, Westergaard P, et al. The effect of hyperbaric oxygen on irradiated oral tissues: transmucosal oxygen tension measurements. J Oral Maxillofac Surg. 1997; 55:1103–1107.
58. Sch€onmeyr BH, Wong AK, Reid VJ, et al. The effect of hyperbaric oxygen treatment on squamous cell cancer growth and tumor hypoxia. Ann Plast Surg. 2008; 60:81–88.
59. Rinaldi B, Cuzzocrea S, Donniacuo M, et al. Hyperbaric oxygen therapy reduces the toll-like receptor signaling pathway in multiple organ failures. Intensive Care Med. 2011; 37:1110–1119.
60. Lu Z, Ma J, Liu B, et al. Hyperbaric oxygen therapy sensitizes nimustine treatment for glioma in mice. Cancer Med. 2016;5: 3147–3155.
61. Wang YG, Long J, Shao DC, et al. Hyperbaric oxygen inhibits production of CD3+ T cells in the thymus and facilitates malignant glioma cell growth. J Int Med Res. 2018; 46:2780–2791.
62. Li Y, Patel SP, Roszik J, et al. Hypoxia-driven immunosuppressive metabolites in the tumor microenvironment: new approaches for combinational immunotherapy. Front Immunol. 2018; 9:1591–1591.

CHAPTER III

FOCUSED ULTRASOUND TREATMENT OF SPONTANEOUS OCCURING CANCERS: LOCAL EFFECTS AND SYSTEMIC IMMUNE EVALUATIONS IN VETERINARY PATIENTS

Parts of this chapter are based on:

Harshini Ashar, Danielle Dugat, Kalyani Ektate, and Ashish Ranjan “Immunological and therapeutic effects of focused ultrasound in canine cancer patients.” *Focused Ultrasound Symposium* (2020).

Harshini Ashar, Deepan Kishore, Danielle Dugat, Tina Neel, Akansha Singh, and Ashish Ranjan. "Final Report FUS Grant." (2021).

Abstract

Over the last decade, the use of novel therapeutic devices to treat solid tumors are on the rise. High-intensity focused ultrasound (HIFU) is a non-invasive therapeutic modality that destroys cancer cells via thermal and mechanical effects. It can be used to treat

tumors of any size and shape or depth, and minimally affects surrounding critical or non-critical structures. The objective of this study was to investigate whether HIFU can be utilized for the treatment of veterinary cancer patients. Companion pet dogs and cats present with a variety of naturally occurring tumors. While the rodent models used for majority of cancer studies allows high throughput studies, they do not mimic the anatomical and physiological stressors that companion animals experience. In addition to providing a desired alternative therapeutic option for pets with cancer, veterinary clinical trials can also be an excellent resource for future use in human patients. The specific aims of our veterinary trials were to investigate the ability of HIFU to induce thermal or mechanical ablation of mostly head, neck, or extremity tumors solid tumors, with or without chemotherapy in patients. Treatment response was characterized by tumor measurements and histopathological examination of the treated site. Additionally, the anti-tumor immune effects of HIFU were assessed by flow cytometry, analysis of blood and tumor samples. Data suggests that HIFU ablation modalities can improve clinical outcomes, and immunologic against certain tumor types.

1. Introduction

Pet dogs get cancer at roughly the same rate as humans. As per the American Veterinary Medical Association approximately 1 in 4 dogs will develop neoplasia at some stage in their life, and about half of the dogs over the age of 10 will develop cancer. This is indicative of spontaneously occurring tumors, many of which are histologically similar to human tumors [1]. Currently, most solid tumors in veterinary patients employ non-

invasive radiation or invasive surgery, and systemic chemotherapy, which can have known side-effects. As an alternative, in this study, we evaluated the feasibility of High-intensity focused ultrasound (HIFU) based solid tumor treatment regimen for improved outcomes in veterinary patients.

High-intensity focused ultrasound is a non-invasive and non-ionizing treatment modality. It focuses ultrasound energy precisely in the target tissue, under ultrasound (US) or magnetic resonance (MR) image-guidance, to produce local and systemic bioeffects [2]. By varying the sonication parameters, it can generate thermal and mechanical effects at various locations in the body. HIFU treatments can also stimulate the patient's immune system against the treated tumor locally and at distant metastases [3, 4]. For e.g., thermal ablation with HIFU causes coagulative necrosis in the focal zone, due to rapid elevation of tissue temperatures to $>60^0$C over short exposures [5]. The exposed proteins and cellular debris can improve antigen presentation and trigger a tumor-specific immune response [6-8]. HIFU can also be used as an adjuvant to augment radiation, chemotherapy, or novel immunotherapies [9-12]. Depending on the HIFU treatments (mild hyperthermia, thermal ablation, or histotripsy), distinct immune responses can be attained [7, 13-18]. In human medicine, HIFU is being increasingly used to treat various malignant and non-malignant conditions, including, breast cancer, uterine fibroids, prostate tumors, and neurological conditions [2]. Combination of HIFU with chemo- and immunotherapies for different cancers are also being extensively investigated in pre-clinical models, with promising results. [10-12].

Application of HIFU in veterinary medicine can not only offer innovative treatment options to veterinarians and pet owners, but tumor-bearing dogs can also act as a unique

resource for translation of novel therapies in human patients. The comparatively similar size and growth rate of tumors and their microenvironmental parameters uniquely positions dogs for translational studies of novel surgical approaches, radiation therapy including HIFU [1]. Like humans, canine patients can be monitored for hematological, biochemical, and immunological parameters and other sophisticated monitoring. Furthermore, due to the large tumor size, serial biopsy and longitudinal assessment of treatment efficacy can be evaluated including temporal endpoints such as remission or progression free survival. This makes clinical trials in client-owned dogs an immense resource.

Recently, studies have been conducted to test the feasibility of using HIFU in canine patients. Seward et al., evaluated the potential of MR-HIFU in targeting canine soft tissue sarcomas (STS). They reported that 81.1% (43/53) of STS were targetable with extremity tumors being the most targetable [19]. Another retrospective study evaluated HIFU therapy for surgically unresectable solid tumor in dogs. Out of the 10 dogs treated, four dogs exhibited decreased tumor size and two dogs had partial remission, with varying transient side effects. Additionally, they reported that HIFU could be used to control local bleeding associated with hemorrhagic tumors [20].

Based on these premises, the purpose of this study was two-fold: 1. To determine the potential of locally targeting solid tumors with HIFU ablation alone, and 2. evaluate the ability of HIFU hyperthermia to enhance chemotherapy delivery in patients with sarcoma tumors. For the HIFU ablation groups, we compared the therapeutic and immunomodulatory effects of thermal vs non-thermal histotripsy protocols. For the hyperthermia + chemotherapy group we compared the drug delivery and

immunomodulatory effects of HIFU heated vs. non-heated sites between Dox alone and Dox-loaded LTSL (LTSL). LTSLs are designed to release encapsulated contents (e.g., doxorubicin or Dox). The premise of these clinical trials stemmed from our various pre-clinical studies in mouse models on developing LTSLs for enhanced Dox penetration in tumors driven by HIFU heating [12, 21, 22] as well as on histotripsy ablation and immune-activation in combination with immunotherapy [10].

2. Materials and methods

2.1 Patient Enrollment and Study Design: All patients were recruited from OSU Veterinary Teaching Hospital and Neel Veterinary Hospital at Oklahoma City. All animal related procedures were approved by the Oklahoma State University Animal Care and Use Committee (OSU-ACUC). Prior to treatment, owner consented to the terms of the study was obtained, including a follow-up post-mortem analysis and release from institutional/ personal (researcher) liability. Canine patients regardless of tumor types were assigned randomly to the ablation and histotripsy group. Biopsy positive canine patients with sarcomas were randomly divided into two groups: 1. Dox + HIFU and 2. LTSL + HIFU.

2.2 Inclusion & Exclusion Criteria: Patients who had received prior treatment (surgery, anticancer drug, or radiotherapy) were not excluded from the trial.

2.3 Endpoints: For Ablation/Histotripsy study, the primary endpoints were local/systemic tumor control and immunological analysis by flow cytometry (FC). For the HIFU hyperthermia + chemotherapy study, the end points included drug delivery

analysis in the heated and unheated regions, and response characterizations. tumor measurements and local and systemic immune characterization by FC. LTSLs (ThermoDox) were provided through a Collaborative Research and Development Agreement with Celsion Corporation. Dox/LTSLs were injected at a dose of 0.7mg Dox/kg body weight, dispersed in D5W (5% dextrose in water), injected intravenous (I/V) over 30min, post HIFU initiation. Biopsies were taken immediately post treatment from the heated and unheated part of the tumor for drug delivery analysis by high-pressure liquid chromatography (HPLC) or spectrophotometrically, as indicated. Prior to Dox therapy, each patient received antihistamines and steroids combinations as follows for two days: 0.5 mg/kg of prednisone orally twice daily; 2 mg/kg of diphenhydramine orally thrice a day and 0.5 mg/kg famotidine orally once a day. A similar regimen of antihistamines and steroids was also utilized against mast cell tumor patients.

HIFU parameters used in the different cohorts of patients were previously optimized in ex vivo tissue phantom and in vivo mouse studies (Table 1). On an average, a patient experienced 3-6 hospital visits. Since client-owned dogs cannot be left untreated, each patient served as its own internal control.

Parameter	Duty cycle (%)	Power (W)	Pulse repetition frequency (PRF)	Treatment time/ focal spot (secs)	% of total tumor volume treated
Ablation	50	70-90	20	30-35	~50-60%
Histotripsy	1	450-600	5	20-25	~30-50%
Hyperthermia	50	8-12	20	300-420	~30-40%

Table 1. Parameters used for treatment of client-owned veterinary patients with spontaneous tumors.

2.4 Pre-treatment clinical exam: Dogs admitted to the hospital were examined for vital parameters (heart rate, temperature, and respiratory rate), by auscultation of the chest, and palpation. The mass lesion was visually examined and palpated to allow for documentation of size, character, color, signs of infection or drainage, and location in relation to other structures. A complete blood count (CBC) and serum biochemistry panel was performed. For metastatic cancer types such as melanomas, sarcomas and with patients that presented with swollen draining lymph nodes, thoracic radiographs were taken to assess for metastases.

2.5 HIFU treatment planning and administration: HIFU treatment was performed in anesthetized patients using an ultrasound guided Alpinion system (Figure 1A). For acoustic coupling, the fur was shaved as closely to the at the treatment site to ensure complete contact with the transducer membrane. Degassed gel was additionally used to provide acoustic coupling. The VIFU planning software was used to select the region of interest and target boundaries in the X, Y, and Z directions for automatic rastering of the transducer as shown in (Figure 1B).

2.6 Sample collection and flow cytometry: Tumor measurements**,** biopsies for immunological analysis by flow cytometry and immunohistochemistry and blood samples were taken before, and 7 to 14 days post treatment. Treatment efficacy was evaluated by tumor caliper measurements and recording of new lesions according to the Veterinary Cooperative Oncology Group (VCOG) response evaluation criteria in solid tumors (RECIST v1.1) guidelines [23]. Complete response (CR) involved disappearance of all target lesions, partial response (PR) involved a > 30% decrease in the sum of tumor diameters, and stable disease (SD) involved a <30% decrease in tumors or <20% increase

in the longest diameters of target lesions after HIFU treatments. Progressive disease (PD) indicated either an appearance of one or more new lesions or at least a 20% in the longest diameters of target lesions.

2.7 Doxorubicin estimation in tumors

Tissue homogenization and sample preparation for HPLC/spectrophotometric analysis was performed using our previously published methods [22, 24]. Briefly, samples were homogenized, and Dox was extracted using HPLC-grade acetonitrile (Sigma-Aldrich, St. Louis, MO). Using daunorubicin as internal standard, tissue Dox was quantified by HPLC d at fluorescence wavelengths at excitation/emission of ex.498/em.595 nm. Data was acquired using Shimadzu LC solution software. Tissue analyte concentrations were determined using peak-area ratios of the sample analyte to the internal standard from the calibration curve. Alternatively, in some cases, homogenized samples were extracted using 2% aqueous acetic acid/acetonitrile, 1:1 v/v and fluorescence (ex. 480 nm, em. 590 nm) and measured using SpectraMax M2 spectrophotometer (Molecular devices, Sunnyvale, CA).

2.8 Immunophenotyping of immune cells with flow cytometry

For flow cytometry, blood samples were collected in BD Vacutainer EDTA tubes, and biopsy samples were collected into RPMI supplemented with 2% FBS. Samples were transported and stored on ice or at 4°C until further analysis. Single-cell suspensions were obtained through mechanical disruption of the tumor biopsy tissues followed by enzymatic digestion with 200 U/ml collagenase IV (Life Technologies, NY, USA) at 37^0C for 1hour. The lysates were filtered through a 70 µm cell strainer (Corning Inc,

Corning, NY). Blood samples collected in EDTA tubes were incubated with 1× RBC lysis buffer (multi-species, Invitrogen) for 10–15 min before antibody staining. The following fluorochrome-conjugated anti-dog antibodies were used to stain cells for 30 min in the dark on ice: anti-$CD3^+$, anti-$CD4^+$, anti-$CD\text{-}8^+$ (dog T lymphocyte cocktail, cat. 558699, BD Pharmingen), and APC labeled anti-$CD45^+$ (YKIX716.13, cat. MCA1042, Bio-Rad). For detecting IFN-Y and $Foxp3^+$ T regulatory (Treg) cells, the cells were washed after surface marker staining, fixed, permeabilized with a transcription factor buffer set (BD Biosciences, San Jose, CA), and incubated with Alexa Fluor 700 labeled anti-IFN-Y (CC302, Novus biologicals) and e-fluor 450 labeled anti-Foxp3 (FJK-16s, cat. 5016374, Fisher) for 50 min in the dark on ice. Stained cells were analyzed with a FACS Aria II (BD Biosciences) within 24–48 h. Compensation was performed with single-stained UltraComp eBeads (Invitrogen). Datasets were analyzed in FlowJo software v.10.2 (Treestar Inc, Ashland, OR, USA).

3. Results

3.1.1 HIFU ablation achieved significant tumor remission.

A total of 8 dogs with different tumor types including mast cell tumors (MCT), mammary, connective tissue, and skin tumors received ablative therapy. The patient characteristics, response rates and treatment side-effects are summarized in Table 2. 50% of treated patients (n= 4/8) exhibited complete response within two weeks after the first treatment (Figure 2). Patient #6 showed gradual tumor regression (data not shown) of >30%, which by RECIST guidelines was considered as a partial response. But the owner

discontinued treatment and hence further longitudinal assessments could not be carried out. Patient #8, although evaluated as PR, showed a significant reduction in tumor mass of ~95% decrease at the end of 11 weeks, following five HIFU treatments covering 50% of tumor in each session (Figure 2). Patient #7 with chondrosarcoma was unresponsive to ablative treatment, showing an open wound and major inflammation, while the MCT of Patient #4, although initially responsive (Figure 2) at the 1-week follow-up, showed a lack of response in subsequent sessions.

Side effects post thermal ablation consisted of moist dermatitis, minor burns, open wounds, and skin inflammation, in the treatment regions. These were managed with periodic hyperbaric oxygen exposures and local and systemic antibiotics. Some patients demonstrated symptoms of diarrhea 1-2 days post-treatment which were managed with fluid therapy. In a few cases (e.g., fibroma and apocrine gland carcinoma), significant healthy tissue damage was noted, especially when the tumors were located very closed to attenuating structures (e.g., bones). These were managed by surgical interventions.

3.1.2 Non-thermal histotripsy treatments were well tolerated in the canine patients.

For the histotripsy arm, 5 canine patients were treated. The tumor types for this trial included mammary, papillary and mast cell tumors. Bubble cloud during histotripsy was monitored using real-time US image guidance (Figure 5). Data suggested that partial histotripsy treatments of tumors kept tumor growth in check, with stable disease persistence (Table 3, Figure 6). Two out of 5 patients showed a partial remission of the treated tumor; both of these tumors were of mammary tumor origin. Unlike thermal ablation treatment that demonstrated complete remission of majority of the treated cases

(Figure 4), the histotripsy exposures were generally well tolerated by all the patients without any alterations in the vital signs. In addition, no side-effects on local, the tumor adjoining healthy tissues, or even systemic reactions were reported by the owners for any of the treated patients.

3.1.3 The immune responses to HIFU exposures depended on the tumor type

The systemic immune responses in blood samples after thermal ablation of tumors showed moderate changes in $CD3^+$ T cells in the blood relative to the pre-treatment levels in almost all patients (Figure 3A). Patient #6 showed a significant spike in $CD3^+$ T cells $CD3^+$ $CD8^+$ T cells on day 14 (Figure 3C). Likewise, patient #3 and #5 showed an increase in $CD3^+$ and $CD3^+$ $CD8^+$ T cells, and these were high IFN-Y expressing $CD4^+$ as well as $CD8^+$ T cells (Figures 3E & F), relative to the pre-treatment levels and a decrease in Tregs (patient #3) but increase in patient #5 (Figure 3D). Overall, the $CD3^+$ $CD4^+$ T cell population in most patients remain unchanged (Figure 3B).

In contrast to thermal ablation, histotripsy treatments increased the populations of $CD3^+$Tcells and $CD8^+$ T cells in the blood of 3 out of the 5 treated patients (Figure 7A & C). Enhanced IFN-Y activity was seen for both CD4+ and CD8+ phenotypes (Figure 7E & F). However, this was accompanied by an increase in the Treg population in almost all patients (Figure 7D).

Ablation Patient #	Breed	Age	Gender	Location	Diagnosis	# of treatments	Response (RECIST)	Side effects
1	Lab retriever	6 y	FS	Tail-base	MCT, low	1	CR	Skin inflammation and open wound after tumor regressed. Prescribed topical antibiotics. Wound healed completely within a week.
2	Great pyrenes	9 y	MI	Rt. Inguinal	Mammary mass	1	CR	
3	Mixed	6 y	MC	Rt. Elbow and thigh	Fibroma	1	CR	Thermal burn lesions noted. Wound managed surgically. Complete healing noted within 2 weeks post-surgery.
4	French bulldog	8 y	MC	Left butt region	MCT, low	1	PD	Treatment area inflamed. Inflammation spread to inguinal region.
5	Yorkshire mix	13 y and 5mo.	FS	Left rump	Apocrine gland carcinoma	1	CR	Owner reported diarrhea. Open wound, surgically closed and healed well.
6	Dach-shund	10 y	FS	Nasal	Amelanotic melanoma	3	PR	Mass was sensitive and bled when touched. Mild ulceration where

								mass was treated and regressed, which healed well.
7	Labrador	9 y	MC	Nasal	Chondro-sarcoma	3	PD	Open wound, tumor non-responsive.
8	Mixed	11y	FS	Nasal	MCT	5	PR	Minor scabbing around treated region.

Table2. Ablation patient characteristics and response evaluation using RECIST guidelines. (CR: complete response, PR: partial response, PD: progressive disease, SD: stable disease, FS: female spayed, FI: female intact, MC: male castrated, MI: male intact, and MCT: mast cell tumor)

Histotripsy Patient #	Breed	Age	Gender	Tumor location	Diagnosis	# of treatments	Response (RECIST)	Side effects
1	Dachshund	-	FS	Left mammary mass	Mammary mass	1	PR	None reported.
2	Pitbull	8 y	MI	Left antebrachium	MCT, low	2	PD	None reported.
3	GSD mix	7 y 7mo	FS	Rump	Lipoma	2	PD	None reported.
4	Mixed	12 y	MC	Oral-rt and left upper	Soft-tissue sarcoma	1	SD	None reported.
5	Mixed	8 y	FS	Left mammary chain	Papillary adenocarcinoma	2	PR	None reported.

Table 3. Histotripsy patient characteristics and response evaluation using RECIST guidelines. (CR: complete response, PR: partial response, PD: progressive disease, SD: stable disease, FS: female spayed, MC: male castrated, MI: male intact, and MCT: mast cell tumor)

Patient #	Breed	Age	Gender	Tumor location	Diagnosis	Route	# of treatments	Response (RECIST)	Side effects
Dox + hyperthermia									
1	Dachshund	11 y	MC	Rt. ventral chest	STS, grade I	I/V	1	PD	No concerns reported
2	Boxer	8 y	MC	Rt. antebrachium	STS, grade I	I/V	1	PD	
3	Mini schnauzer	9 y 6 mo.	FS	Rt. shoulder	STS, grade I	I/V	1	PD	
LTSL + hyperthermia									
4	Mixed	12 y	MC	Oral-rt. and left maxilla	STS, grade I	I/V	1	SD	No concerns reported
5	Giant Schnauzer	12 y	MC	Left proximal humerus	Osteosarcoma	I/V	1	PR	Lethargy and transient loss of appetite was reported

Table 4. Hyperthermia + chemotherapy patient characteristics and response evaluation using RECIST guidelines. (CR: complete response, PR: partial response, PD: progressive disease, SD: stable disease, FS: female spayed, MC: male castrated, STS: soft tissue sarcoma, and I/V: intravenous)

3.2.1 HIFU hyperthermia enhanced delivery of Dox in the heated regions of tumor.

Tumor Dox concentrations were 0.26 ± 0.02 and 0.325 ± 0.01μg Dox/g tissue in the unheated and heated regions of the tumor, respectively, following Dox + HIFU treatment. Overall, the Dox delivery to heated regions significantly exceeded those of the unheated in the sarcoma tumors (Figure 9).

3.2.2 HIFU + Dox treatment induced tumor regressions.

The efficacy of FUS at the indicated time points was evaluated with tumor volume measurements as per the RECIST guidelines (Table 4). Distinct tumor regression compared with the pre-treatment value was observed on day 7 in all the treated dogs (Figure 10). In patient #3, a regrowth of the treated mass was noted by day14 post-treatment. In contrast, in patients #1 and #2, tumors continued to regress at 2 weeks post-treatment. As per RECIST criteria, all the cases experienced partial tumor regressions to stable disease, however, the removal of the HIFU treatment caused regrowth and a progressive disease.

3.2.3 HIFU + Dox stimulated a local and systemic T cell response in all the treated patients.

Local and systemic evaluation of the immune responses of harvested tumor biopsy and blood samples after HIFU + Dox revealed moderate changes in $CD3^+$ T cells in the blood, but a significantly increased infiltration (~3-fold) in tumors post treatment, relative to the pre-treatment levels (Figure 11A & B). A concomitant increase in the $CD3^+$ T cell subset of $CD3^+$ $CD4^+$ cells in the biopsy samples was observed. However, the population of $CD3^+$ $CD8^+$ cells were not altered, except for minor fluctuations, in both blood and

biopsy samples. Additionally, there was an increase in the IFN-Y expressing T cells relative to the pre-treatment paired control levels, accompanied with an increased population of $CD4^+$ $Foxp3^+$ Tregs in the blood and biopsy samples (Figure 11C).

3.2.4 HIFU + LTSL for targeted drug delivery in sarcoma patients

In this treatment group, 2 dogs sarcoma patients were enrolled (Table 4). Since the case requirements varied amongst the three patients, results for each patient are reported separately.

Patient #4: 12 yr. old dog with soft-tissue sarcoma in the right and left maxillary masses.

Compared to Dox alone cohorts, the drug delivery from LTSL increased by ~4-fold in the heated region, and 2-fold in the unheated regions of the treated tumor (Figure 12A). This suggests that clinical-grade LTSL can significantly improve drug delivery to tumor tissues compared to Dox alone, when combined with local hyperthermia.

A resulting decrease in tumor volumes was observed at Day7 post-treatment (Figure 12B). HIFU + LTSL treatment led to an increase in $CD3^+$ T cells in the blood (Figure 12C). However, no differences were seen in the CD3+ subsets (Figure 12C). This patient dropped out of the study 1week post-treatment, preventing longitudinal follow-ups or additional treatments.

Patient #5: 12 yr. old dog with end-stage metastatic osteosarcoma in the left proximal humerus.

This patient had a history of prior chemo- and stereotactic radiation therapy at Colorado state university and was referred to OSU. CT revealed significant pulmonary metastasis in the patient. HIFU + LTSL was administered in the affected bone as described above (Figure 13A). A slight improvement in clinical symptoms was reported by the owner's post-treatment. Blood immune analysis revealed a gradual but significant increase in population of $CD3^+$ T cells as well as the $CD8^+$ T cell subset (Figure 13B). Additionally, a gradual decrease in the blood Treg populations was also observed. Unfortunately, due to poor overall health, the patient was put to sleep at 1 week post treatment. Biopsy samples were collected post-mortem to evaluate local treatment effects, from treated leg as well as contralateral bone, which could help tailor future treatments for similar cases. The analysis showed a promising treatment effect with significant increase in $CD3^+$ T cells and concurrent decrease in Tregs, in the heated tumor regions, which contrasted with the respective cell populations in the unheated tumor region (Figure 13C). Furthermore, an abscopal increase in $CD3^+$ T cells and $CD3^+CD8^+$ T cells was observed in the contralateral bone, along with increased Tregs, compared to the heated bone biopsy.

Immunologically, an increase in the populations of $CD3^+$T cells was seen, over time, with moderate changes in the T cell subsets (Figure 13C). In contrast, a decreased population of the pro-tumoral Treg cells was observed in blood post-treatment.

4. Discussion

Each year in the United States, more than 1 million new cases of cancer occur, and it is the most common cause of death in dogs (~30% estimated rate) based on retrospective studies on canine mortality [25, 26]. Conventional therapies including surgery, radiation, and chemotherapy provide clinical benefit, but can be associated with adverse effects. HIFU achieves diverse tissue bioeffects, thus its incorporation in the existing cancer regimens can be an important step forward [3, 27]. In this pilot study, we tested the feasibility and effectiveness of HIFU alone and in combination with doxorubicin chemotherapy for the treatment of a variety of solid tumors in dogs.

Spontaneously occurring tumors in dogs are a unique cancer population for investigation of experimental therapeutics [28, 29]. Success of clinical trials can herald new therapies for veterinary patients and also be guide for translation to humans. Veterinary clinical trials allow highest quality management and data collection and be relatively less costly than human oncology trials. These benefits have spurred the enrollment of dog patients with spontaneously occurring tumors in translational radiation therapy studies, novel surgical approaches, drug delivery, amongst others [1]. For e.g., critical proof-of-concept studies for accurate radiation dosimetry by Gilette et. al., conducted in the 1970's in dog patients is still in use for human radiation dosing [30-33]. Observations and surgical refinements developed in dogs with spontaneous osteosarcomas, by human and veterinary surgical oncologists, led to use of these approaches in human limb-sparing surgery [34].

Tumor ablation modalities such as HIFU that offer alternatives to surgical resection are sought-after by veterinarians and companion animal caregivers, committed to the overall welfare of their pets. The most common application of HIFU, tissue destruction, can be achieved either by thermal energy to induce tissue protein denaturation [35] or mechanical energy (histotripsy) to induce cell membrane destruction via cell stress [36]. We compared the effectiveness of using thermal ablation and histotripsy in n=8 dogs and n=5 dogs, respectively (Figure 4). Our findings suggest that in terms of tumor remissions, thermal ablation was relatively more effective compared to histotripsy. Regardless of tumor type, most of the canine patients treated with thermal ablation responded to treatment (Table 2; Figure 2). N=4 patients showed complete remission while n=2 showed partial remission. Treatment was well-tolerated by the patients with minor episodes of open wounds post tumor mass denaturation and skin ulceration around the treated region, which were effectively managed by hyperbaric oxygen therapy as previously reported by us [37]. Most of the ablation patients were prescribed with antibiotics for wound management. This was also instituted by Ryu et. al. while investigating use of HIFU for non-resectable tumors or refractory to chemotherapy [20]. They reported mild side effects, including transient hyperthermia in multiple patients, enteritis in one dog, and skin ulceration in two dogs. Four out of the 10 dogs treated with thermal ablation exhibited a decrease in tumor size, with two dogs showing partial tumor response as per RECIST. Kopelman et. al., reported the successful use of MR-guided HIFU for the treatment of hepatocellular adenoma in a canine patient. The 10 yr. old dog was given four ablative treatments over the course of 8 weeks [38] and tumor was resected surgically 21 days after the fourth ablative procedure. The MRgHIFU created

necrosis and tissue destruction, accurately and in accordance with treatment planning. They did report a focal thermal injury by the ribs post fourth treatment which was surgically managed without further complications, quite similar to our findings. Interestingly, out of the 3 patients with mast cell tumors (MCT), one showed CR, one showed PR and one showed PD. All three patients had MCT in different anatomic locations, were of different breeds, between 6 yr.- 11yr, and the 2 patients that responded were spayed females while the non-responder was castrated male. Interestingly, the non-responding MCT patient initially presented with the inguinal lymph node (LN) metastasis, but with HIFU treatment, the LN reduced significantly and shrank back to normal palpable size, however, the primary tumor underwent massive inflammation, which gradually spread from the perineal regions to the inguinal regions. Historically, MCTs located in the perineal/inguinal regions are reported to require intensive trimodality therapy with surgery, radiation, and chemotherapy [39]. Additionally, dogs with LN metastasis had significantly shorter median survival times than dogs without nodal metastasis [40]. More studies focused on metastatic MCTs will need to be carried out to conclusively differentiate responders from non-responders.

To overcome the thermally induced side-effects of HIFU, HIFU treatments relying on histotripsy, are increasingly be used in patients. Histotripsy uses high power and short duration ultrasound pulses to create a large pressure change in the tissue leading to acoustic cavitation [41]. Cavitation creates highly precise tissue fractionation minimizing unwanted tissue damage [42]. Canine prostate models used to evaluate the potential of histotripsy modality previously demonstrated the ability of histotripsy to yield acellular disruption of targeted tissues [43-45]. Similarly, histotripsy treatments of canine STS and

OS tumors conducted with a clinical histotripsy prototype, indicated precise volumetric ablation of targeted regions [46]. In this study we determined the effectiveness of histotripsy against many types of solid tumors in canine patients (Table 3). Compared to ablation, histotripsy did not elicit a complete tumor remission in any of the 5 patients treated. All the dogs showed an initial decrease in mass, however they began regrowing by 3-4 weeks post-treatment (Figure 6). In the two patients that showed PR, histotripsy shrunk the tumor enough to surgically resect it without having to excise major margins of surrounding tissues. This indicated that histotripsy can be used in conjunction with surgery to effectively reduce risk and morbidity associated with surgical resection of tumors [46]. It should be noted that only 30-50% of tumors were treated with histotripsy, and the results may be tremendously different if the histotripsy levels are enhanced or decreased per-treatment session. Although histotripsy is known to induce enhanced tumor antigen release [15], which leads to anti-tumor immune-stimulation, we reasoned that a rapid release of tumor antigens into systemic circulation may also cause tumor lysis syndrome (TLS). This has in fact been reported in a uterine myoma patient, where HIFU induced TLS and acute kidney injury [47]. The blood reports in our initial studies did not indicate any such occurrences. In effect, unlike ablation, histotripsy did not cause any side effects or discomfort in the treated patients. Thus, having tested the safety of treating canine tumors with histotripsy alone in smaller volumes, our next goal is to treat of larger tumor volumes with histotripsy for effective tumor remission. In addition, we reason that an increased frequency of histotripsy treatments may induce CR of tumor masses with histotripsy alone treatments and more studies in a larger cohort of patients will be carried out to evaluate this. Additionally, results on pre-clinical use of histotripsy in our lab and

others have indicated that histotripsy modality is effective in stimulating an anti-tumor immune response and is most effective when used in combination with drug delivery systems and immunotherapy treatments, thereby pointing towards a need to institute these regimens in patients [9, 10, 14, 48].

Several pre-clinical and human clinical studies have shown the positive effects of thermal ablation and histotripsy on local tumor control and systemic immune responses [14, 49-53]. We sought to analyze the T cell based immune responses in canine patients treated with thermal ablation and histotripsy and found that it is highly patient dependent (Figure 3 & 7). Although by different mechanisms, in both treatment groups, patients showed an overall increased frequency of CD3+ T cells. Most treated patients demonstrated an increased frequency of IFN-Y expressing $CD3^{+}CD4^{+}$ and $CD3^{+}CD8^{+}$T cells in the blood, as compared with the pre-treatment levels. This is in line with study by Lu et. al., increased tumor infiltrating lymphocytes (TILs) particularly cytotoxic CD8+ cells and NK cells after HIFU ablation of human breast cancer [51]. Clinical evidences suggest that ablative HIFU treatment may also enhance local antitumor immunity in prostate cancer patients [54] and upregulated expression of HSP70 in breast cancer tumor debris [55]. Studies investigating this have linked these pro-oncogenic effects to upregulation of inflammatory pathways in this region, including the IL-6-HGF/c-Met-STAT3-VEGF axis and the HSP70 related pathways [56-58]. Distinctively, histotripsy generates subcellular fragments through mechanical fractionation, releasing damage associated molecular patterns (DAMPs) which, in turn, enhance tumor inflammation, and anti-tumor immune effects [9, 48, 59, 60]. In addition, critical cytokines and chemokines have been found to be significantly altered, especially IFN-Y, in multiple histotripsy studies [9, 15, 61, 62], which is consistent

with our clinical findings. While IFN--Y is the most consistently reported cytokine across therapies and tumor types, other important cytokines including IL-6, IL-2, TNF, IL-8, IL-13, and IL-10 have been reportedly upregulated post histotripsy treatment [9, 15, 53, 62]. Our present study lacks the investigation of the local and systemic cytokine/chemokine responses, but studies are underway to assess these important end points, which will help us in better assessing our clinical treatment outcomes. In contrast to mice studies reporting a reduction in Tregs post histotripsy [63], some of our patients showed an increased population of Tregs, with both histotripsy and ablation treatments. Therefore, a detailed study of the implication of the enhancement of these cell types will need to be performed to verify such effects in a larger cohort of patients.

A second major objective of our project was to evaluate the ability of HIFU hyperthermia to influence Dox delivery in veterinary patients with sarcoma tumors. HIFU mediated mild-moderate hyperthermia (42- 45^0C) has been shown to increase vascular as well as cellular permeability, and enhance the metabolic activity of the hyperthermic targets [3]. Our data suggests that addition hyperthermia to intravenous Dox therapy enhanced drug delivery in the heated regions of the tumor (Figure 9). This is in line with several studies that have shown that elevating and maintaining tissue temperature to a mild 42°C for several minutes can increase blood flow and drug absorption in the targeted region [64]. Hyperthermia increases blood flow to the heated region, increasing tissue perfusion drastically [18] which also increases oxygen delivery to the area, thus enhancing the metabolic activity and sensitivity of the targeted cells to drugs [65]. All patients were given a single treatment of the combination therapy and assessed longitudinally over 8 weeks (Table 4; Figure 10). Tumor regressions were observed in all 3 patients at 1-2 weeks post-treatment. however,

with a single treatment, the tumors started to grow back for all patients at 3 weeks post-treatment. This suggests that a greater number of treatments, 2 weeks apart, may enhance the anti-tumor response by keeping the tumor growth in check and inducing further tumor regressions. It is important to note that since each patient served as an internal control for non-heated tumor region, only ~40% of the tumor mass was given local hyperthermia treatment. It is possible that if the entire tumor mass was to be heated, it would induce a better tumor regression response to the hyperthermia + Dox treatment. Immunologically, the local and systemic T-cell responses were supportive of the tumor regressions seen at 1-2 weeks post-treatment (Figure 10). Statistically significant levels of $CD3^+$ T cells were observed in the tumor biopsies at 2-weeks post-treatment, along-with an increase in the $CD4^+$ and anti-tumoral $CD8^+$ T cell subsets. Additionally, release of IFN-Y , which is a key moderator of cellular immunity and CD8 T cell cytotoxic functions [66], was seen to be increased locally and systemically. However, there was a dip in the IFN-Y levels, accompanied by a substantial increase in the Treg population, at 2-weeks post-treatment. This may be indicative of a waning anti-tumoral immune response stimulated by the treatment and could explain the sudden and subsequent increase in tumor size after the 3-week follow-up.

In addition, we compared Dox alone therapy with LTSLs loaded with Dox. When local hyperthermia is applied to tumor tissue, the heat accentuates the leakiness of tumor vasculature caused more LTSLs to be carried into the tumor, as well as to release their contents rapidly ‘on-demand, directly into the tumor tissue. This is based on studies from our lab and others that demonstrate the efficacy of HIFU hyperthermia triggered drug release and accumulation using TSL (temperature-sensitive liposomal) formulations [21,

22, 67]. Furthermore, Hauck et. al., performed a similar phase I pharmacokinetic trial of liposome-encapsulated Dox combined with microwave induced local hyperthermia in canine sarcomas and carcinomas [68]. Twenty-one patients were treated with LTSL-Dox (0.7-1.0 mg/kg body weight) and toxicity and pharmacokinetic profiles were evaluated. They reported decreased plasma Dox clearance with LTSL compared to free Dox as well as ~10-fold higher intra-tumoral drug levels at 1.0 mg/kg dose levels. With our dose rate of 0.7 mg/kg body weight, we saw similar increases in intra-tumoral Dox levels of ~4-fold and ~2-fold in the heated and unheated regions, respectively, compared to the Dox alone cohorts (Figure 12). This is further supported by a clinical trial in phase 1 human clinical trial that demonstrated the safety and feasibility of ultrasound-triggered Dox delivery from LTSLs in liver tumors [69]. Additional plasma pharmacokinetic studies are currently ongoing to determine Dox clearance levels in Dox alone and LTSL treated patients in the current study. The patients treated with ThermoDox combination were given appropriate premedication and did not show any treatment/dose related renal or cardiac toxicities [68]. The 3 patients enrolled in this group had different types of sarcomas, unlike the Dox alone group which had patients with soft tissue sarcomas. Thus, results and hence the discussion is reported case-wise. Although patient #4 (Table 4) showed tumor regressions at 1-week post-treatment, accompanied by an increased levels of $CD3^+$ T cells in the blood (Figure 12), the case dropped out of the study due to overall old age and weak health. Similarly, patient #5 had to be euthanized at 1-week post-treatment due to significant metastasis, despite some improvements in clinical symptoms as reported by the owner. Since this patient had metastasis and was too old to be repeatedly anesthetized for CT tumor measurements, post-treatment tumor regression

data could not be obtained (Table 4). Immunologically though, patient #5 showed promising results with enhanced $CD3^+$ T cells and anti-tumoral $CD3^+CD8^+$ T cells in the blood (Figure 13). This was accompanied by a slight decrease in Tregs, which are known to hamper effective antitumor immunity. Moreover, this trend was also observed in post-mortem tumor biopsy samples of the heated region, compared to the control unheated region. These results agree with reports that show that temperature-sensitive drug-loaded nanoparticles can induce immunogenic cell death and facilitate the antigen-presenting ability of DCs to naive T cells, further promoting their differentiation into CTLs rather than Tregs [11, 70, 71]. This suggests that in high grade tumors like sarcomas, combinatorial treatments can induce a robust anti-tumoral response.

Clinical trials include studies that test new drugs, devices, or other forms of treatments. Many clinical trials look at new ways of diagnosing, detecting, or even preventing diseases (American Cancer Society). They are usually designed to answer important questions not limited to but including- Does the new treatment/device work? Is it safe? Do the benefits outweigh the associated risks, if any? Is the new treatment better than the standard-of-care treatment? Answering these questions usually requires to be done in steps or ‘phases’ that build on one another, each designed to answer specific questions pertaining to the treatment/device being tested. Following this stepwise procedure ensures patient safety as well as accuracy of results [72]. Our pilot studies, testing the feasibility and effectiveness of HIFU for the treatment of a variety of solid tumors in dogs, encompass the goals of phase I and some phase II clinical trials, as described in Table 5. Building on the current data, further studies will be planned to advance our knowledge regarding efficacy and applicability of HIFU in veterinary science.

In summary, the tumor remissions were durable in low-grade tumors in patients who underwent ablative treatments. Assessing the same in high grade tumors can help establish this technology as a possible surgical adjuvant. Ablative therapy can cause significant adverse effects. Although most can be managed by hyperbaric oxygen therapy or by other available interventions, additional investigations using histotripsy protocols that targets the entire tumor volume in one-session or a mixture of ablation/histotripsy protocols can hypothetically further improve outcomes. LTSL+ HIFU demonstrated greater Dox delivery compared to other treatments, presumably due to higher release of encapsulated content from LTSLs. It also appears that enhanced Dox delivery in sarcoma tumors correlates with improved local and systemic antitumor immunity, and tumor regressions. More longitudinal studies need to be carried out in a larger cohort of patients to generate statistically significant correlations. Additional systemic and local immune analyses of other innate and adaptive cell populations as well as cytokine and chemokine measurements, need to be included in the study design. Together, results from these initial pilot studies demonstrate the effectiveness of HIFU for non-invasive treatment of spontaneous canine tumors and the potential of utilizing veterinary oncology populations for conducting more clinically relevant studies for cancer applications.

	What happens in different phases of clinical trials?			
Phase	**What doctors want to learn**	**Type of treatment being tested**	**Do people in the clinical trial get different treatments?**	**Length and number of people**
Phase I	If the new drug or treatment is safe. The highest dose of a treatment that people can get without major side effects or problems.	A new drug, medical device, test, or surgery.	Everyone gets the same treatment. But people might get different strengths or amounts.	10 to 30 people Several months to a year.
Phase II	If the new drug or treatment works.	A new drug, medical device, test, surgery, or combination of treatments.	People sometimes get different treatments. This depends on the clinical trial.	Up to several hundred people. About 2 years.
Phase III	If the new drug or treatment works better than the regular treatment.	A new drug, medical device, surgery, test, or combination of treatments.	People get different treatments. Doctors compare the new drug or treatment with the regular one.	300 to 3,000 people. Several years.
Phase IV	What happens once doctors are using the new drug or treatment.	A new drug, medical device, surgery, test, or combination of treatments.	People do not get different treatments. Doctors only collect information on what happens with the treatment they are studying.	Thousands of people. Several years to many years.

Table 5. Different phases of clinical trials. Source: http://www.cancer.net/clinicaltrials

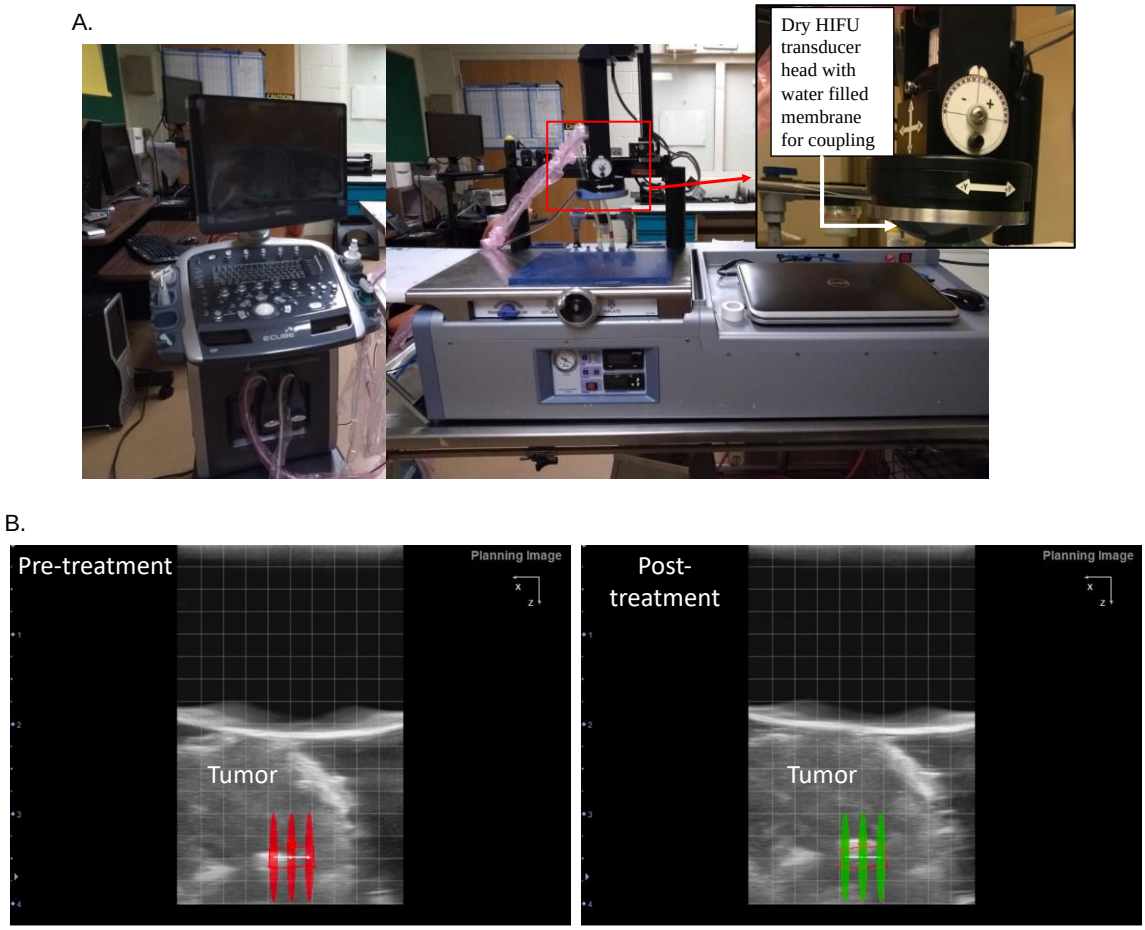

Figure 1. Ultrasound-guided high-intensity focused ultrasound system used for dog treatments. A. The figure inset shows the treatment transducer filled with distilled water, with a membrane. The membrane can be inflated to adjust for the depth at which the target lesion needs to be treated, and B. The VIFU planning software was used to select the region of interest and target boundaries for automatic raster treatment.

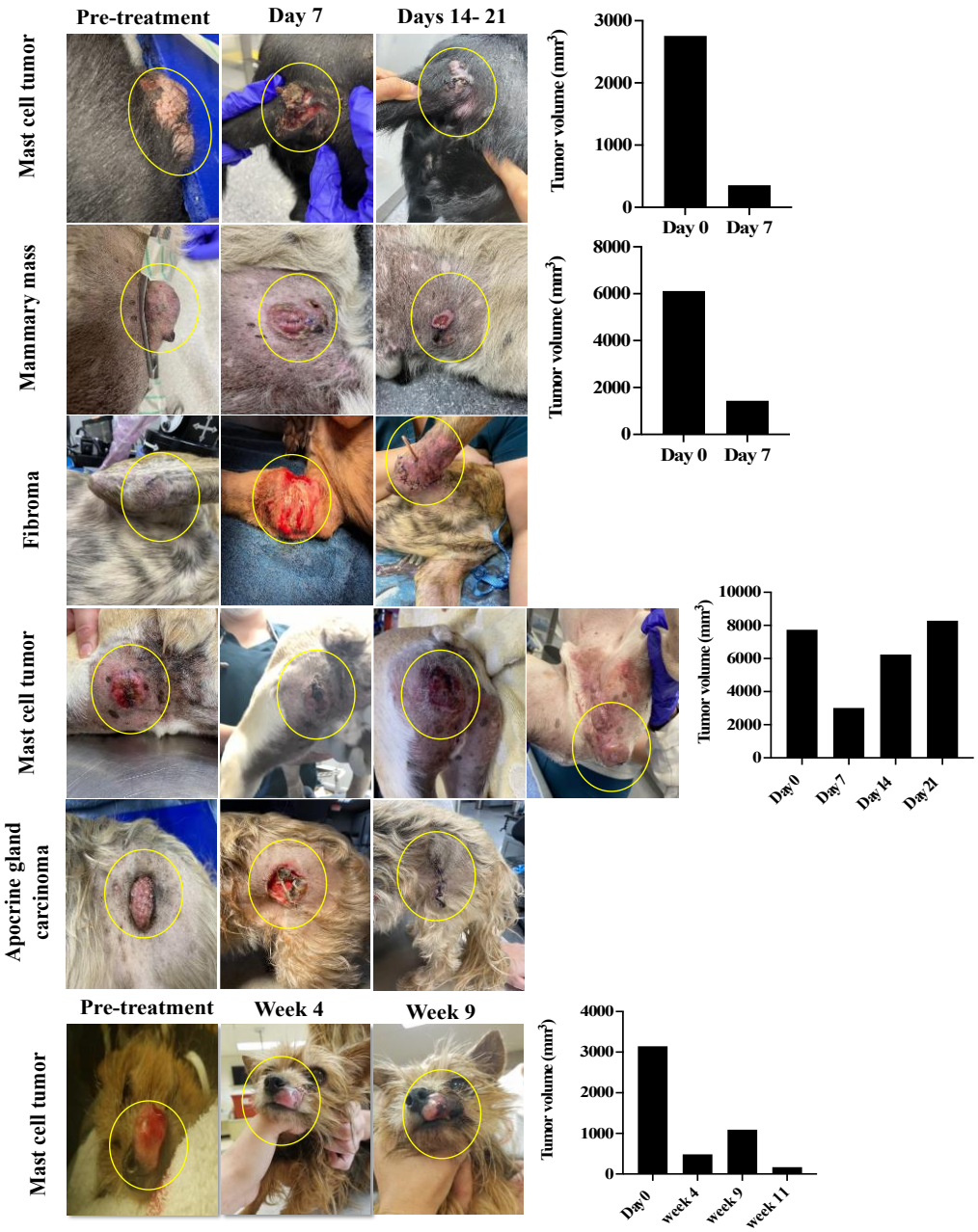

Figure 2. Representative images showing changes in tumors post treatment with thermal ablation protocol. Tumor remissions for most cases were noted around day 7, and the masses became undetectable after 2-weeks. In some cases, minor to significant damage of skin and adjoining tissues were observed, and the cases were managed by surgical intervention.

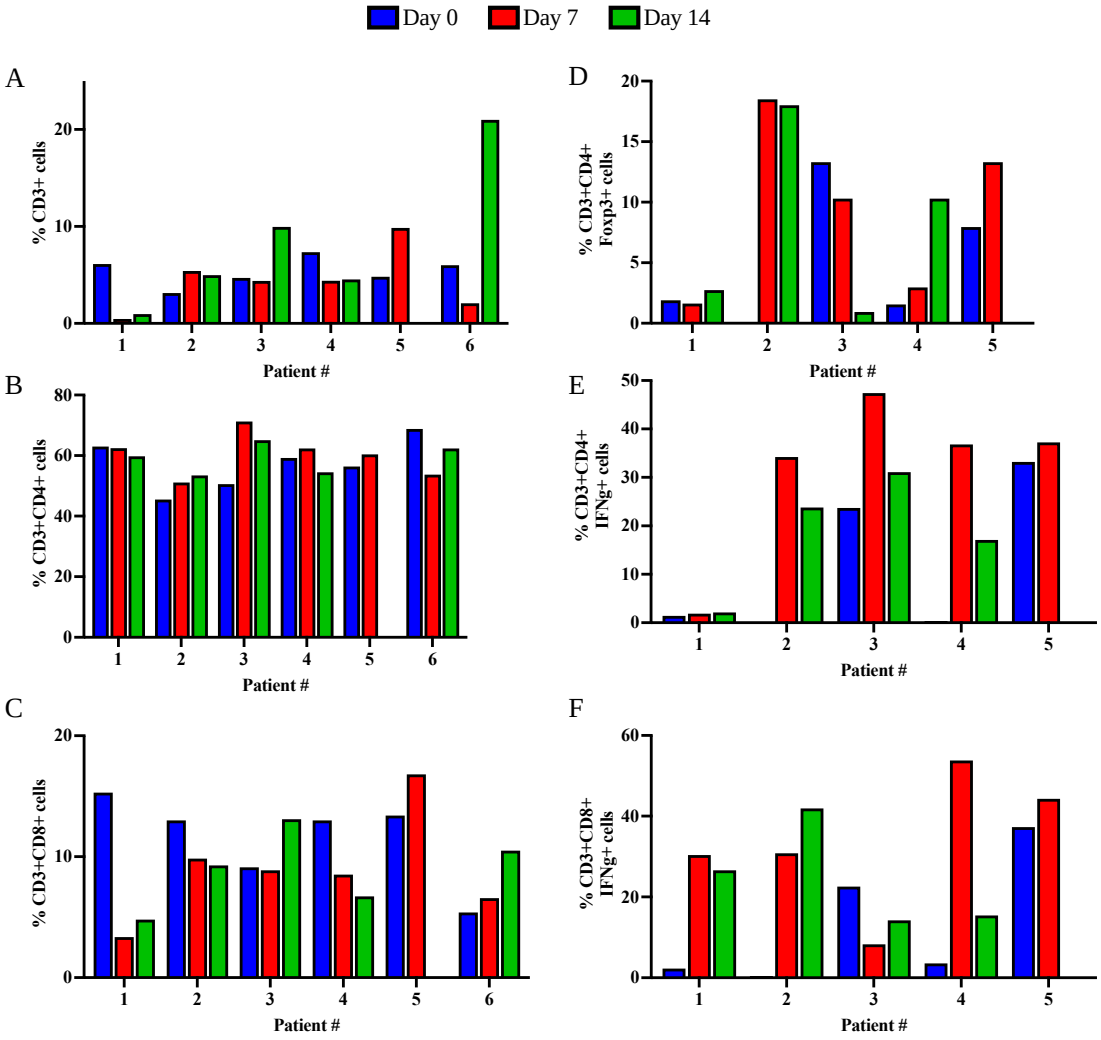

Figure 3. Immunological analyses of blood samples of ablation-treated patients. A-F) Trends in the treatment effects on T cells in the blood over time, relative to the pre-treatment controls. Patient# 3, 5 & 6 showed an overall increased frequency of CD3+ T cells. Most treated patients demonstrated an increased frequency of IFN-Y expressing $CD3^{+}CD4^{+}$ and $CD3^{+}CD8^{+}$T cells 1-2 weeks post-treatment in the blood, as compared with the pre-treatment levels. An increased population of Tregs was also observed in patient #2, 4 and 5.

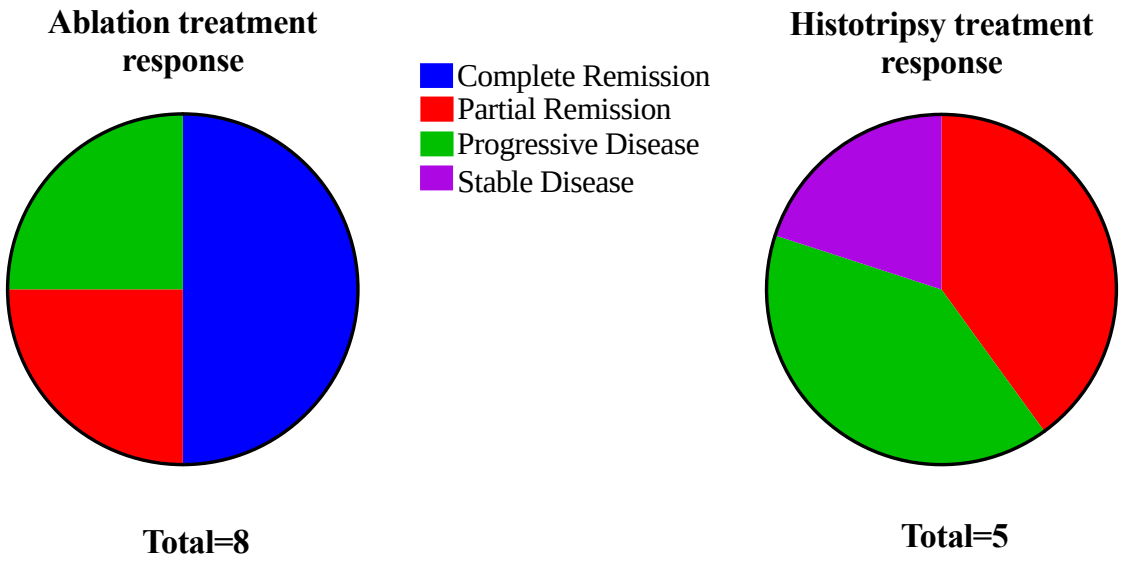

Figure 4. Comparison of overall treatment response with HIFU- mediated thermal ablation vs. non-thermal histotripsy treatments. 4 out of the 8 patients treated with ablation, showed complete remission within 1-2 weeks post-treatment. Of the remaining 4 patients, 2 showed partial remission with more follow-ups needed to determine case outcome, while the other 2 were unresponsive to treatment with progressive disease. From the histotripsy treated cohorts, 2 showed partial regression, 1 showed stable disease and the remaining 2 showed progressive disease.

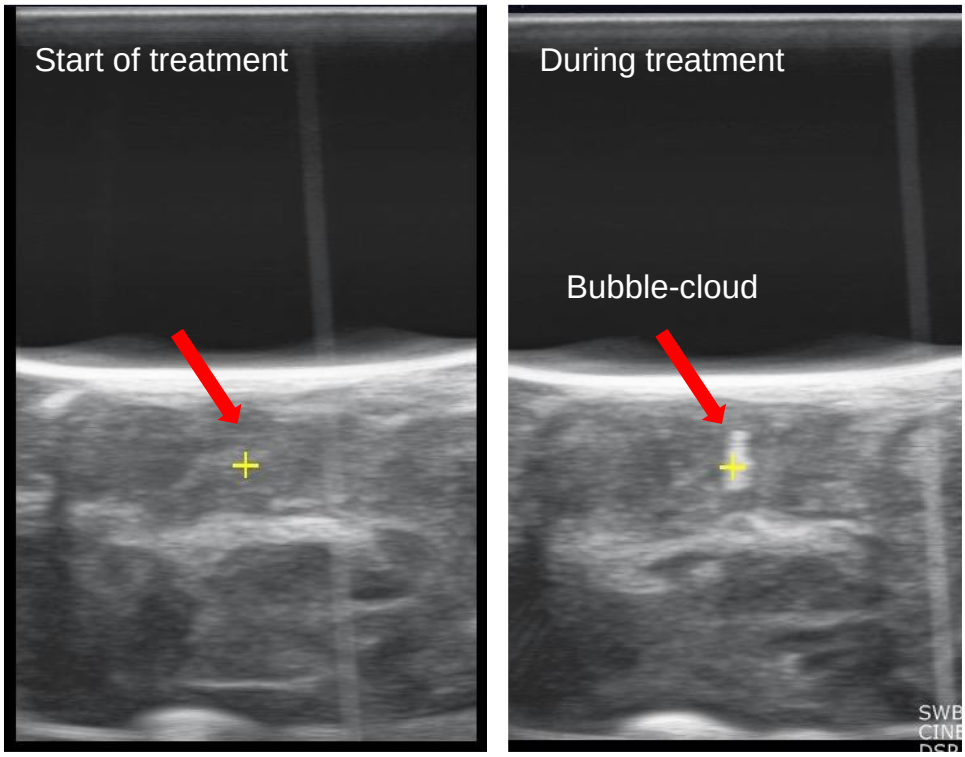

Figure 5. Visualizing the histotripsy cavitation process. Bubble cloud formation generated from intrinsic gas nuclei was captured on the ultrasound imaging during histotripsy treatment of the tumors.

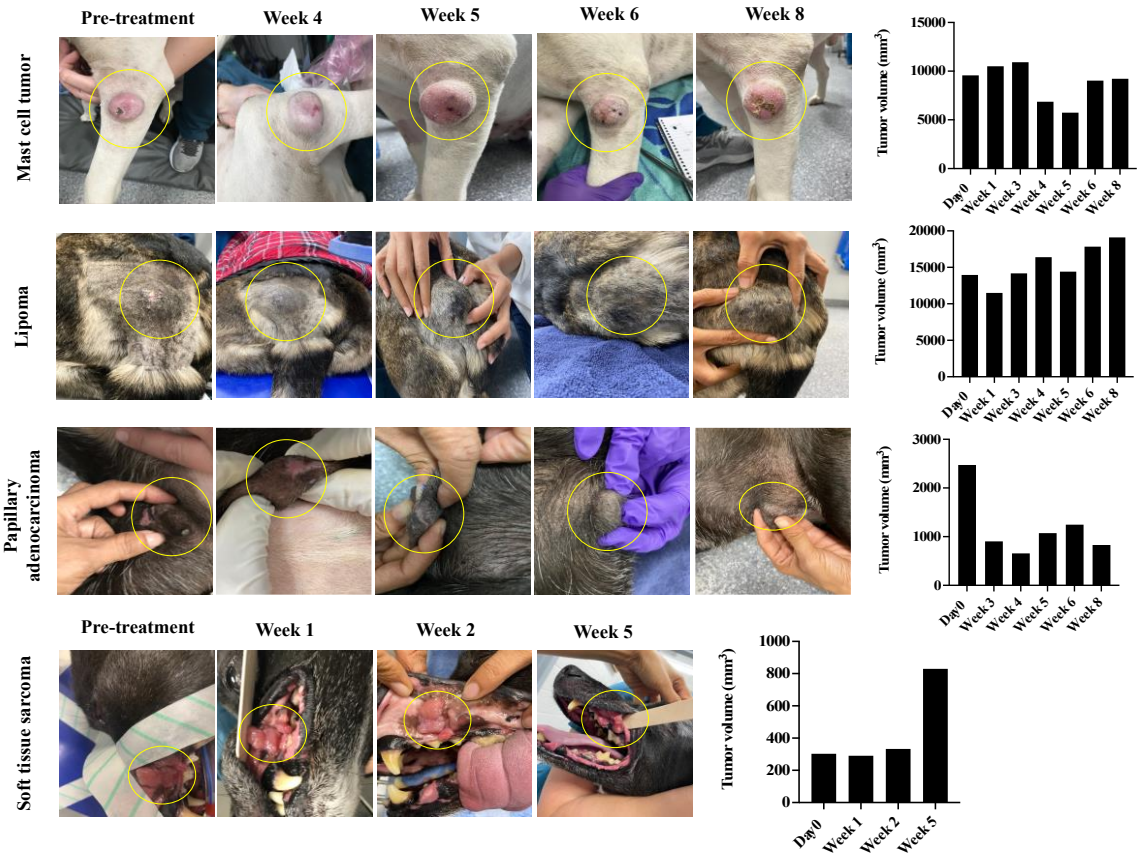

Figure 6. Representative images showing changes in tumors post treatment with histotripsy protocol. Histotripsy attained partial to stable disease in the treated patients. No adverse effects were noted in the treated patients.

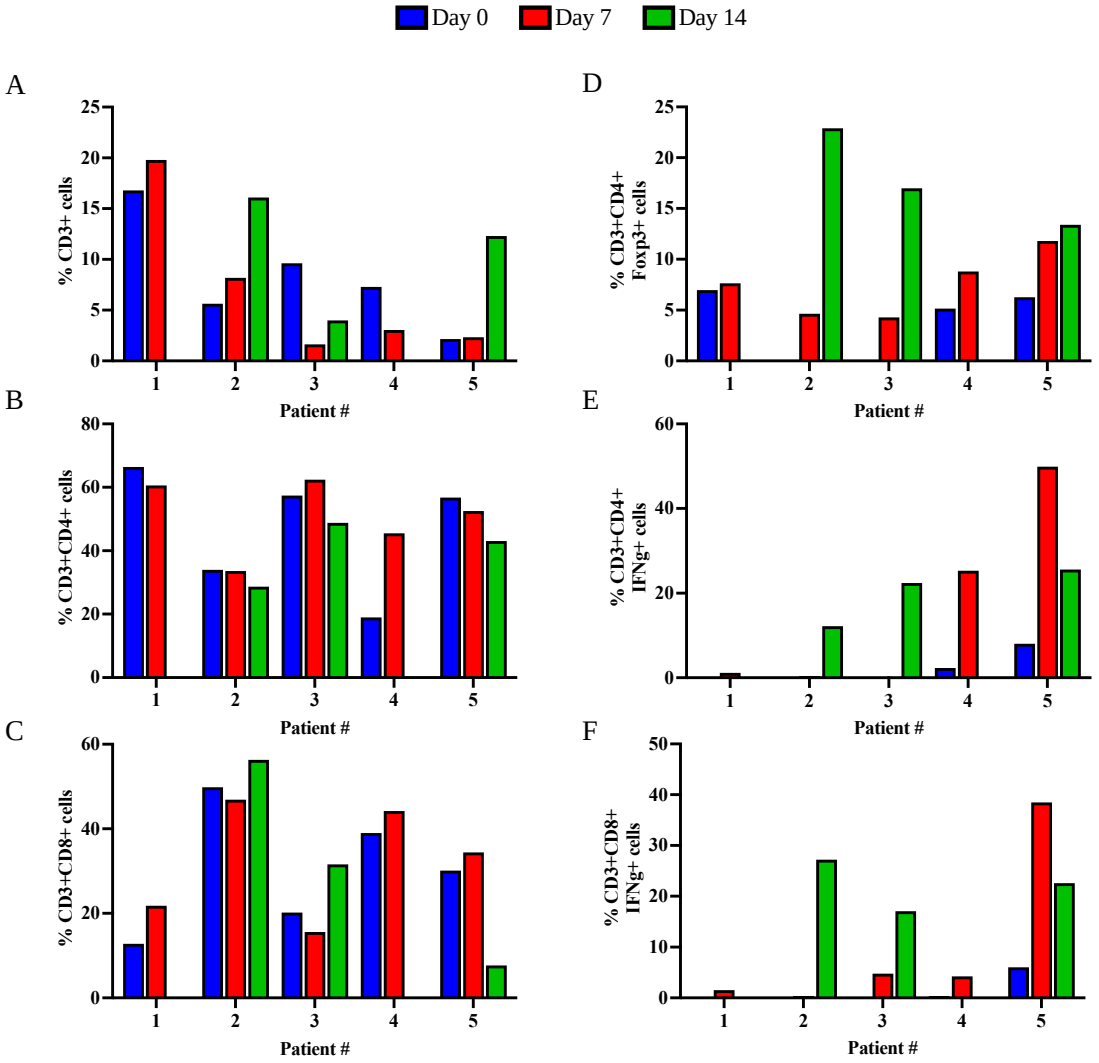

Figure 7. Immunological analyses of blood samples of histotripsy-treated patients. A-F) Patient #1,2 & 5 showed an increased frequency of $CD3^+$ T cells. Most treated patients demonstrated an increased frequency of $CD3^+CD4^+$ and IFN-Y expressing $CD3^+CD4^+$ and $CD8^+$ T cells at 1-2 weeks post-treatment, as compared with the pre-treatment levels. A concurrent increase in Treg populations was also observed in most patients.

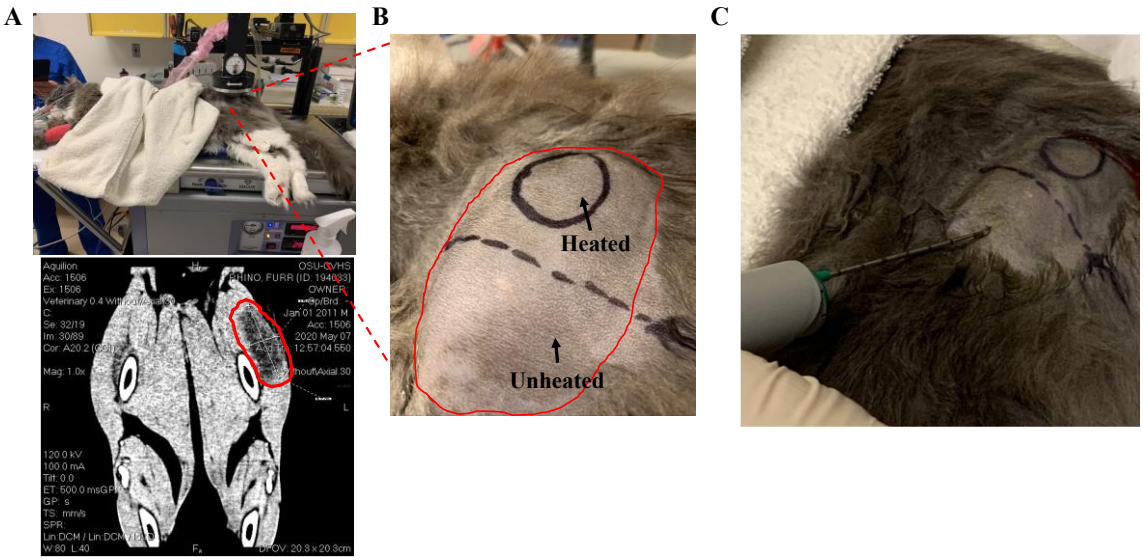

Figure 8. Representative images showing the HIFU hyperthermia + chemotherapy treatment distribution and sample collection. A) Representative image of combination treatment in patient #6 (cat patient) with spindle cell sarcoma in the hip region close to the femur (CT). B) Treatment regions were divided into HIFU heated and unheated parts. C) Biopsies were collected from the farther ends of the respective regions for estimation of Dox delivery by the combination therapy.

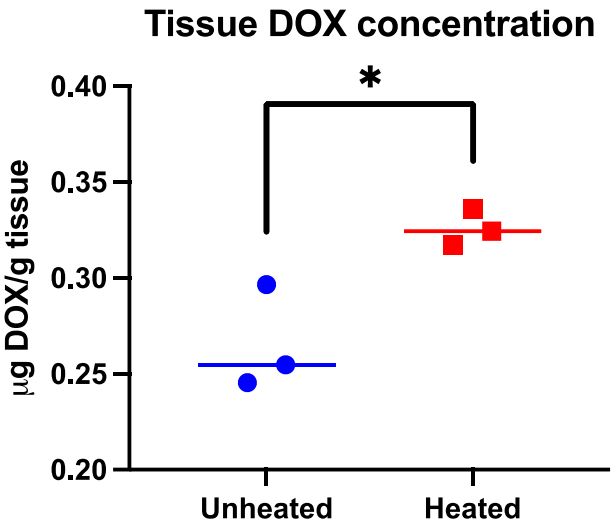

Figure 9. Drug delivery in µg Dox/g of tumor in the heated and unheated regions of tumors. Following HIFU initiation, a 0.7 mg/kg body weight I/V injection of doxorubicin alone was given to all the patients. Data are shown as mean Dox concentration ± standard error of mean (n=3; pairwise comparison; *Indicates significant difference with unheated region; $p<0.05$).

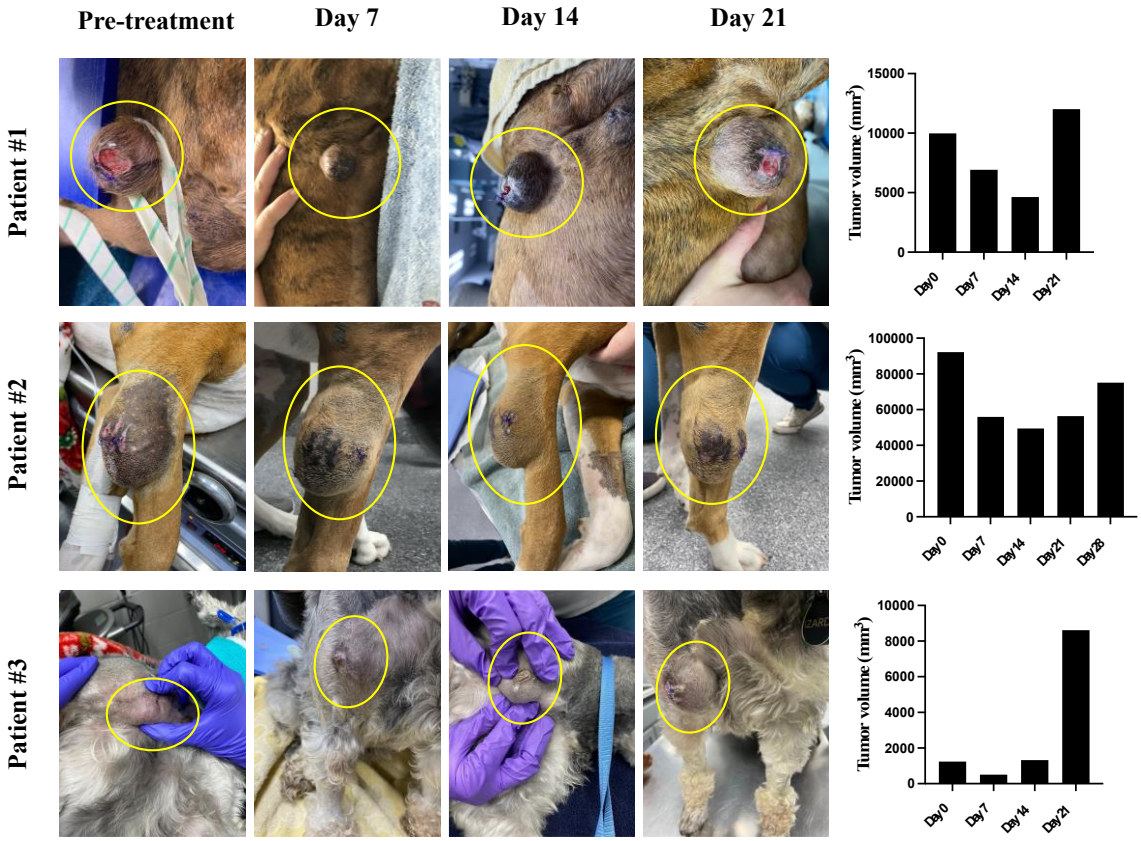

Figure 10. Representative images showing changes in tumors post treatment with hyperthermia + Dox protocol. Tumor regressions were observed in all patients at 1-2 weeks post-treatment. With a single treatment, tumors grew back for all patients at 3 weeks post-treatment.

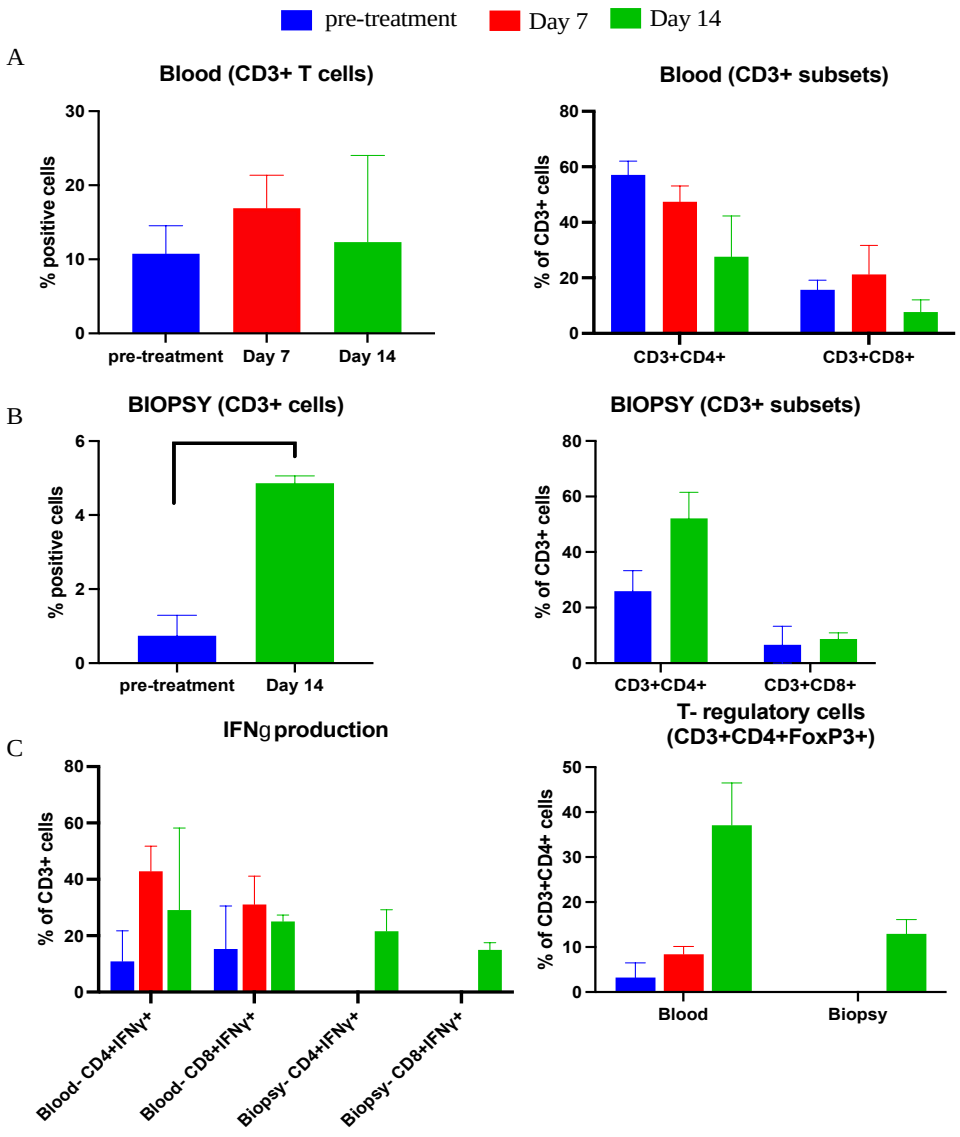

Figure 11. Immunological analyses of blood and biopsy samples of combination (Dox alone)-treated patients. A-B) Trends in the treatment effects on T cells in the tumor and blood over time, relative to the pre-treatment levels. Tumor biopsy samples showed significant infiltration of $CD3^+$ lymphocytes and an increased frequency of $CD3^+CD4^+$ T cells post HIFU + Dox treatment. C) Increased frequency of IFN-Y expressing $CD3^+CD4^+$T cells and $CD3^+CD8^+$T cells as well as Tregs at 1-2 weeks post-treatment in the tumor and blood, as compared with the pre-treatment levels.

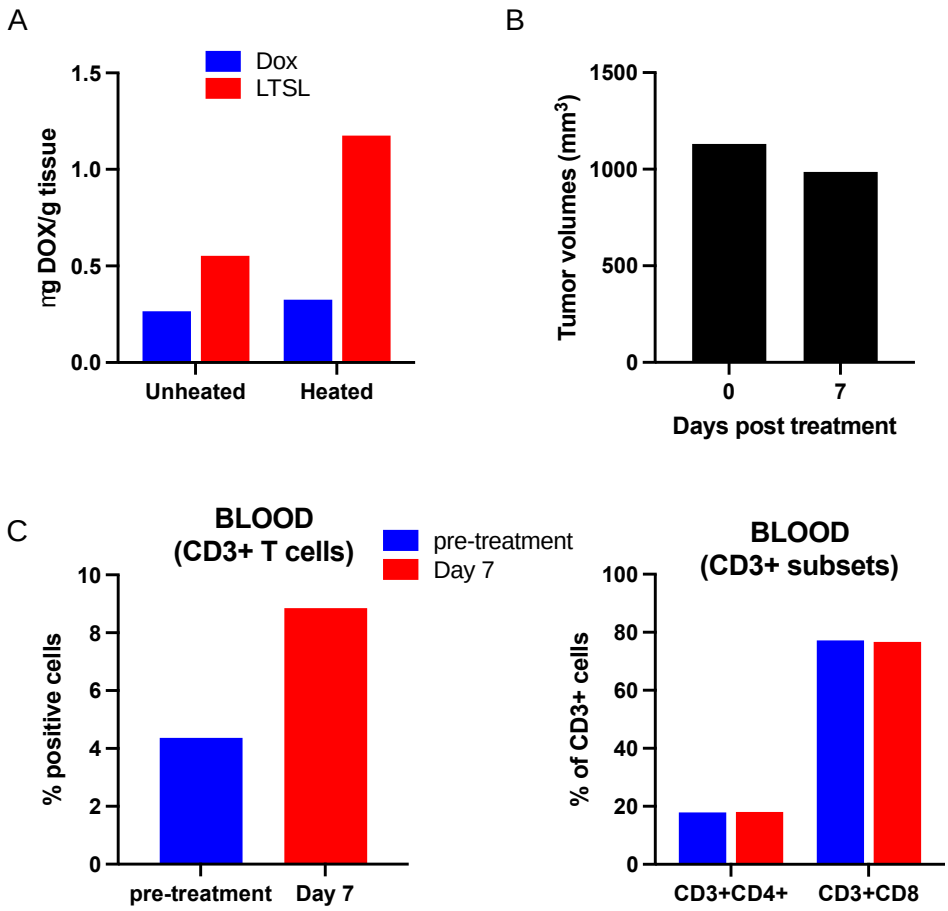

Figure 12. Treatment outcomes of patient #4 treated with combination hyperthermia + LTSL therapy. A) Comparison of µg Dox/g of tumor for heated and unheated regions of tumors following a 0.7 mg/kg body weight injection of LTSL and Dox alone. LTSL enhanced Dox delivery to the heated regions compared to the unheated and Dox alone controls. B) Tumor slightly regressed at day 7 post-treatment. C) An enhanced population of CD3+ T cell was noted on day 7, however, this was not associated with changes in the $CD3^{+}CD4^{+}$ and $CD3^{+}CD8^{+}$ subsets.

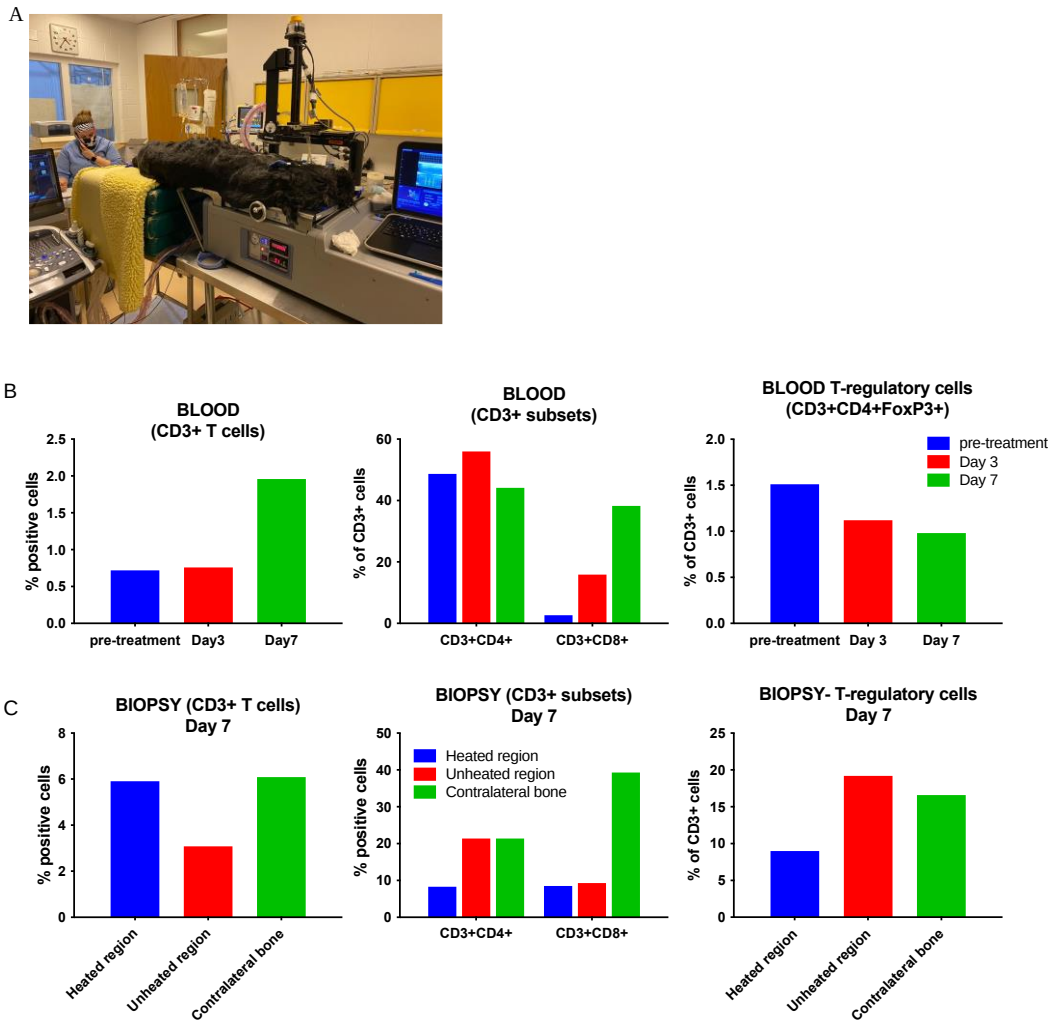

Figure 13. Treatment outcomes of patient #5 treated with combination hyperthermia + LTSL therapy. A) Image showing positioning and treatment of the dog with HIFU B) An enhanced population of $CD3^+$ T cells was noted on day 7. Additionally, a trend towards an increased frequency of $CD3^+CD8^+$ T cells and a slight decrease in the populations of Tregs in blood was observed C) Post-mortem analysis of biopsy tissue indicated increased levels of $CD3^+$ T cells in the heated region of tumor and contralateral bone, compared to the unheated region. Presence of $CD4^+$ and $CD8^+$ T cell subsets observed in the biopsies and a decreased Treg population in the heated region as compared to the unheated region and contralateral bone.

References

1. Thamm, D.H., *Canine cancer: strategies in experimental therapeutics.* Frontiers in oncology, 2019. **9**: p. 1257.
2. Bachu, V.S., et al., *High-Intensity Focused Ultrasound: A Review of Mechanisms and Clinical Applications.* Ann Biomed Eng, 2021.
3. Foundation, F.U. *An Overview of the Biological Effects of Focused Ultrasound*. 2015.
4. van den Bijgaart, R.J., et al., *Thermal and mechanical high-intensity focused ultrasound: perspectives on tumor ablation, immune effects and combination strategies.* Cancer Immunol Immunother, 2017. **66**(2): p. 247-258.
5. Chu, K.F. and D.E. Dupuy, *Thermal ablation of tumours: biological mechanisms and advances in therapy.* Nature Reviews Cancer, 2014. **14**(3): p. 199-208.
6. den Brok, M.H., et al., *In situ tumor ablation creates an antigen source for the generation of antitumor immunity.* Cancer research, 2004. **64**(11): p. 4024-4029.
7. Ito, F., et al., *In situ thermal ablation augments antitumor efficacy of adoptive T cell therapy.* International Journal of Hyperthermia, 2019. **36**(sup1): p. 22-36.
8. Wissniowski, T.T., et al., *Activation of tumor-specific T lymphocytes by radio-frequency ablation of the VX2 hepatoma in rabbits.* Cancer research, 2003. **63**(19): p. 6496-6500.
9. Eranki, A., et al., *High-Intensity Focused Ultrasound (HIFU) Triggers Immune Sensitization of Refractory Murine Neuroblastoma to Checkpoint Inhibitor Therapy.* Clinical Cancer Research, 2020. **26**(5): p. 1152-1161.
10. Singh, M.P., et al., *Boiling histotripsy and in-situ CD40 stimulation improve the checkpoint blockade therapy of poorly immunogenic tumors.* Theranostics, 2021. **11**(2): p. 540.
11. Sethuraman, S.N., et al., *Novel calreticulin-nanoparticle in combination with focused ultrasound induces immunogenic cell death in melanoma to enhance antitumor immunity.* Theranostics, 2020. **10**(8): p. 3397.
12. Ektate, K., et al., *Chemo-immunotherapy of colon cancer with focused ultrasound and Salmonella-laden temperature sensitive liposomes (thermobots).* Scientific Reports, 2018. **8**(1): p. 13062.
13. Wu, F., et al., *Activated anti-tumor immunity in cancer patients after high intensity focused ultrasound ablation.* 2004. **30**(9): p. 1217-1222.
14. Hendricks-Wenger, A., et al., *Immunological Effects of Histotripsy for Cancer Therapy.* Frontiers in Oncology, 2021. **11**: p. 1999.
15. Qu, S., et al., *Non-thermal histotripsy tumor ablation promotes abscopal immune responses that enhance cancer immunotherapy.* Journal for immunotherapy of cancer, 2020. **8**(1).
16. Hurwitz, M.D., *Hyperthermia and immunotherapy: clinical opportunities.* International Journal of Hyperthermia, 2019. **36**(sup1): p. 4-9.

17. May, J.P. and S.-D. Li, *Hyperthermia-induced drug targeting.* Expert opinion on drug delivery, 2013. **10**(4): p. 511-527.
18. PAWAR, P. and M. JOSHI, *Hyperthermia Therapy in Cancer Treatment.* 2013.
19. Seward, M.C., et al., *Feasibility of targeting canine soft tissue sarcoma with MR-guided high-intensity focused ultrasound.* International Journal of Hyperthermia, 2018. **35**(1): p. 205-215.
20. Ryu, M.O., et al., *Treatment of solid tumors in dogs using veterinary high-intensity focused ultrasound: A retrospective clinical study.* The Veterinary Journal, 2018. **234**: p. 126-129.
21. Ektate, K.P., *Development of Targeted Liposomal Formulation Approaches for Enhanced Colorectal Cancer Therapy*. 2019, Oklahoma State University: Ann Arbor. p. 137.
22. VanOsdol, J., et al., *Sequential HIFU heating and nanobubble encapsulation provide efficient drug penetration from stealth and temperature sensitive liposomes in colon cancer.* Journal of controlled release : official journal of the Controlled Release Society, 2017. **247**: p. 55-63.
23. Nguyen, S., et al., *Response evaluation criteria for solid tumours in dogs (v1. 0): a Veterinary Cooperative Oncology Group (VCOG) consensus document.* Veterinary and comparative oncology, 2015. **13**(3): p. 176-183.
24. Staruch, R., R. Chopra, and K. Hynynen, *Hyperthermia in bone generated with MR imaging–controlled focused ultrasound: Control strategies and drug delivery.* Radiology, 2012. **263**(1): p. 117-127.
25. Fleming, J., K. Creevy, and D. Promislow, *Mortality in North American dogs from 1984 to 2004: an investigation into age-, size-, and breed-related causes of death.* Journal of Veterinary Internal Medicine, 2011. **25**(2): p. 187-198.
26. Alvarez, C.E., *Naturally occurring cancers in dogs: insights for translational genetics and medicine.* ILAR journal, 2014. **55**(1): p. 16-45.
27. Maloney, E. and J.H. Hwang, *Emerging HIFU applications in cancer therapy.* Int J Hyperthermia, 2015. **31**(3): p. 302-9.
28. Vail, D.M. and E.G. Macewen, *Spontaneously occurring tumors of companion animals as models for human cancer.* Cancer investigation, 2000. **18**(8): p. 781-792.
29. MacEwen, E.G., *Spontaneous tumors in dogs and cats: models for the study of cancer biology and treatment.* Cancer and Metastasis Reviews, 1990. **9**(2): p. 125-136.
30. Gillette, S.M., et al., *Response of canine soft tissue sarcomas to radiation or radiation plus hyperthermia: a randomized phase II study.* International journal of hyperthermia, 1992. **8**(3): p. 309-320.
31. Gillette, E.L., S.L. McChesney, and P.J. Hoopes, *Isoeffect curves for radiation-induced cardiomyopathy in the dog.* International Journal of Radiation Oncology* Biology* Physics, 1985. **11**(12): p. 2091-2097.
32. Gavin, P.R. and E.L. Gillette, *Radiation response of the canine cardiovascular system.* Radiation research, 1982. **90**(3): p. 489-500.
33. Gillette, E.L., G.D. Maurer, and G.A. Severin, *Endothelial repair of radiation damage following beta irradiation.* Radiology, 1975. **116**(1): p. 175-177.

34. Withrow, S.J. and R.M. Wilkins, *Cross talk from pets to people: translational osteosarcoma treatments.* ILAR journal, 2010. **51**(3): p. 208-213.
35. Webb, H., M.G. Lubner, and J.L. Hinshaw. *Thermal ablation*. in *Seminars in roentgenology*. 2011. Elsevier.
36. Jang, H.J., et al., *Current and future clinical applications of high-intensity focused ultrasound (HIFU) for pancreatic cancer.* Gut and liver, 2010. **4**(Suppl 1): p. S57.
37. Ranjan, A., et al., *Focused ultrasound ablation of a large canine oral tumor achieves efficient tumor remission: a case report.* International Journal of Hyperthermia, 2021. **38**(1): p. 552-560.
38. Kopelman, D., et al., *Magnetic resonance-guided focused ultrasound surgery (MRgFUS). Four ablation treatments of a single canine hepatocellular adenoma.* HPB, 2006. **8**(4): p. 292-298.
39. Sfiligoi, G., et al., *Outcome of dogs with mast cell tumors in the inguinal or perineal region versus other cutaneous locations: 124 cases (1990–2001).* Journal of the American Veterinary Medical Association, 2005. **226**(8): p. 1368-1374.
40. Garrett, L.D., *Canine mast cell tumors: diagnosis, treatment, and prognosis.* Veterinary Medicine: Research and Reports, 2014. **5**: p. 49.
41. Leighton, T., *The Acoustic Bubble.| Academic.* Press, London, 1994: p. 234-243.
42. Wrenn, S.P., et al., *Bursting bubbles and bilayers.* Theranostics, 2012. **2**(12): p. 1140.
43. Hempel, C.R., et al., *Histotripsy fractionation of prostate tissue: local effects and systemic response in a canine model.* The Journal of urology, 2011. **185**(4): p. 1484-1489.
44. Schade, G.R., et al., *Histotripsy focal ablation of implanted prostate tumor in an ACE-1 canine cancer model.* The Journal of urology, 2012. **188**(5): p. 1957-1964.
45. Hall, T.L., et al., *Histotripsy of the prostate: dose effects in a chronic canine model.* Urology, 2009. **74**(4): p. 932-937.
46. Hendricks-Wenger, A., et al., *Histotripsy Ablation in Preclinical Animal Models of Cancer and Spontaneous Tumors in Veterinary Patients: A Review.* IEEE Transactions on Ultrasonics, Ferroelectrics, and Frequency Control, 2021.
47. Park, J.-H., et al., *High intensity focused ultrasound treatment-induced tumor lysis syndrome in uterine myoma patient.* Soonchunhyang Medical Science, 2015. **21**(2): p. 99-101.
48. Eranki, A., et al., *Mechanical fractionation of tissues using microsecond-long HIFU pulses on a clinical MR-HIFU system.* International Journal of Hyperthermia, 2018. **34**(8): p. 1213-1224.
49. Dromi, S.A., et al., *Radiofrequency ablation induces antigen-presenting cell infiltration and amplification of weak tumor-induced immunity.* Radiology, 2009. **251**(1): p. 58-66.
50. Kruse, D., et al., *Short-duration-focused ultrasound stimulation of Hsp70 expression in vivo.* Physics in Medicine & Biology, 2008. **53**(13): p. 3641.
51. Lu, P., et al., *Increased infiltration of activated tumor-infiltrating lymphocytes after high intensity focused ultrasound ablation of human breast cancer.* Surgery, 2009. **145**(3): p. 286-293.

52. Widenmeyer, M., et al., *Analysis of tumor antigen-specific T cells and antibodies in cancer patients treated with radiofrequency ablation.* International Journal of Cancer, 2011. **128**(11): p. 2653-2662.
53. Schade, G.R., *Evaluation of the Systemic Response to Boiling Histotripsy Treatment for Renal Carcinoma.*
54. Kramer, G., et al., *Response to sublethal heat treatment of prostatic tumor cells and of prostatic tumor infiltrating T-cells.* The Prostate, 2004. **58**(2): p. 109-120.
55. Wu, F., et al., *Expression of tumor antigens and heat-shock protein 70 in breast cancer cells after high-intensity focused ultrasound ablation.* Annals of surgical oncology, 2007. **14**(3): p. 1237-1242.
56. Velez, E., et al., *Hepatic thermal ablation: effect of device and heating parameters on local tissue reactions and distant tumor growth.* Radiology, 2016. **281**(3): p. 782-792.
57. Ahmed, M., et al., *Hepatic radiofrequency ablation–induced stimulation of distant tumor growth is suppressed by c-Met inhibition.* Radiology, 2016. **279**(1): p. 103-117.
58. Ahmed, M., et al., *Radiofrequency ablation (RFA)-induced systemic tumor growth can be reduced by suppression of resultant heat shock proteins.* International Journal of Hyperthermia, 2018. **34**(7): p. 934-942.
59. Khokhlova, T.D., et al., *Controlled tissue emulsification produced by high intensity focused ultrasound shock waves and millisecond boiling.* The Journal of the Acoustical Society of America, 2011. **130**(5): p. 3498-3510.
60. Hu, Z., et al., *Investigation of HIFU-induced anti-tumor immunity in a murine tumor model.* Journal of translational medicine, 2007. **5**(1): p. 1-11.
61. Schade, G.R., et al., *Boiling histotripsy ablation of renal cell carcinoma in the eker rat promotes a systemic inflammatory response.* Ultrasound in medicine & biology, 2019. **45**(1): p. 137-147.
62. Pahk, K.J., et al., *Boiling Histotripsy-induced Partial Mechanical Ablation Modulates Tumour Microenvironment by Promoting Immunogenic Cell Death of Cancers.* Scientific reports, 2019. **9**(1): p. 1-12.
63. Huang, X., et al., *M-HIFU inhibits tumor growth, suppresses STAT3 activity and enhances tumor specific immunity in a transplant tumor model of prostate cancer.* PloS one, 2012. **7**(7): p. e41632.
64. Thanou, M. and W. Gedroyc, *MRI-guided focused ultrasound as a new method of drug delivery.* Journal of drug delivery, 2013. **2013**.
65. Ko, A. and M. Dollinger, *Everyone's guide to cancer therapy: How cancer is diagnosed, treated, and managed day to day*. 2008: Andrews McMeel Publishing.
66. Bhat, P., et al., *Interferon-γ derived from cytotoxic lymphocytes directly enhances their motility and cytotoxicity.* Cell death & disease, 2017. **8**(6): p. e2836-e2836.
67. Kneidl, B., et al., *Thermosensitive liposomal drug delivery systems: state of the art review.* International journal of nanomedicine, 2014. **9**: p. 4387.
68. Hauck, M.L., et al., *Phase I trial of doxorubicin-containing low temperature sensitive liposomes in spontaneous canine tumors.* Clinical Cancer Research, 2006. **12**(13): p. 4004-4010.
69. Lyon, P.C., et al., *Safety and feasibility of ultrasound-triggered targeted drug delivery of doxorubicin from thermosensitive liposomes in liver tumours*

(TARDOX): a single-centre, open-label, phase 1 trial. The Lancet Oncology, 2018. **19**(8): p. 1027-1039.
70. Singh, M.P., et al., *In-situ vaccination using focused ultrasound heating and anti-CD-40 agonistic antibody enhances T-cell mediated local and abscopal effects in murine melanoma.* International Journal of Hyperthermia, 2019. **36**(sup1): p. 64-73.
71. Qi, J., et al., *Synergistic effect of tumor chemo-immunotherapy induced by leukocyte-hitchhiking thermal-sensitive micelles.* 2021.
72. Sedgwick, P., *Phases of clinical trials.* BMJ, 2011. **343**.

CHAPTER IV

ANTIBIOTIC TREATMENT OF METHICILLIN-RESISTANT *S. AUREUS* (MRSA) BONE INFECTION CAN BE IMPROVED WITH FOCUSED ULTRASOUND COMBINED HEAT-SENSITIVE LIPOSOMES

This chapter is based on:

Harshini Ashar, Kalyani Ektate, Ashish Ranjan. "Feasibility of treating implant-associated osteomyelitis with focused ultrasound and antibiotic-laden thermally sensitive liposomes." *Focused Ultrasound Symposium* (2020)

Harshini Ashar, Akansha Singh, Kalyani Ektate, Sunil More, Ashish Ranjan. "Treating non-healing bone infections with focused ultrasound and antibiotic-loaded thermally sensitive liposomes." *International Symposium for Therapeutic Ultrasound* (2021)

Abstract

Objective: Chronic osteomyelitis is a destructive bony infection typically caused by *Staphylococcus aureus* biofilms in children and adults. It is characterized by reduced

penetration and susceptibility to antibiotic treatment within infected bone tissues, and is exacerbated in patients with diabetes, vascular diseases, open fractures, artificial hip or knee joint replacements, or other bone surgery. To improve outcomes, the objective of this study was to assess “heat-targeted, on-demand” antibiotic delivery and *S. aureus* killing by combining ciprofloxacin (CIP) laden Low Temperature-Sensitive Liposomes (LTSLs) with local High Intensity Focused Ultrasound (HIFU)-induced bone heating (>40°C) in a rat model of osteomyelitis.

Methods: LTSL was loaded with CIP, and characterized for size, zeta-potential, and targeted antimicrobial release at >40°C in physiological buffers in vitro. A rat model of osteomyelitis was established by surgically implanting an orthopedic K-wire into the femurs of rats and colonized with methicillin-resistant *S. aureus* (MRSA) strain. Infected rats were randomly assigned to the following treatment groups to determine biodistribution and therapeutic efficacy: (1) Control, (2) HIFU, (3) CIP, (4) CIP+HIFU, (5) LTSL, and (6) LTSL + HIFU. For bone heating, HIFU exposures were performed under ultrasound guidance to achieve a local temperature of >40°C (~15min) following intravenous injection of CIP-LTSL and CIP (10 mg CIP/kg body weight), Biodistribution analysis of bone tissues were determined spectrophotometrically 24h post LTSL injection. Therapeutic efficacy of rats that underwent two treatments every 3 days were determined by bacteriological and histological assessment of treated tissues. Additionally, the implanted wires were visualized with scanning electron microscopy to evaluate changes in biofilm masses.

Results: Our metal implantation method yielded medullary disease by day 10 in bones and adjoining muscle tissues. This was evidenced by suppurative changes (bacterial and

pus pockets) with remodeling and colonization of bone tissues. Adding HIFU heating improved antibiotic delivery in the heated region by >1-fold for LTSL (2.16μg CIP/g) *vs*. CIP (1.47μg CIP/g) and unheated femur (1.33μg CIP/g). The increased CIP delivery correlated with the therapeutic effects of the CIP-LTSL combination treatment, achieving significant reductions of MRSA load in the infected bone (2.3-log and 2.9-log) compared to HIFU alone and free CIP groups, respectively. These were also confirmed in the SEM imaging where a distinct reduction in *S. aureus* populations of the infected metal wires was noted.

Conclusions: Our results demonstrate that HIFU improved CIP delivery to bones increase the clearance of MRSA biofilm from infected metal implants. This approach can be used to improve targeting of bone pathogens and therapeutic clearance of hard-to-treat bacteria.

1. Introduction

Osteomyelitis is caused by the formation of bacterial biofilms in bone, bone marrow and surrounding tissue. It is one of the most feared clinical complications incurring significant health care costs. In total, the cost for treatment of implant-associated infection is projected to exceed $1.62 billion by 2020 [230]. Osteomyelitis caused by biofilms demonstrate reduced sensitivity to antibiotics (~1000 times) compared to planktonic bacteria, and often requires multiple revision surgeries, resulting in functional impairments and even amputations [231]. Notably, the risk of reinfection increases after every revision surgery with the bacteria within such biofilms exhibiting altered growth

rates, gene expression profiles, and protein synthesis [232]. This thereby makes the bacterial pathogens even more resistant to the effector mechanisms of the host's immune system. In fact, antibiotic resistance including those that involves osteomyelitis is estimated to cause 10 million deaths/year by 2050 [233].Thus, there is a critical clinical need to develop innovative and novel treatment approaches that addresses the complex variables of osteomyelitis biofilms for improved therapeutic outcomes.

In all osteomyelitis treatment scenarios, success depends on the complete removal of infected devitalized tissues and metallic hardware. An essential factor governing infection management is also the antibiotic-targeting of the pathogens. In this regard, the prophylactic and therapeutic use of antibiotic loaded implant depots to allow a means of antibiotic release near the bone surface is an innovative approach. However, it has met with moderate clinical success [233]. Alternatively, biodegradable antibiotic laden spacers post-surgery can be tried [234], but the high initial in-situ burst release followed by a sub-therapeutic delivery of antibiotics can enhance the incidence of drug resistance [234, 235]. To address this, in the present study, we investigated the feasibility of combining high intensity focused ultrasound (HIFU) therapy with low temperature sensitive liposome (LTSL) nanoparticles (NPs). LTSLs release antibiotics slightly above the body temperature (>40^{o}C). We hypothesized that LTSLs administered systemically can be activated by HIFU heating to achieve chemotherapy of implant-associated osteomyelitis.

HIFU is well-established clinically to achieve heating in deep seated regions of the body non-invasively. HIFU exposure conditions can be varied by changing the parameters to achieve thermal and/or mechanical effects, features that are particularly attractive for

biofilm targeting. Furthermore, it can enhance delivery/passage of drugs and immune cells, and increase bio-availability and sensitivity to chemotherapy [79]. Previously, we demonstrated the combined effects of HIFU and CIP loaded LTSLs for management of superficial chronic wounds [131]. However, whether LTSLs and HIFU treatment can disrupt biofilms resident in hard-to-reach marrow regions of bones and improve antibiotic therapy is not known. To investigate this goal, in this study, we developed a chronic implant-associated osteomyelitis in a rat-model and optimized *in vivo* bone heating with ultrasound guided treatment planning, determined localized antibiotic delivery from CIP-LTSLs in rat femurs, and evaluated the treatment efficacy in rats. Our study suggests that HIFU sensitizes *S. aureus* biofilm to CIP killing compared to free CIP, and thus may pave the way for a minimally invasive, non-surgical treatment platform for recurrent biofilm infections.

2. Materials and methods:

2.1 Materials

The lipids- 1-stearoyl-2-hydroxy-sn-glycero-3-phosphocholine (Lyso PC), 1,2-dipalmitoyl sn-glycero-3-phosphocholine (DPPC), and 1,2-distearoyl-sn-glycero-3-phosphoethanolamine-N- [methoxy (Polyethylene glycol) 2000] (DSPE-mPEG2000) were obtained from Avanti Polar Lipids (AL, USA). Ciprofloxacin HCl was obtained from Alfa Aesar (MA, USA). Reagent grade ammonium sulfate, sodium chloride, and triton X-100 (Amresco) were purchased from VWR (PA, USA). Whatman polycarbonate membrane filters (0.2µm, 25mm) and PD-10 columns were obtained from GE Healthcare

(IL, USA). Trypticase soy agar and broth (TSA and TSB, respectively) were obtained from BD (NJ, USA). A human clinical isolate of bioluminescent methicillin-resistant *Staphylococcus aureus* (MRSA), strain SAP231, was obtained from the Center of Biologics Evaluation and Research, FDA (MD, USA).

2.2 Synthesis of LTSLs and ciprofloxacin (CIP) loading

LTSLs were prepared by hydration of thin phospholipid film followed by the high-pressure extrusion through a polycarbonate membrane filter [236] (Fig. 2). Briefly, phospholipids DPPC: LysoPC: DSPE-mPEG were dissolved in chloroform at a molar ratio of 85.3:9.7:5.0. The organic solvent was evaporated using a rotary evaporator and the resulting thin lipid film was hydrated using 350 mM ammonium sulfate. Hydrated lipids were extruded five times through double stacked 200 nm polycarbonate filters to yield blank liposomes (LTSLs). CIP loading (5mg of CIP per 100mg of lipids) was carried out using the ammonium sulfate gradient as described previously [237, 238]. Unencapsulated CIP was removed using a PD-10 desalting column equilibrated with 150 mM NaCl.

2.3 Characterization of LTSLs and CIP release from CIP-LTSLs

LTSLs were characterized for size and polydispersity index (PDI) using dynamic light scattering (DLS) with a NanoBrook 90Plus PALS device (Brookhaven Instruments Corporation, NY, USA). Briefly, 10 µl of LTSLs were added to 1 ml of distilled water in a cuvette and DLS measurements were recorded at room temperature. An average of five measurements was taken and mean size and standard deviation were calculated. For zeta potential measurements, 10 µl of LTSLs were added to 1.5 ml of distilled water in a

cuvette, and an average of five measurements was taken to calculate the mean zeta potential. CIP release was measured spectrophotometrically using a Cary Eclipse Fluorescence Spectrometer (Agilent Technologies, CA, USA). Briefly, 10 µl of CIP-LTSLs were diluted 300-fold in distilled water and 10X triton, and 3 ml of sample was placed in a quartz cuvette with a magnetic stirrer. Fluorescence intensity of the completely released CIP was recorded at an excitation wavelength of 330 nm and emission wavelength of 445 nm from 25ºC-45ºC. Encapsulation efficiency of the CIP-LTSLs was assessed using our previously published protocol [131].

2.4 Establishment of *S. aureus* osteomyelitis in rat model

All animal-related procedures were approved and carried out under the regulations and guidelines of the Oklahoma State University Animal Care and Use Committee. 6–8-week-old male Wistar rats (Charles River, MA, USA) were anesthetized with 1 L/min oxygen and 5% Isoflurane induction and 3% maintenance dose. Meloxicam was administered subcutaneously (S/C) at 1mg/kg BW of the rat. For metal implantation, the rat was placed on left lateral recumbency and the surgical area around femur was shaved and disinfected with chlorhexidine and iodine to create a sterile field. A medial incision was made along the knee joint using a scalpel blade (No. 11). Fascia was bluntly separated to provide better visualization of the medial patellar ligament, followed by medial parapatellar arthrotomy and lateral patella subluxation to expose the knee joint. Next, 100 µl MRSA grown overnight in TSB, centrifuged, washed, and diluted with 1X PBS at a concentration 1.5×10^8 CFU/ml was injected into the medullary cavity of the femur through the distal end of the femur using an 18-gauge hypodermic needle (Fig. 1A). The needle was slowly removed and a sterile orthopedic wire (22 gauge, ~2 cm

long, stainless steel; IMEX veterinary inc., TX, USA) was inserted to fit inside the medullary cavity while avoiding any irritation or infection in the knee joint. After metal insertion, the site was rinsed with sterile saline solution, and the incision was closed using simple interrupted intradermal skin sutures (4-0, PDS*II, Ethicon) and tissue adhesive (3M Vetbond). The surgical region was sprayed with a taste deterrent spray (Grannick's bitter apple) to avoid rats from biting or licking the suture site. Finally, Rats were X-rayed (Bruker In-Vivo Xtreme II, MA, USA) to confirm successful implantation of wire and all animals were given S/C meloxicam injections for 2 days post infection for pain management.

2.5 *In vivo* drug delivery and efficacy study design

To optimize infection rates, initially the rats were evaluated histopathologically on 7-, 10-, 14-, or 21-days to track progression of osteomyelitis infection. Histological and radiological features indicative of bone infection were observed at 10 days post MRSA infection (Fig. 3), and thus this time-point was selected for biodistribution and efficacy evaluations in rats. Animals with osteomyelitis were randomized into the following groups: 1&2. *S. aureus* (±HIFU) 3&4. Free CIP (±HIFU) 5&6. CIP-LTSL (±HIFU). For the drug delivery study, rats were sacrificed 24 hours post LTSL treatment and CIP concentration was determined in the heated bone and adjoining muscle and compared between the free CIP+/- HIFU and CIP-LTSL+/- HIFU groups (n=3) (Fig. 5A). To assess treatment efficacy, rats were given two treatments, three days apart, and sacrificed 24 hours post second treatment (Fig. 6A).

2.6 HIFU treatment set-up and methodology

An integrated ultrasound–HIFU Alpinion system (VIFU2000, WA, USA) with a 1.5-MHz transducer frequency, 45-mm radius and 64-mm aperture diameter with a central opening of 40 mm in diameter was used for treatment planning and HIFU exposure. Rats were anesthetized with 2%–5% isoflurane and a tail vein I/V catheter was secured prior being restrained in custom-built animal holders, mounted on a 3-D positioning stage, and lowered into a 37^0C degassed water bath for coupling (Fig. 4A). The right femur was aligned to HIFU beam axis using real-time ultrasound guidance. VIFU software was used to define the target boundaries in the x, y, and z directions for automatic rastering of the transducer. HIFU treatment parameters used were: 50% duty cycle, 5 Hz pulse repetitive frequency, and 8 W power (equivalent to 3.6 W acoustic power). These parameters achieved a mean target temperature of 42-45^0C at the focus measured using a temperature sensor at the bone-muscle interface. Each focal point (1x1x10 mm on the x, y, and z axes, respectively) within the raster treatment pattern was heated for 120 seconds, and the entire length of the femur was treated for a total treatment time of 30-35 mins (Fig. 4B). Free CIP or CIP-LTSLs were injected intravenously at 10 mg/kg CIP concentration post initiation of HIFU treatment.

2.7 Gait/pain analysis post HIFU treatments

To assess the impact of HIFU treatment of bone on the ambulation of rats, the rats were scored on a scale of 0-4, where 0= normal gait and behavior, 1= animal moving around while infrequently lifting treated leg, 2= animal moving with a slight limp (partial weight-bearing), 3= animal reluctant to move much, moving with occasionally setting

down the treated foot (toe-touch), and 4= animal is non-weight-bearing (Fig. S1). The rats were monitored immediately post-treatment 1&2, at 6-hours post-treatment 1&2, 24-hours post-treatment 1, and 48-hours post-treatment 1, since they were sacrificed for efficacy studies at 24 hours post-treatment 2.

2.8 Post-treatment tissue analysis

Upon completion of treatment, rats were euthanized. The treated and untreated bone and surrounding muscles and skin were collected for drug delivery, bacteriological, and histological analysis.

2.8.1 Bacteriological assessment

For bacteriological analysis, the right femur bone and surrounding muscles and skin were collected, weighed, and homogenized in 1XPBS using a bead-vial homogenizer (Mini-Beadbeater-16, BioSpec, OK, USA) at 3450 oscillations/min for 3 min in 7mL polypropylene screw-cap micro vials (BioSpec) using zirconia beads (1mm diameter, BioSpec). Homogenized tissue samples were covered in foil and stored at -80C before and after use. 1:10 serial dilutions were made in 1XPBS, up to 7 dilutions, and plated on TSA plates using the drop plate method. The resulting discrete colonies were counted for the highest dilution containing 30-300 colonies. The results were expressed as CFU/ml of homogenized tissue.

2.8.2 Analysis of ciprofloxacin in tissues

100 mg of the homogenized tissues was added to 1.2 mL extraction medium (2% aqueous acetic acid/acetonitrile, 1:1 v/v) and mixed using the bead-vial homogenizer with zirconia

beads. The sample lysate was transferred to 1.5mL tubes and centrifuged to pellet cell debris at 16,000 g for 15 min. The supernatant was transferred to another 1.5mL tube and re-centrifuged. For CIP detection, 500µl of clarified supernatant was added to a 700µl quartz cuvette, and fluorescence (ex: 330nm, em: 445nm) was measured using a SpectraMax M2 spectrophotometer (Molecular devices, CA, USA).

2.8.3 Histopathological assessment

For histopathological analysis, the surgical limb was removed, cut into half in a way that the surrounding muscle can be viewed in layers with the bone, and stored in formalin. The paraffin embedded tissue sections were stained for Hematoxylin and Eosin (H&E) staining and Gram staining. The samples were scored for relative abundance of intraosseous Gram-positive cocci and extent of tissue damage by an experienced pathologist blinded for this study.

2.8.4 Scanning electron microscopy (SEM) of *S. aureus* biofilms on explanted wire

For electron microscopy, the femur was cut into half and the implants were carefully removed from the femur with sterile forceps and immediately fixed for 2 h in 2.0% glutaraldehyde in 0.1M cacodylate buffer washed with sodium cacodylate buffer, incubated for 1h in 1% osmium tetraoxide in cacodylate buffer, serially dehydrated in increasing concentrations of ethanol (50, 70, 90, 95 and 100%), and dried in hexamethyldisilazane. Individual samples were then mounted on microscopy stubs with tape and coated with gold–palladium and viewed under scanning electron microscope.

2.9 Statistical analysis

All analyses were performed using GraphPad Prism 9.0 (GraphPad Software Inc.). All data were reported as the mean ± standard error of mean (SEM). A one-tailed *t*-test was performed to compare the mean micrograms of CIP in heated vs. unheated bone. An ordinary one-way analysis of variance (ANOVA) followed by Fisher's LSD test was performed for comparing the specificity of drug delivery in bone: adjoining muscle. Treatment groups were compared for differences in mean CFU by two-way ANOVA followed by Tukey's multiple comparison test. All p values were two- sided, and $p < 0.05$ was taken to indicate statistical significance.

3. Results

3.1 LTSL particle characterization and CIP release kinetics

The hydrodynamic diameter of LTSLs measured by DLS was in the range of 183.5 nm ± 1.91 (n=5) with a polydispersity index of 0.134 ± 0.009. The LTSLs had a negative surface charge indicated by the zeta potential of -21.56 mV ± 0.58 (Fig. 2B).

Ciprofloxacin loading via transmembrane ammonium sulfate gradient yielded an encapsulation efficiency of >70% in the LTSLs. % CIP release from LTSLs started gradually at 40^{o}C and was rapid and complete with 100% release at 41-42^{o}C (Fig. 2C).

3.2 Establishment of rat model of peri-implant MRSA biofilm associated osteomyelitis

All animals included in the study survived the metal-implant surgery. Post-operation, the infected rats showed an initial decrease in body weight and mild limping. These signs gradually disappeared within 3-7 days post-surgery and most rats had full weight-bearing gait with no signs of distress or pain. No marked differences in rectal temperatures were found in the rats postoperatively.

Analysis of radiographs at 10 days post infection showed obvious signs of osteomyelitis with a clear difference between the infected right femur vs. the uninfected left femur in the rats. These included periosteal reaction and osteolysis of the femur as well as septic arthritic changes at the knee joint (Fig. 3A). This was also confirmed by histopathological analysis of infected bone where salient features of osteomyelitis including but not limited to loss of periosteal lining of bone and presence of extensive inflammation, fibrosis, and clumps of bacteria especially around the distal end of femur (Fig. 3B) could be noted. Specifically, bone necrosis and subperiosteal scalloping of cortex was observed along with presence of intracellular bacteria and the infiltration of the immune cells infiltrated in the infected regions.

3.3 Combining HIFU thermal therapy with LTSL increases local CIP concentration

Treatment with HIFU caused mild discomfort in the rats immediately post-treatment, which was alleviated by 6 hours post-treatment, without any significant impact on the ambulation (Fig. S1) or overall health. LTSL alone treatment delivered 1.33 ± 0.71 µg CIP/g in the bones (Fig. 5B). In contrast, adding HIFU to LTSLs increased CIP levels to 2.16 ± 0.07. In contrast, HIFU achieved 1.47 ± 0.16 µg ciprofloxacin/g of tissue from free CIP+HIFU. Overall, LTSL+HIFU resulted in a 1.5-fold greater CIP delivery

compared to its free CIP counterpart ($p< 0.05$). Also, addition of HIFU to LTSL achieved a 1.6-fold greater CIP delivery to the bones compared to LTSL alone. We also assessed the targeted drug delivery to the heated bone regions compared to the adjacent muscle (bone: muscle). The relative CIP levels were 1.4-fold and 2.2-fold greater in the LTSL+HIFU group compared to the free CIP+HIFU and CIP-LTSL groups, respectively ($p< 0.05$; Fig. 5C).

3.4 Combinatorial therapy enhanced MRSA bactericidal activity and biofilm eradication

The tissue CFU counts were analyzed for heated bones, adjoining muscles (the lateral muscle layer was directly overlying the heated bone region while the medial muscle was farther away from the HIFU heated regions), skin and joint space in all treatment groups. LTSL+HIFU decreased the bacterial load by 1.4-log and 1.1-log in the overlying lateral muscles and medial muscles respectively compared to control (n=5; Fig. 6B). This trend was also noted in the skin and joint, compared to the other treatment groups. In line with CIP delivery, the treatment efficacy of CIP-LTSL+ HIFU group was best observed in the heated bones with a 2.3-log and 2.9 log decrease in tissue MRSA load compared to the HIFU alone and free CIP+ HIFU groups respectively ($p< 0.05$; Fig. 6C). To verify our findings, the bacterial burden was visualized on the SEM of the wire explants (Fig. 7). Untreated control wires showed a thick film of *S. aureus* with extracellular matrix. Treatment with HIFU alone showed changes in the density and structure of the *S. aureus* biofilm compared to the control. CIP alone also reduced the biofilm mass on the wire.

However, a greater change in the structure of the extracellular matrix network was observed with the LTSL treatment. Interestingly, rats treated with CIP-LTSL+ HIFU showed the greatest reduction in the overall bacterial density as well as biofilm structure, with reduction in the extent of the extracellular matrix cover and presence of sparsely scattered *S. aureus*. These were similarly observed in the histopathological analysis of the bones and surrounding muscle layer, which exhibited a reduction in the bacterial burden and extent of tissue necrosis in the treatment groups compared to the non-treated control group (Fig. S2). In general, the LTSL+ HIFU group consistently decreased the *S. aureus* burden and the extent of tissue necrosis compared to the other HIFU treated groups (Fig. 8).

4. Discussion

Eradication of biofilms from implant materials is a challenging aspect of orthopedic surgery [233]. Especially, *S. aureus* biofilm that extends to bone and intramedullary tissues is a serious complication of open fractures and surgical repairs [239, 240]. These biofilms show poor antibiotic penetration, making chemotherapy challenging [241, 242]. To address this, HIFU has been investigated to improve biofilm therapy *in vitro* and *in vivo* [243-246]. Resdiske et al. combined continuous ultrasound at 100 mW/cm^2 with gentamicin, but this approach did not reduce bacterial viability. In contrast, at 300 mW/cm^2, the bacterial killing was significant, but it was also associated with some skin damage [246]. Rieck et al. measured the killing of MRSA murine abscesses with moderate HIFU temperature (MT: $52.3^0C \pm 5.1^0C$) and high temperature (HT: $63.8^0C \pm$

7.5^{0}C). MT and HT groups reached target temperatures after four 9-s ultrasound exposures applied in a square 1 x 1 mm grid, with a 1-min pause between exposures. This resulted in a significant reduction in MRSA bacterial count in the treated areas compared with the untreated control at days 1 and 4 post-treatment [247]. To further augment the HIFU effects with antibiotics, we recently combined localized HIFU hyperthermia with LTSLs to improve outcomes against *S. aureus* induced murine abscess [131]. We found that our combinatorial approach improved CIP delivery, and also enhanced *S. aureus* clearance compared to the unheated control [86]. Unlike superficial abscess wounds, delivering antibiotics through the calcified tissues of bone is highly challenging due to ultrasound attenuation of heat. The objective of this study was to determine whether combining HIFU with LTSL is similarly capable of effectively clearing *S. aureus* bone biofilms via heat-targeted and mechanical effects of sound waves.

A variety of animals models that mimic the presentation and pathophysiology of osteomyelitis have been employed in previous research [248, 249]. To test our objective, we utilized a rat model of osteomyelitis. A sterile orthopedic K-wire was surgically inserted into the distal end of rat femurs to mimic intramedullary nailing. To be as close to clinical disease representation, no promoters of infection were used besides implant and *S. aureus*. We chose to do our studies with *S. aureus* as it is the most common pathogen in osteomyelitis infections [233, 250] and over 50% of clinical cases are caused by methicillin resistant strains [251]. The amount of bacteria inoculated in previous studies ranged from 10^3 to 10^9 CFU of *S. aureus* [239, 240, 252-256]. For our studies, we used an inoculum of 10^6 CFU of MRSA strain SAP231 injected directly into the medullary cavity of rat femur. Histopathological and radiological evaluation showed

clinically classifiable signs of osteomyelitis infection after 10 days (Fig.3) including acute destructive to chronic localized and stable infection in all animals with the selected dose of MRSA.

Over the years, the development and spread of multiple antibiotic resistant organisms has gained much attention [257]. Moreover, clinical presentation of open wounds, diabetic wounds as well as osteomyelitis is frequently a multi-bacterial infection including MRSA, *S. epidermidis*, *Pseudomonas aeruginosa*, *Klebsiella pneumoniae* and others [258, 259]. Ciprofloxacin is fluoroquinolone antibiotic that is active against both Gram-negative and Gram-positive bacteria. It is indicated for the treatment of a variety of bacterial infections, including bone and joint infections [260]. Although resistance to fluoroquinolones, including CIP emerged rapidly due to clonal spread, especially in MRSA and *P. aeruginosa* spp. [261], a clinical trial by Mulligan et. al., reported that CIP can still be used for eradication of MRSA colonization alone or in combination therapies [262]. Our motivation to use CIP in our study is, therefore, multi-factorial. The current therapeutic approach is feasible against not only Staphylococcal/ gram-positive organisms but can also be used against similar gram-negative infections. In addition, the increased potential for resistance development allows us to address an important question of whether our therapeutic approach can potentially reverse the antibiotic resistance. This will have far-reaching effects considering the increasing difficulty in discovering and developing new antibiotics. This is based on the premise that HIFU enhances the effectiveness of antibiotics by promoting oxygenation to enhance bacterial metabolism of the compound [263]. HIFU being a rapid focal technique, the bacteria may not have time to adapt to the applied stresses [264].

For treatments, we chose the liposome based delivery systems since they have already shown great potential against *S. aureus* and MRSA [265, 266]. Their excellent biocompatibility, controlled release of loaded antibiotics and biofilm penetrating features are clinically relevant [182]. Ferreira et al. tested positively charged liposomes attachment and anti-biofilm activity against *S. aureus* biofilm. While strong attachment to biofilms were noted, it did not translate into an improved anti-biofilm efficacy. On the contrary, the negatively charged liposomes showed a higher therapeutic potential [267]. Our LTSLs have a slightly negative zeta-potential and has been widely utilized for localized delivery of anti-cancer drugs (e.g., doxorubicin) [132, 203, 268, 269]. We found that HIFU hyperthermia combined with LTSLs similarly achieved higher CIP delivery compared to the CIP-LTSL alone and free CIP+HIFU groups, respectively (Fig. 5B). Also, the targeted drug delivery to the heated bone was superior compared to the adjacent muscle (bone: muscle) for LTSL+ HIFU treatments (Fig. 5C). Likely, the increased bone perfusion mediated by stable and long duration hyperthermia by HIFU induced greater LTSL uptake in the infected tissues [132, 270, 271]. We also theorize that an increase of localized temperature by HIFU resulted in an increased metabolic activity in bacterial cells, which in turn, facilitated the uptake of antibiotic by biofilm bacteria. This may be supported by the previous findings of transcriptomic and metabolic data of *S. aureus* in response to an exposure of a sub-lethal (43^0C) temperature, where increased metabolic activities including ATP-generating pathways were activated [272].

Treatment of implant-associated osteomyelitis consists of implant removal, extensive surgical debridement, and prolonged antibiotic treatment. Additionally, implant coatings to inhibit bacterial adhesion with antibiotics, antiseptics, or metal ions can be attempted

[233, 239]. However, to our best knowledge, the application of non-invasive means to improve the therapeutic efficacy of HIFU for MRSA biofilm treatment in an animal model of peri-implant osteomyelitis has not been investigated. Our study shows a correlation of decreased *S. aureus* load in the heated bones as well as adjacent and overlying muscles with improved CIP-LTSL delivery (Fig. 6). Our SEM images also showed a distinct reduction of biofilm biomass on the wires explanted from the rat femurs with LTSL +HIFU (Fig. 7). This is similar to our findings of *S. aureus* biofilms in abscesses exposed to 42^0C -46^0C, where the cocci appeared damaged in presence of HIFU [86]. Gera and Doores similarly found that E. coli treated with ultrasound showed damaged cell wall and cell membrane [273]. Our results are also in agreement with previous *in vitro* studies demonstrating biofilm detachment upon mild hyperthermia treatments [274, 275]. These visualization of treatment effects on biofilms on explanted intramedullary wires with HIFU provides important information about the effects of this therapy, a further improvement in outcomes in presence of an antibiotic *in vivo*. Interestingly, our histopathology analysis suggested that all the treatment groups exhibited reduced bacterial burden and extent of tissue necrosis compared to the untreated control group (Fig.8), without significant differences between the different treatment groups. This discrepancy between histopathology with SEM could be due to the limitation posed by the tissue collection process. The femurs had to sawed open to remove the intramedullary wired without disturbing the biofilm biomass. Infected bones being fragile, some bones were fragmented in that process, and this could have influenced histological enumerations. Finally, some treated subjects did demonstrate mild-to-moderate pain with HIFU exposures. This could be managed medically using

anti-inflammatory drugs and thus we proposed that the treatments did not have a significant impact on ambulatory status with the chosen US parameters.

In summary, our findings for the first time demonstrate the feasibility of utilizing HIFU for physical eradication of MRSA biofilm bone infections or at a minimum, biologically significant reduction of bacterial biomass with LTSLs in a non-surgical manner. Although the current study assessed the effects of two treatments, a complete eradiation of biofilm may require additional optimization of treatment duration and frequency. Studies to address these limitations are currently underway. We propose that the combinatorial methodology can serve as an effective adjuvant to combat recalcitrant chronic bacterial biofilm infections.

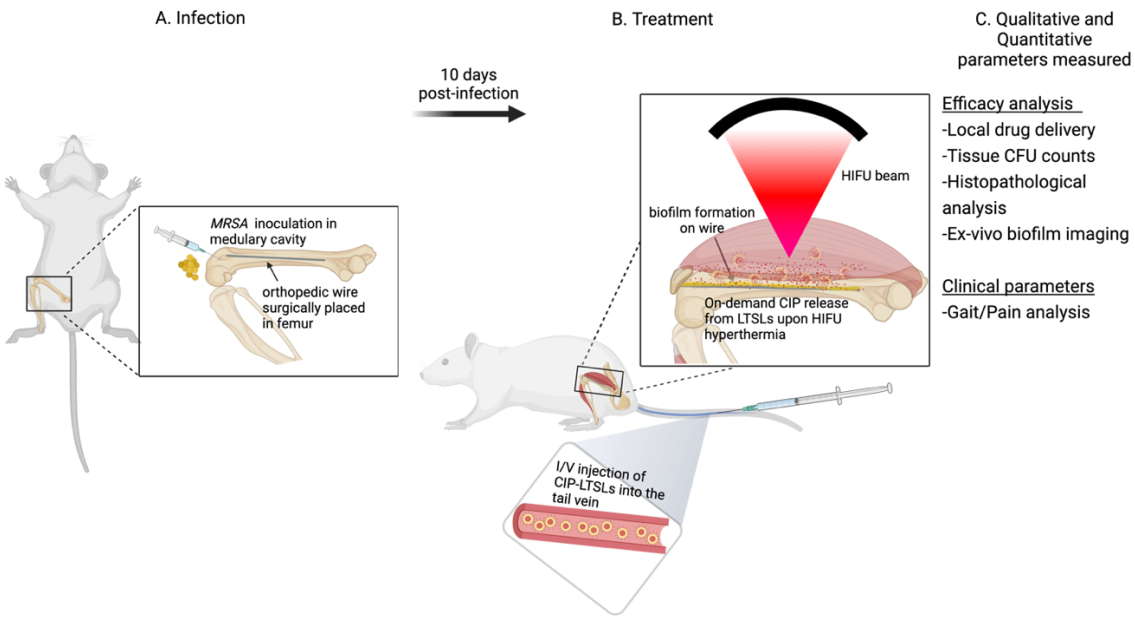

Figure 1- Graphical representation of minimally invasive HIFU-hyperthermia combined chemotherapy approach for the treatment of peri-implant biofilm-associated osteomyelitis. Created with BioRender.com.

A.

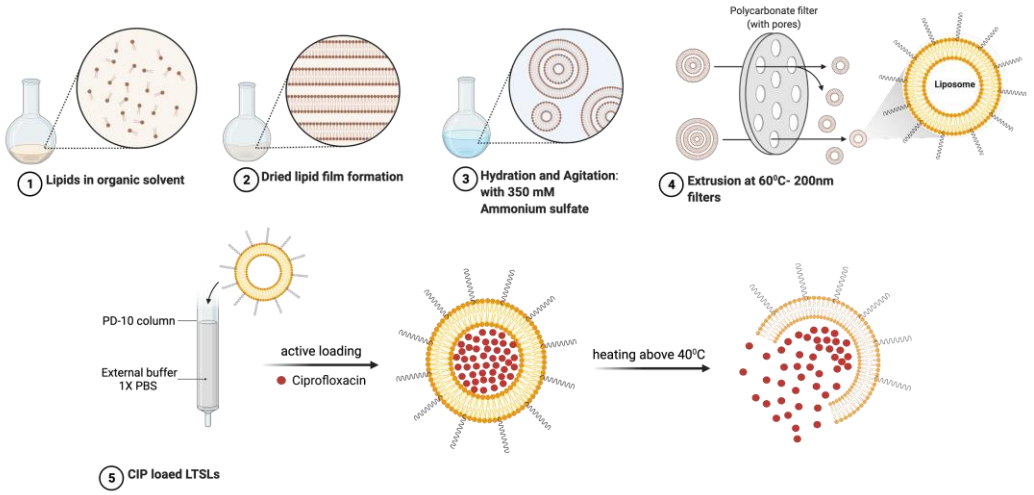

B.

SIZE	183.5 nm ± 1.91
PDI	0.134 ± 0.009
Zeta potential	-21.56 mV ± 0.58

C.

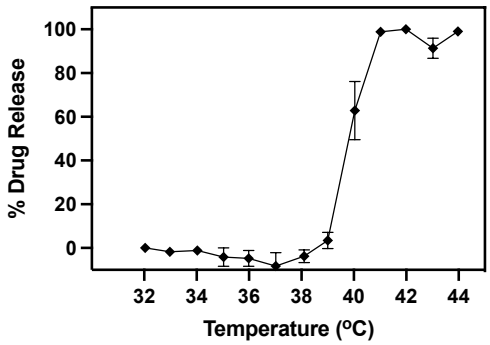

Figure 2. Ciprofloxacin loaded low temperature sensitive liposomes release their payload when heated to temperatures above 40^0C. A. Graphical representation of LTSL synthesis, B. LTSL characterization, and C. CIP release from LTSLs as a measure of temperature. Created with BioRender.com.

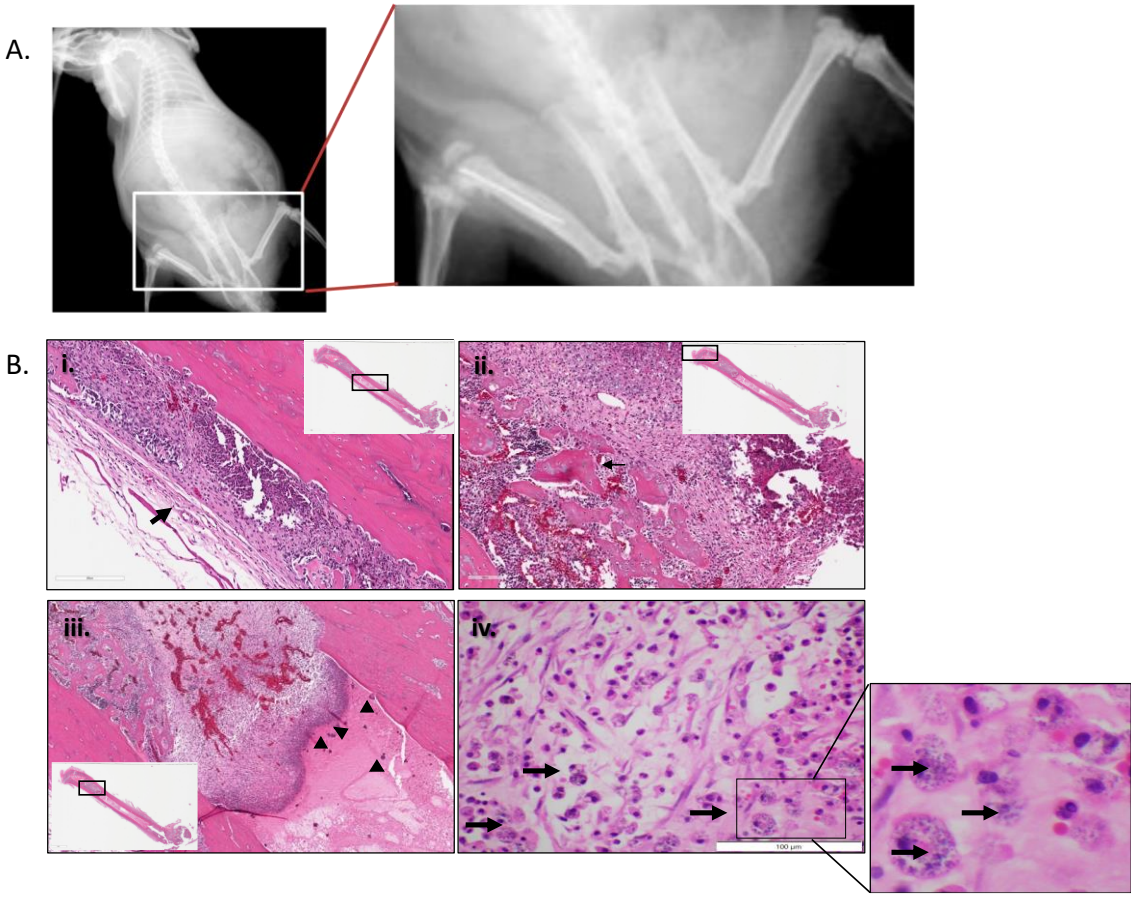

Figure 3. Establishment of rat model of peri-implant MRSA biofilm associated osteomyelitis. A. Radiographic evidence of rat at 10 days post infection shows signs of periosteal reaction, osteolysis and swelling in infected right femur compared to the uninfected left femur, and B. Histopathological changes in the rat model of osteomyelitis in the femur illustrate salient features of osteomyelitis, i. Extensive inflammation and fibrosis seen in the periosteal lining of the bone; ii. Pieces of necrotic bone (black arrow) surrounded by micro-abscess, inflammation, and fibrosis; iii. Inflammation and presence of clumps of bacterial (black arrow heads) in the distal end of the femur; iv. Presence of immune cells with intracellular bacteria (black arrows) was observed. Scale bars=100**µ**m.

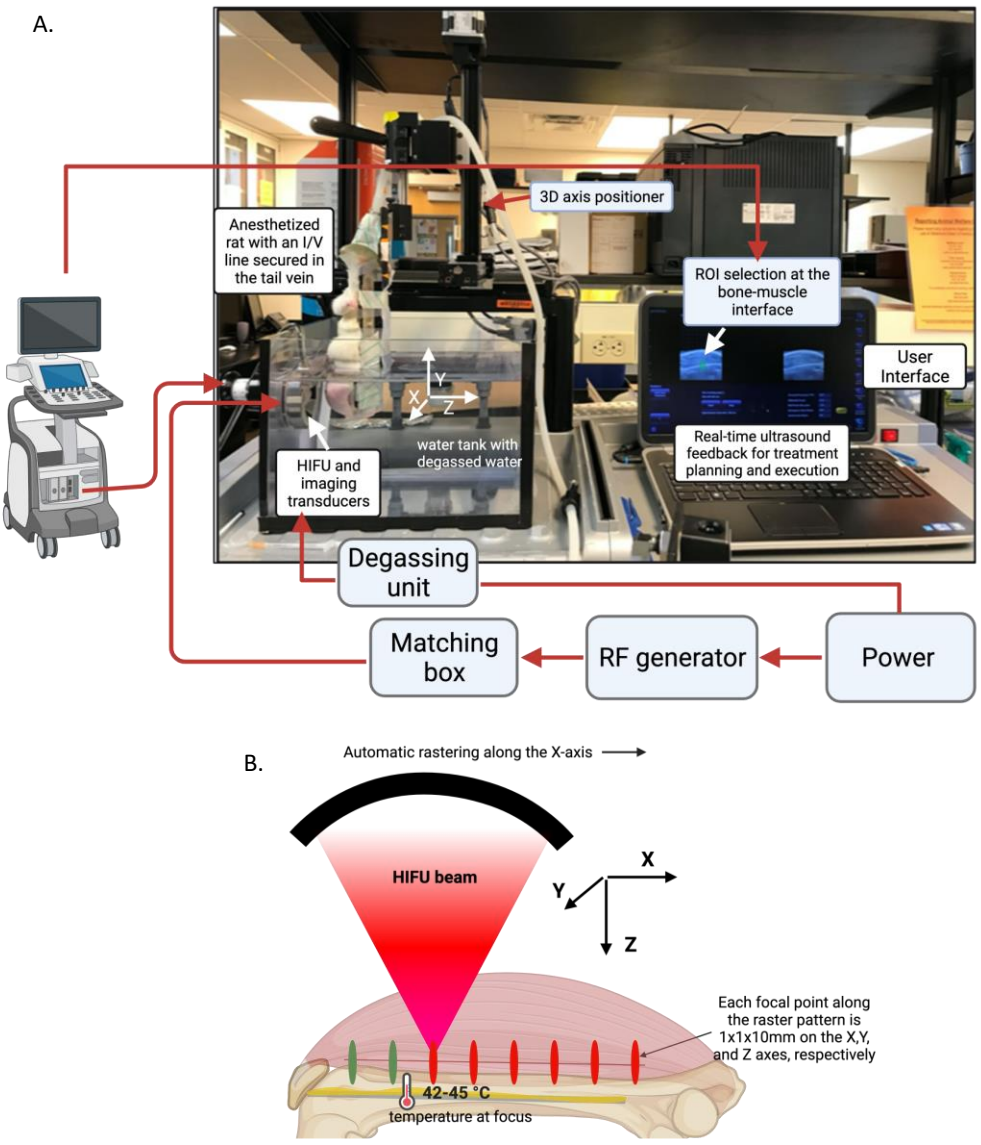

Figure 4. Experimental setup for HIFU hyperthermia treatment. A. 1.5 MHz HIFU transducer with a coaxially aligned imaging probe was used for targeting and treatment guidance. Anesthetized rat in a holder was mounted on a computer-controlled 3D positioning system and lowered into a water bath filled with circulating degassed water maintained at 37^0C, and B. HIFU hyperthermia was achieved by selecting a ROI with raster treatment pattern at the bone: muscle interface while delivering the specified treatment protocol at each focal point. Created with BioRender.com.

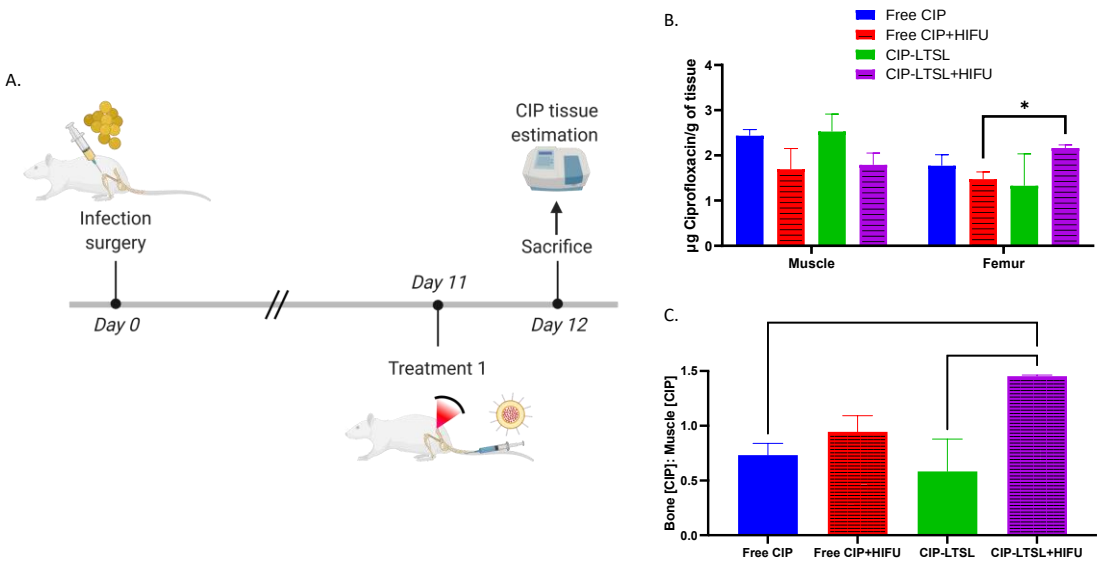

Figure 5. Combining HIFU with ciprofloxacin laden liposomes significantly increases antibiotic delivery to treated bones. A. Experimental timeline of combinatorial treatment in rats with established infections. Rats were infected on Day 0, treated with CIP-LTSL or Free CIP +/- HIFU on Day 11, followed by sacrifice 24 hours later and tissue CIP estimation (Created with BioRender.com), B. Bar graphs showing µg ciprofloxacin concentration per g of tissue, in muscle and HIFU targeted bones, and compared to respective controls. Significance was calculated using a one-tailed t-test ($p < 0.05$), and C. Bar graphs showing targeted drug delivery in heated bones with adjoining muscle. Significance was calculated using ANOVA with Fisher's LSD.

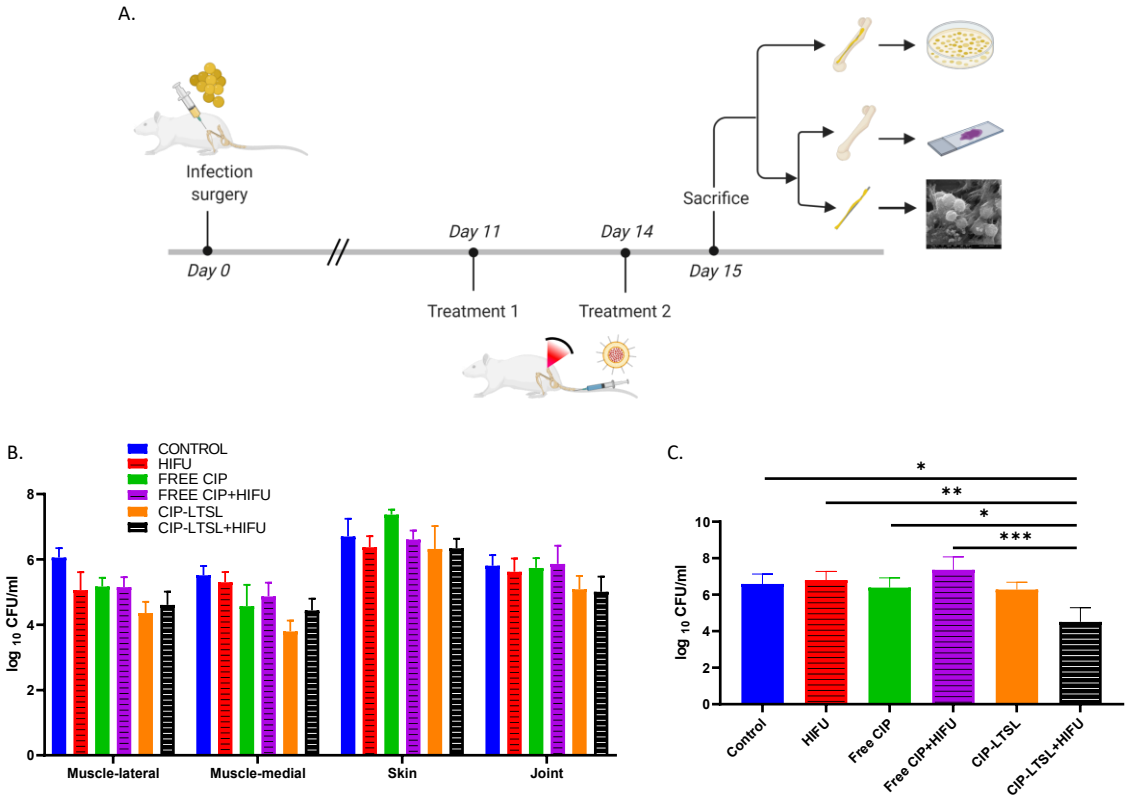

Figure 6. Non-invasive CIP-LTSL+ HIFU treatments of biofilm infected bones lead to reductions in tissue bacterial load. A. Experimental timeline of combinatorial treatment in rats with established infections. Rats were infected on Day 0, treated with CIP-LTSL or Free CIP +/- HIFU on Days 11 and 14, followed by sacrifice on Day 15. Tissues were processed for bacteriological and histological analyses (Created with BioRender.com), B. Bar graphs presenting $\log_{10}$ colony forming units (CFU) per ml of homogenized tissue, in muscle, skin and joint space between different treatment groups, and C. Bar graphs presenting $\log_{10}$ colony forming units (CFU) per ml of homogenized tissue in the HIFU targeted bones, between different treatment groups. Significance was calculated using two-way ANOVA with Tukey's multiple comparisons test ($p < 0.05$).

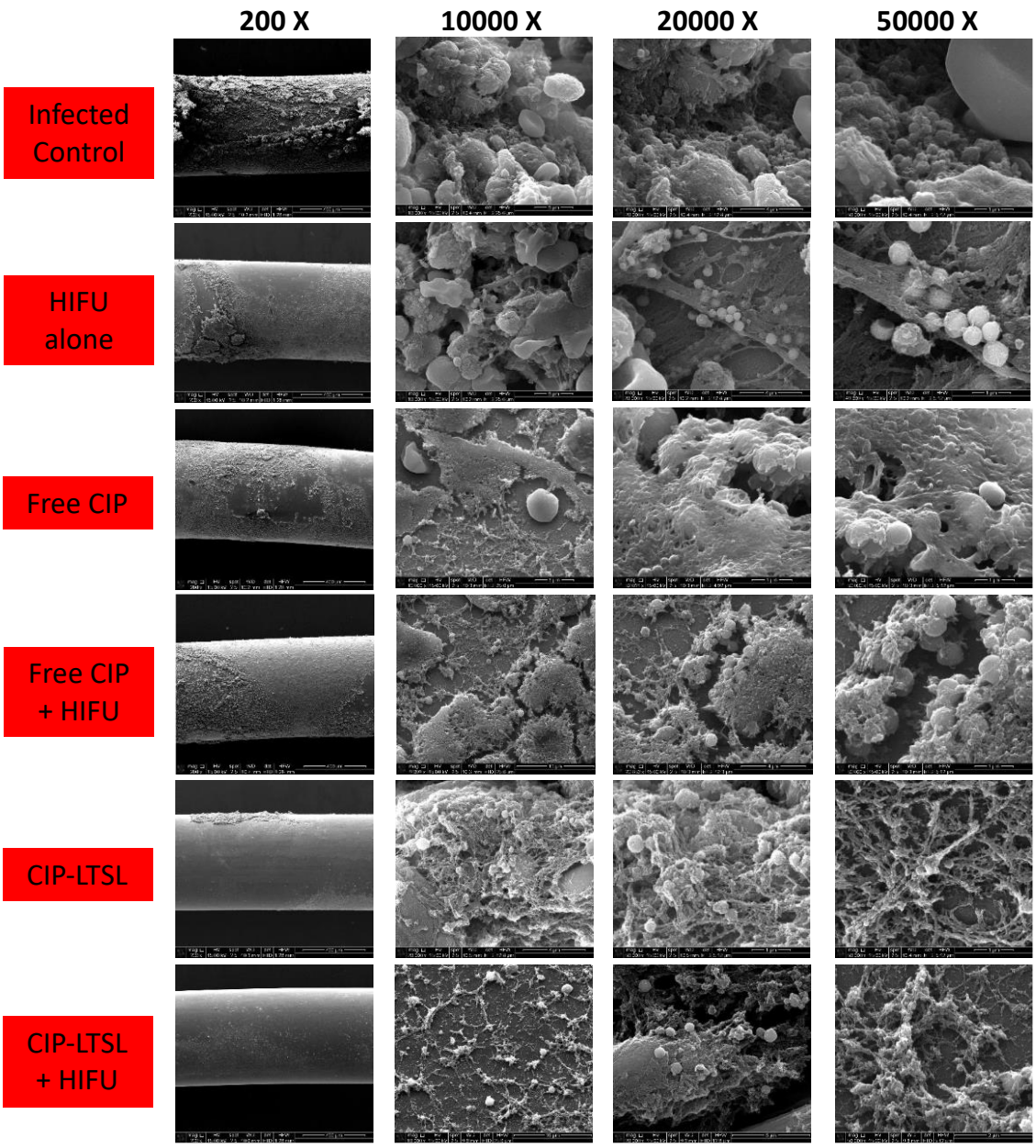

Figure 7. Reduction in bacterial burden caused by CIP-LTSL+ HIFU treatments of biofilm infected bones was visualized by scanning electron microscopy (SEM) of biofilm-contaminated wire explants. Increasing magnifications showing extent of biofilm dispersal between different treatment groups, post second treatment (n=1).

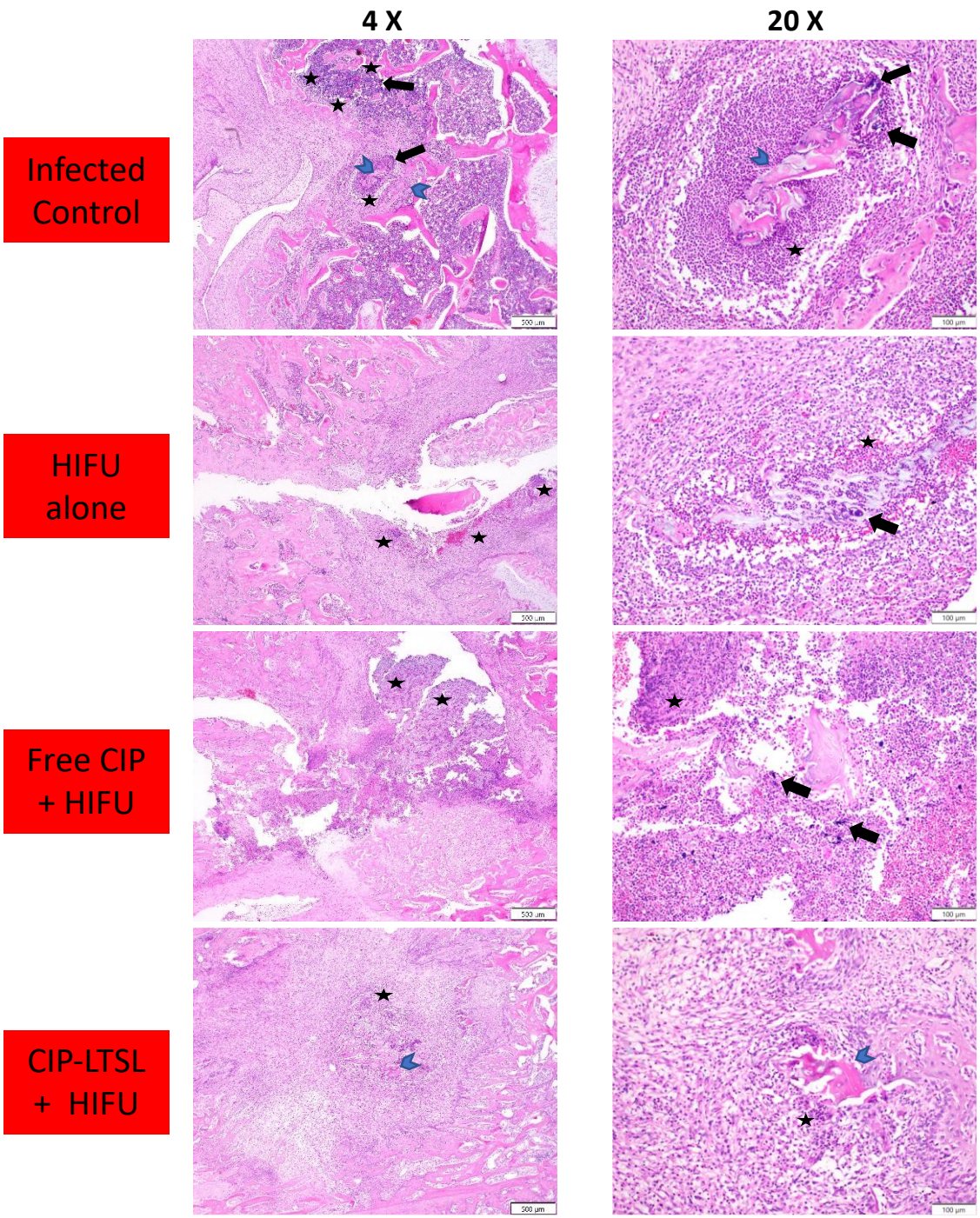

Figure 8. Hematoxylin and eosin (H&E) staining of HIFU treated femurs show reduced bacterial burden (black arrows), suppurative inflammation (black stars) and osteonecrosis (blue arrowheads) in the HIFU treated groups compared to the untreated infected control, post second treatment (n=1). Scale bars- 4X= 500µm, 20X= 100µm.

SUPPLEMENTARY FIGURES:

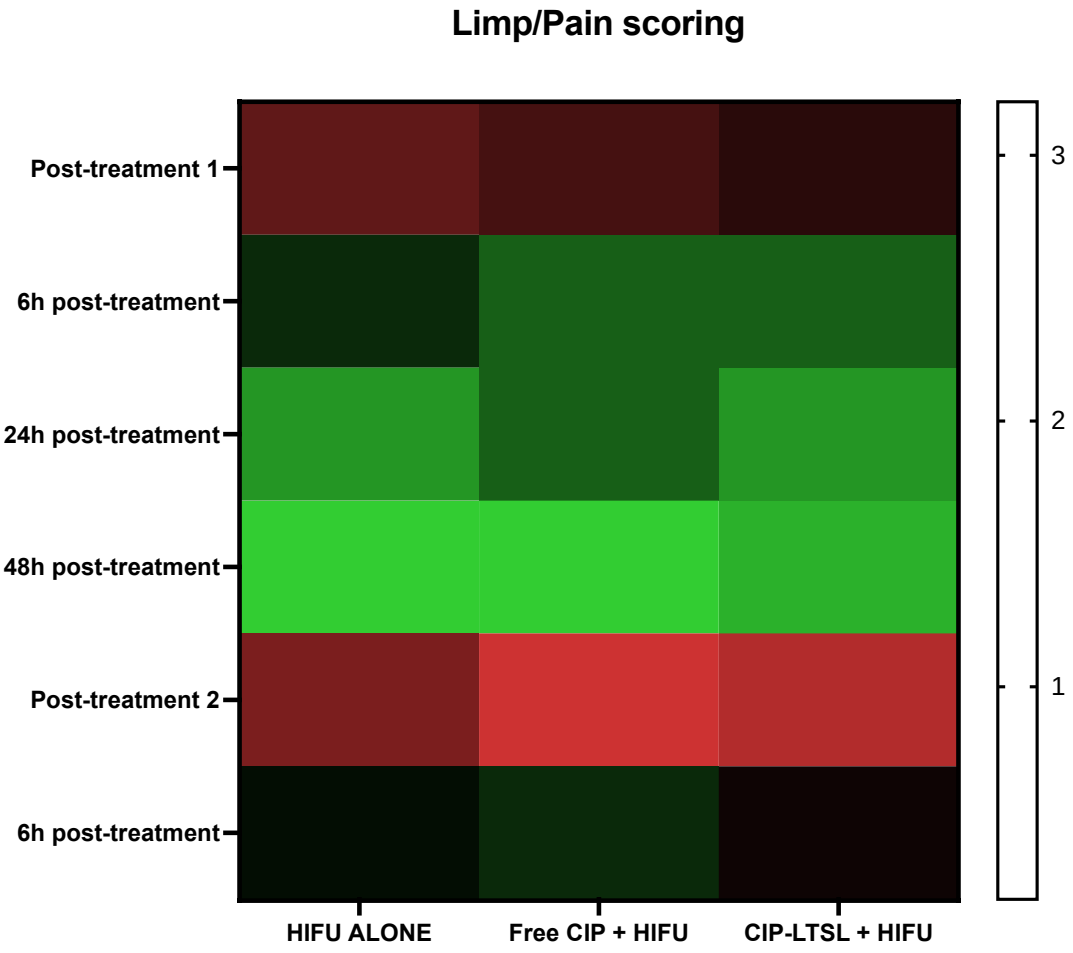

Figure S1. Gait and pain scoring in rats treated with HIFU over the course of treatments. All the rats showed discomfort immediately post-treatment 1 & 2. Signs of pain and resultant limping resolved over 6 hours post treatments and the rats had normal gait and behavior over the next 24-48 hours post-treatment 1. Rats were sacrificed for therapeutic analysis at 24 hours post-treatment 2. Rats were scored from 0-4, where 0= normal gait and behavior, 1= animal moving around while infrequently lifting treated leg, 2= animal moving with a slight limp (partial weight-bearing), 3= animal reluctant to move much, moving with occasionally setting down the treated foot (toe-touch), and 4= animal is non-weight-bearing.

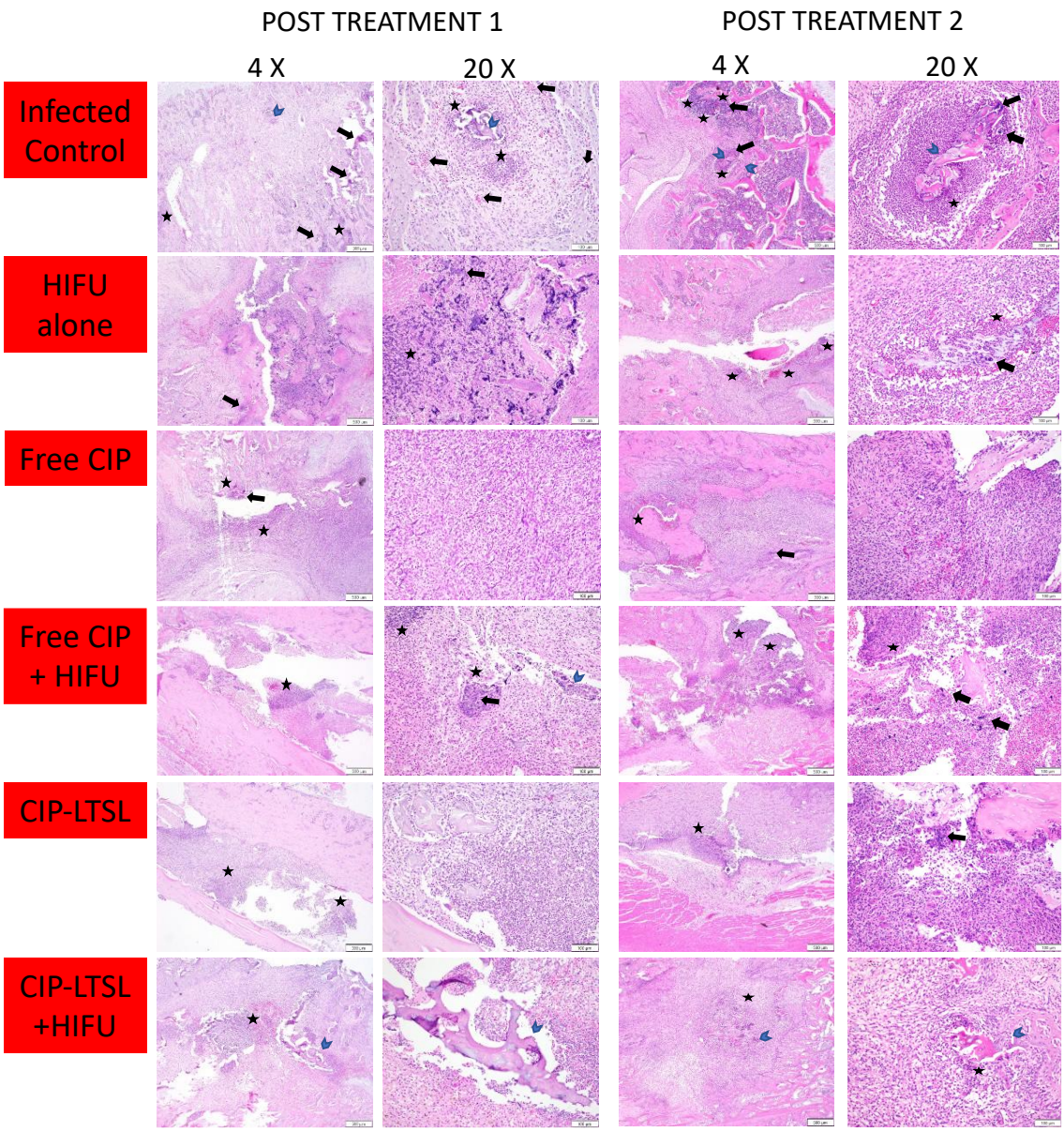

Figure S2. Hematoxylin and eosin (H&E) staining of HIFU treated femurs show reduced bacterial burden (black arrows), suppurative inflammation (black stars) and osteonecrosis (blue arrowheads) in all treatment groups compared to the untreated infected control, post treatment 1 and 2 (n=1). Scale bars- 4X= 500µm, 20X= 100µm.

References

1. Schwarz, E.M., et al., *2018 International Consensus Meeting on Musculoskeletal Infection: Research Priorities from the General Assembly Questions.* Journal of Orthopaedic Research, 2019. **37**(5): p. 997-1006.
2. Lattwein, K.R., et al., *Sonobactericide: An emerging treatment strategy for bacterial infections.* Ultrasound in medicine & biology, 2020. **46**(2): p. 193-215.
3. Hofstee, M.I., et al., *Current Concepts of Osteomyelitis: From Pathologic Mechanisms to Advanced Research Methods.* The American Journal of Pathology, 2020.
4. Masters, E.A., et al., *Evolving concepts in bone infection: redefining "biofilm","acute vs. chronic osteomyelitis","the immune proteome" and "local antibiotic therapy".* 2019. **7**(1): p. 20.
5. Jiranek, W.A., A.D. Hanssen, and A.S. Greenwald, *Antibiotic-loaded bone cement for infection prophylaxis in total joint replacement.* JBJS, 2006. **88**(11): p. 2487-2500.
6. Ma, D., et al., *Viable bacteria persist on antibiotic spacers following two-stage revision for periprosthetic joint infection.* Journal of Orthopaedic Research®, 2018. **36**(1): p. 452-458.
7. Foundation, F.U. *An Overview of the Biological Effects of Focused Ultrasound*. 2015.
8. Wardlow, R., et al., *Targeted antibiotic delivery using low temperature-sensitive liposomes and magnetic resonance-guided high-intensity focused ultrasound hyperthermia.* International Journal of Hyperthermia, 2016. **32**(3): p. 254-264.
9. Maples, D., et al., *Synthesis and characterisation of ultrasound imageable heat-sensitive liposomes for HIFU therapy.* Int J Hyperthermia, 2015. **31**(6): p. 674-85.
10. Maurer, N., et al., *Anomalous solubility behavior of the antibiotic ciprofloxacin encapsulated in liposomes: a 1H-NMR study.* Biochimica et Biophysica Acta (BBA)-Biomembranes, 1998. **1374**(1-2): p. 9-20.
11. Tazina, E., K. Kostin, and N. Oborotova, *Specific features of drug encapsulation in liposomes (A review).* Pharmaceutical Chemistry Journal, 2011. **45**(8): p. 481-490.
12. Fang, C.H., et al., *Magnetic hyperthermia enhance the treatment efficacy of peri-implant osteomyelitis.* BMC Infect Dis, 2017. **17**(1): p. 516.
13. Lucke, M., et al., *A new model of implant-related osteomyelitis in rats.* Journal of Biomedical Materials Research Part B: Applied Biomaterials: An Official Journal of The Society for Biomaterials, The Japanese Society for Biomaterials, and The Australian Society for Biomaterials and the Korean Society for Biomaterials, 2003. **67**(1): p. 593-602.

14. Santos-Ferreira, I., A. Bettencourt, and A.J. Almeida, *Nanoparticulate platforms for targeting bone infections: meeting a major therapeutic challenge.* Nanomedicine, 2015. **10**(20): p. 3131-3145.
15. Ferreira, M., et al., *Lipid-based nanosystems for targeting bone implant-associated infections: Current approaches and future endeavors.* Drug Delivery and Translational Research, 2021. **11**: p. 72-85.
16. Pitt, W.G., et al., *Ultrasonic enhancement of antibiotic action on gram-negative bacteria.* Antimicrobial agents and chemotherapy, 1994. **38**(11): p. 2577-2582.
17. Rediske, A.M., et al., *Ultrasonic enhancement of antibiotic action on Escherichia coli biofilms: an in vivo model.* Antimicrobial Agents and Chemotherapy, 1999. **43**(5): p. 1211-1214.
18. Ensing, G.T., et al., *Effect of pulsed ultrasound in combination with gentamicin on bacterial viability in biofilms on bone cements in vivo.* J Appl Microbiol, 2005. **99**(3): p. 443-8.
19. Rediske, A.M., et al., *Pulsed Ultrasound Enhances the Killing ofEscherichia coli Biofilms by Aminoglycoside Antibiotics In Vivo.* 2000. **44**(3): p. 771-772.
20. Rieck, B., et al., *Focused ultrasound treatment of abscesses induced by methicillin resistant Staphylococcus aureus: Feasibility study in a mouse model.* 2014. **41**(6Part1).
21. Wardlow, R., et al., *High Intensity Focused Ultrasound (HIFU) Heating Improves Perfusion and Antimicrobial Efficacy in Mouse Staphylococcus Abscess.* Ultrasound in Medicine and Biology, 2018. **44**(4): p. 909-914.
22. Patel, M., et al. *Animal models for the study of osteomyelitis*. in *Seminars in plastic surgery*. 2009. © Thieme Medical Publishers.
23. Lebeaux, D., et al., *From in vitro to in vivo models of bacterial biofilm-related infections.* Pathogens, 2013. **2**(2): p. 288-356.
24. Pulido, L., et al., *Periprosthetic joint infection: the incidence, timing, and predisposing factors.* Clinical orthopaedics and related research, 2008. **466**(7): p. 1710-1715.
25. Kaplan, S.L., *Recent lessons for the management of bone and joint infections.* Journal of Infection, 2014. **68**: p. S51-S56.
26. Carli, A.V., et al., *Quantification of Peri-Implant Bacterial Load and in Vivo Biofilm Formation in an Innovative, Clinically Representative Mouse Model of Periprosthetic Joint Infection.* 2017. **99**(6): p. e25.
27. Spagnolo, N., et al., *Chronic staphylococcal osteomyelitis: a new experimental rat model.* Infection and immunity, 1993. **61**(12): p. 5225-5230.
28. Solberg, B.D., A.P. Gutow, and M.R. Baumgaertner, *Efficacy of gentamycin-impregnated resorbable hydroxyapatite cement in treating osteomyelitis in a rat model.* Journal of orthopaedic trauma, 1999. **13**(2): p. 102-106.
29. Littlewood-Evans, A., et al., *Local expression of tumor necrosis factor alpha in an experimental model of acute osteomyelitis in rats.* Infection and immunity, 1997. **65**(8): p. 3438-3443.
30. Haenle, M., et al., *A Model of Implant-Associated Infection in the Tibial Metaphysis of Rats.* The Scientific World Journal, 2013. **2013**: p. 481975.

31. Gade, N.D. and M.S. Qazi, *Fluoroquinolone therapy in Staphylococcus aureus infections: where do we stand?* Journal of Laboratory physicians, 2013. **5**(02): p. 109-112.
32. Yin, L.-Y., M.M. Manring, and J.H. Calhoun, *A rabbit osteomyelitis model to simulate multibacterial war wound infections.* Military medicine, 2013. **178**(6): p. 696-700.
33. Ibelli, T., S. Templeton, and N. Levi-Polyachenko, *Progress on utilizing hyperthermia for mitigating bacterial infections.* International Journal of Hyperthermia, 2018. **34**(2): p. 144-156.
34. LeBel, M., *Ciprofloxacin: chemistry, mechanism of action, resistance, antimicrobial spectrum, pharmacokinetics, clinical trials, and adverse reactions.* Pharmacotherapy: The Journal of Human Pharmacology and Drug Therapy, 1988. **8**(1): p. 3-30.
35. Dalhoff, A., *Quinolone resistance in Pseudomonas aeruginosa and Staphylococcus aureus. Development during therapy and clinical significance.* Infection, 1994. **22**(2): p. S111-S121.
36. Mulligan, M., et al., *Ciprofloxacin for eradication of methicillin-resistant Staphylococcus aureus colonization.* The American journal of medicine, 1987. **82**(4A): p. 215-219.
37. Carmen, J.C., et al., *Ultrasonically Enhanced Vancomycin Activity Against Staphylococcus Epidermidis Biofilms in Vivo.* 2004. **18**(4): p. 237-245.
38. Vollmer, A.C., et al., *Bacterial stress responses to 1-megahertz pulsed ultrasound in the presence of microbubbles.* Applied and environmental microbiology, 1998. **64**(10): p. 3927-3931.
39. Bhatia, E., et al., *Combinatorial liposomes of berberine and curcumin inhibit biofilm formation and intracellular methicillin resistant Staphylococcus aureus infections and associated inflammation.* Journal of Materials Chemistry B, 2021. **9**(3): p. 864-875.
40. Portilla, S., et al., *Encapsulation of the antistaphylococcal endolysin lysrodi in ph-sensitive liposomes.* Antibiotics, 2020. **9**(5): p. 242.
41. Rukavina, Z. and Ž. Vanić, *Current trends in development of liposomes for targeting bacterial biofilms.* Pharmaceutics, 2016. **8**(2): p. 18.
42. Ferreira, M., et al., *Liposomes as a Nanoplatform to Improve the Delivery of Antibiotics into Staphylococcus aureus Biofilms.* Pharmaceutics, 2021. **13**(3): p. 321.
43. Staruch, R., R. Chopra, and K. Hynynen, *Localised drug release using MRI-controlled focused ultrasound hyperthermia.* International Journal of Hyperthermia, 2011. **27**(2): p. 156-171.
44. de Smet, M., et al., *Magnetic resonance imaging of high intensity focused ultrasound mediated drug delivery from temperature-sensitive liposomes: an in vivo proof-of-concept study.* Journal of Controlled Release, 2011. **150**(1): p. 102-110.
45. VanOsdol, J., et al., *Sequential HIFU heating and nanobubble encapsulation provide efficient drug penetration from stealth and temperature sensitive liposomes in colon cancer.* Journal of controlled release : official journal of the Controlled Release Society, 2017. **247**: p. 55-63.

46. Ektate, K., et al., *Chemo-immunotherapy of colon cancer with focused ultrasound and Salmonella-laden temperature sensitive liposomes (thermobots).* Scientific Reports, 2018. **8**(1): p. 13062.
47. Gasselhuber, A., et al., *Targeted drug delivery by high intensity focused ultrasound mediated hyperthermia combined with temperature-sensitive liposomes: computational modelling and preliminary in vivo validation.* International Journal of Hyperthermia, 2012. **28**(4): p. 337-348.
48. Hijnen, N., S. Langereis, and H. Grüll, *Magnetic resonance guided high-intensity focused ultrasound for image-guided temperature-induced drug delivery.* Advanced drug delivery reviews, 2014. **72**: p. 65-81.
49. Fleury, B., et al., *Transcriptomic and metabolic responses of Staphylococcus aureus exposed to supra-physiological temperatures.* BMC microbiology, 2009. **9**(1): p. 76.
50. Gera, N. and S. Doores, *Kinetics and mechanism of bacterial inactivation by ultrasound waves and sonoprotective effect of milk components.* Journal of food science, 2011. **76**(2): p. M111-M119.
51. Nguyen, T.-K., et al., *Iron oxide nanoparticle-mediated hyperthermia stimulates dispersal in bacterial biofilms and enhances antibiotic efficacy.* Scientific Reports, 2015. **5**: p. 18385.
52. Kaplan, J.B. and D.H. Fine, *Biofilm dispersal of Neisseria subflava and other phylogenetically diverse oral bacteria.* Applied and Environmental Microbiology, 2002. **68**(10): p. 4943-4950.

CHAPTER V

SUMMARY OF FINDINGS AND FUTURE DIRECTIONS

High-intensity focused ultrasound (HIFU) induced thermal and non-thermal effects can generate a variety of bioeffects in target tissues anywhere in the body, thereby transforming the treatment of many medical disorders. The goal of this dissertation was to investigate the role of thermal and non-thermal HIFU in improving treatment outcomes against spontaneously occurring canine tumors and peri-implant biofilm-associated bone infections. A variety of solid tumors in canine cancer patients were treated to establish the safety and efficacy of HIFU with or without adjuvant low-temperature sensitive liposomes (LTSL) chemotherapy. Additionally, the local and systemic immune responses to HIFU ablation of the tumors was determined. Further, the ability of combinatorial treatment to kill biofilms on osteomyelitis implants was evaluated. The key findings of the various research works are described below.

Chapter II

The objective of this study was to investigate whether HIFU- thermal ablation induce remission of a spontaneous oral tumor and enhance anti-tumor immunity. A canine patient with a benign and solitary lesion oral schwannoma, a rare tumor occurring around

the lips, jaws, tongue, and mucosa was enrolled. Three thermal ablation treatments over 3 weeks., treating ~50% of the tumor at each treatment session were performed. Our longitudinal assessment indicated that the patient tolerated the treatments and showed a normal appetite with minimal to mild pain at the treated region. Renal function examination did not indicate any signs of acute toxicity due to tumor lysis syndrome. Progressive tumor remission was observed with each treatment, and the tumor became undetectable 4 weeks post-treatment. Mechanistically, **HIFU** exposures induced coagulative necrosis and increased the populations of inflammatory cells in the treated tumor and blood samples collected during the course of the treatments. In particular, an increase in the populations $CD4^+$ and $CD8^+$ T cells as well as increased IFN-Y production in tumor and blood samples compared with the pretreatment levels was noted. Although our treatments were highly conformal, treatment related adverse events, primarily thermal burns, were observed on the buccal mucosa, which were managed with periodic hyperbaric oxygen therapy and surgical closure of the underlying exposed bones with gingival flaps. In summary, data from this study suggested that HIFU thermal ablation can induce regression of a large oral masses and the local treatments generate an inflamed tumor microenvironment that may possibly increase antitumor immunity.

Chapter III

The aim of this study was to compare the therapeutic and immunological properties of HIFU ablation versus mechanical histotripsy in canine patients. Additionally, the ability of HIFU hyperthermia to enhance anti-tumor immunity and delivery of free doxorubicin from LTSL in patients with sarcoma tumors were investigated. Results showed that benign local masses were highly responsive to thermal ablative treatments but were

associated with adverse effects in some cases. These adverse effects (minor to moderate burns) were manageable by hyperbaric oxygen therapy or other available interventions. In contrast, no adverse effects were noted with histotripsy, but the therapeutic protocols were not sufficient to sustain tumor regressions. Immunologically, systemic T cell activation was observed with both ablation and histotripsy. In the HIFU + adjuvant study, LTSL+ HIFU demonstrated greater Dox delivery compared to other treatments, presumably due to higher release of encapsulated content from LTSLs in sarcoma tumors. The enhanced Dox delivery correlated with improved local and systemic antitumor immunity, and tumor regressions. In summary, results from our pilot trials demonstrate the effectiveness of HIFU for non-invasive treatment of spontaneous canine tumors and its potential to improve local drug delivery and systemic anti-tumor immunity in patients.

Chapter IV

The goal of this study was to understand the ability of HIFU to enhance targeting of non-healing MRSA bone infections that causes chronic osteomyelitis. Osteomyelitis is characterized by a reduced susceptibility to treatment, and poor penetration/non-uniform distribution of antimicrobials within bone tissues. We hypothesized that antibiotic laden Low Temperature-Sensitive Liposomes (LTSLs), applied systemically with High Intensity Focused Ultrasound (HIFU)-induced bone heating (>40°C) can overcome this barrier, by enabling externally controlled “heat-targeted, on-demand” antibiotic delivery and synergistic MRSA killing within infected bony tissue, reducing, or obviating the need for ultimate surgical manipulation and debridement. To investigate our hypothesis, we developed a rat model of metal-implanted osteomyelitis, by surgically implanting

orthopedic wires into the right femurs of rats to induce osteomyelitis. Our metal implantation method yielded medullary disease by day 10 in bones and adjoining muscle tissues. Histologically, suppurative changes (bacterial and pus pockets) with remodeling and colonization of tissues with *S. aureus* was observed. LTSL containing ciprofloxacin for targeted release at >40°C with HIFU were administered intravenously immediately after the initiation of HIFU. 24h later, the rats were sacrificed, and CIP bone delivery of was estimated. We found the CIP delivery in the heated region was increased by >1-fold with LTSL (2.16µg CIP/g) *vs.* CIP (1.47µg CIP/g) and unheated femur (1.33µg CIP/g), demonstrating that our approach can be used to improve drug delivery to infected bones. To measure the therapeutic efficacy, rats underwent two treatments and were sacrificed 24h post second treatment for bacteriological and histological assessment of treated tissues. Our data suggested that the increased CIP delivery in the bones correlated with the therapeutic effects of the CIP-LTSL combination treatment, achieving significant reductions of tissue MRSA load in the infected bone (2.3-log and 2.9-log) compared to HIFU alone and free CIP groups respectively. These could also be verified via scanning electron microscopy where distinct reduction in biofilm density on the implanted wire was visualized. Our data suggests that HIFU hyperthermia and targeted antibiotic release using LTSLs can non-invasively disrupt biofilm bacteria on implant surfaces, in vivo, rendering the MRSA more susceptible to antibiotic clearance.

Future directions

This dissertation work established the applicability and effectiveness of HIFU for non-invasive treatment of spontaneous canine tumors and recalcitrant musculoskeletal infections. Although our results are highly encouraging, certain issues need to be

addressed. First, it would be valuable to conduct HIFU canine clinical trials in a bigger cohort of patients with low-grade and high-grade tumors. This will allow to draw more meaningful study conclusions regarding therapeutic efficacies. Secondly, correlations between the breed, gender, tumor type or tumor locations need to be assessed, to personalize HIFU therapy. Third, in addition to the T cells responses, cellular responses like antigen presenting cells as well as changes in the chemokine/cytokine levels, to gain a better understanding of the immunomodulatory effects of HIFU treatments should be instituted. Additionally, the molecular mechanisms driving canine cancer treatments, using next-generation sequencing methods, can help explore novel immunotherapy approaches

Long term exposure to bacterial antigens leads to immune cell dysfunction associated with ineffective clearance and persistence of disease. *S. aureus* persistence in bone cells further contributes to drug resistance. Thus, a successful treatment strategy, for effective and complete recovery from chronic biofilm *S. aureus* infections, needs to be multitarget. HIFU was shown to induce systemic immune response against cancer cells, thus it may be interesting to discover if a similar mechanism operates in bone biofilms treated with HIFU. Furthermore, with the recent transformative clinical success of checkpoint inhibitors in cancer immunotherapy, similar advances for treatment of chronic bone infections warrant investigation.

VITA

Harshini Kailash Ashar

Candidate for the Degree of

Doctor of Philosophy

Dissertation: TRANSLATING FOCUSED ULTRASOUND COMBINED NANOMEDICINES FOR TREATMENT OF BONE INFECTIONS AND CANINE CANCER PATIENTS

Major Field: Veterinary Biomedical Sciences

Biographical:

Education:
Completed the requirements for the Doctor of Philosophy/Education in Veterinary Biomedical Sciences at Oklahoma State University, Stillwater, Oklahoma in December, 2021.

Completed the requirements for the Master of Veterinary Sciences at Bombay Veterinary College, Mumbai, Maharashtra/India in 2013.

Completed the requirements for the Bachelor of Veterinary Sciences and Animal Husbandry at Nagpur Veterinary College, Nagpur, Maharashtra/India in 2011.

Experience:
Small animal veterinarian (2011- 2013)

Graduate teaching assistant for Gross and Developmental Anatomy, College of Veterinary Medicine, Oklahoma State University (2017-2020)

Graduate research assistant at Oklahoma State University (2014-2016; 2020-2021)

Professional Memberships:
Women In Focused Ultrasound (WIFUS)